PNNL-13320

Gas Generation from K East Basin Sludges – Series I Testing

C. H. Delegard
S. A. Bryan
A. J. Schmidt
P. R. Bredt
C. M. King
R. L. Sell
L. L. Burger
K. L. Silvers

September 2000

Prepared for Fluor Hanford, Inc.

Work Supported by
the U.S. Department of Energy
under Contract DE-AC06-76RL01830

Pacific Northwest National Laboratory
Richland, Washington 99352

PACIFIC NORTHWEST NATIONAL LABORATORY
operated by
BATTELLE
for the
UNITED STATES DEPARTMENT OF ENERGY
under Contract DE-AC06-76RL01830

PNNL-13320

Gas Generation from K East Basin Sludges – Series I Testing

C. H. Delegard
S. A. Bryan
A. J. Schmidt
P. R. Bredt
C. M. King
R. L. Sell
L. L. Burger
K. L. Silvers

September 2000

Prepared for Fluor Hanford, Inc.

Work Supported by
the U.S. Department of Energy
under Contract DE-AC06-76RL01830

Pacific Northwest National Laboratory
Richland, Washington 99352

Summary and Conclusions

The path forward for the management of Hanford K Basin sludge calls for it to be packaged, shipped, and stored at T Plant until final processing at a future date. An important consideration for the design and cost of retrieval, transportation, and storage systems is the potential for heat and gas generation through oxidation reactions between uranium metal and water. Another sludge component, uranium hydride, could also contribute to heat and gas generation. This report, the first in a series, describes work performed at the Pacific Northwest National Laboratory (PNNL) to examine the gas generation behavior of K Basin sludge materials using actual K East (KE) Basin floor and canister sludge. Two other test series will be described in future reports. The work is being conducted under the direction of the Spent Nuclear Fuel Sludge Handling Project managed by Fluor Hanford, Inc.

The overall goals for this testing were to collect gas generation rate and composition data to better understand the quantity and reactivity of the metallic uranium present in the K Basin sludge. Specific objectives included:

1. Determine the chemical reactivity of KE floor sludge compared with KE canister sludge.
2. Determine the quantity of uranium metal present in each sludge type.
3. Determine the reactivity of the uranium metal in KE canister sludge.
4. Determine how reactivity varies with particle size for the various KE sludges.
5. Provide data for input into sludge thermal stability models for safe sludge handling practices (e.g., uranium metal content, reaction rates).
6. Provide gas generation data that can be used as design input into sludge transportation and storage systems.
7. Estimate the uranium metal surface area per unit mass of sludge (combined with sludge calorimetry and particle size distribution data).
8. Determine if the oxidation rate measured for uranium in actual sludge agrees with the baseline project-accepted kinetic model for uranium oxidation in water (Reilly 1998).

The conclusions resulting from this first series of tests are summarized as follows:

- The floor sludge has low chemical reactivity, provides little gas generation, and is estimated to contain less than 0.15 wt% metallic uranium (settled-sludge basis).
- Sludge made up of fine particles (<250 μm) from both the KE floor and canisters also has low chemical reactivity and gas generation.
- The canister sludge (including <250 μm and > 250 μm fractions) is estimated to contain 1.9±0.2 wt% metallic uranium (settled-sludge basis).
- Larger-particle canister sludge (>250 μm) exhibits moderate chemical reactivity and gas generation (i.e., contains some metallic uranium).
- The reaction rates observed for larger particle canister sludge agree reasonably well with the rate equation for uranium metal with oxygen-free water given in the Spent Nuclear Fuel Project Technical Databook (Reilly 1998). Use of a reaction rate enhancement factor is probably not necessary.

Test Materials and Description

The sludge used for the gas generation testing was taken from the KE Basin floor and fuel canisters in March and April 1999 by Duke Engineering & Services Hanford. A consolidated sampling technique was employed for collecting the material (i.e., sludge from several locations was combined to form "consolidated samples"). Three sludge samples were used: fuel canister sludge (KC-2/3); floor sludge collected from between slotted fuel canisters containing highly damaged fuel (KC-4); and floor sludge collected away from fuel canisters and away from areas known to contain high concentrations of organic ion exchange resin (KC-5). The canister sludge used in this testing (KC-2/3) was prepared by combining two consolidated sludge samples (i.e., KC-2, collected from canisters containing highly damaged fuel, and KC-3, collected from canisters containing moderately damaged fuel). Portions of these samples were sieved to separate particles greater than or "plus" 250 µm (P250) from particles less than or "minus" 250 µm (M250). This separation was made to mimic the separation operations that are planned for the retrieval of certain K Basin sludge types and to gain a better understanding of how uranium metal is distributed in the sludge. [The separation point for certain K Basin sludge types was subsequently changed from 250 µm to 500 µm (Pearce and Klimper 2000).] Fine uranium metal particles have a high surface area and will react rapidly. Larger uranium metal particles will react at a slower rate, since their surface area per unit mass of sludge is lower.

For the testing described here, sludge samples were placed into four large-scale vessels (850 ml) and eight small-scale reaction vessels (30 ml). The gas pressure in the vessels was monitored continuously, and gas samples were collected intermittently and analyzed via mass spectrometry. The large-scale testing was initiated in August 1999, and three tests continued through June 2000. One large-scale test is still underway, and will continue into FY2001. These test vessels contained 70 to 440 grams of settled sludge held at ambient hot cell temperature (~32ºC). The large-scale-test conditions are expected to be prototypical of those that will be experienced during long-term storage of the sludge at T Plant (i.e., large-scale tests serve as a mock-up for prolonged T Plant storage). The small-scale tests, which were conducted with about 15 grams settled sludge each, were initiated on October 6, 1999, and completed in June 2000. The small-scale tests were conducted at elevated temperatures (six tests at 80ºC, one at 60ºC, and one at 40ºC) to accelerate the reactions and provide conclusive gas generation data within a reasonable testing period. The temperature in all of the small-scale test vessels was increased to 95°C for a period at the end of the tests to force completion of the reactions. The table below shows the test matrix.

Experimental Matrix for Large- and Small-Scale Gas Generation Tests

Temperature and Test Scale	**KC-2/3**		**KC-4**		**KC-5**	
	M250 µm	**P250 µm**	**M250 µm**	**P250 µm**	**M250 µm**	**P250 µm**
40ºC-small		X[(a)]				
60ºC-small		X[(a)]				
80ºC-small	X[(a)]	X[(a)]	X[(a)]	X[(a)]	X[(a)]	X[(a)]
Ambient (~32ºC)-large		X	X X (Dup)		X	

Note: Large-scale tests at ambient temperatures (~32ºC) are being conducted with the >250 µm fraction of KC-2/3 Composite and the intact (before sieving) samples from KC-4, KC-4 Dup, and KC-5.
(a) Tests completed at 95°C.

Results of Gas Generation Testing

The results from the tests with small- and large-scale vessels are summarized here.

Small-Scale Gas Generation Testing with Canister Sludge (KC-2/3 P250)

Small-scale gas generation tests were conducted with KC-2/3 P250 at three temperatures: 40ºC, 60ºC, and 80ºC. Each test was then subjected to a period of heating to 95°C to force completion of the reactions. The KC-2/3 P250 sample, which is more reactive than the other samples tested, exhibited a gas generation profile (moles of gas generated as a function of time) that includes an induction period, a linear region, and a declining region (as reactants are depleted). The time of the induction period increased with decreasing reaction temperature.

In the linear region at 80ºC, gas was generated at a rate of 1600 ml total gas [at standard temperature and pressure (STP)] per kg settled sludge-day. A 27-hour induction period was observed in this test. During the first 730 hours for the test conducted at 80ºC, about 95% of the initial uranium metal was depleted, and the composition of the gas ranged from about 75% to 85% H_2 and 15% to 25% CO_2. Small quantities of other gases (e.g., methane, ethane, krypton, and xenon) were also present.

Several actions were taken to obtain additional confidence in the data generated from the KC-2/3 P250 test. After the gas generation rate slowed down, the KC-2/3 P250 reaction vessel was agitated aggressively for about 20 minutes with a high-energy vibrator. After this agitation, the gas generation quantity and rate were essentially unchanged. Also, near the end of the test, the temperature was raised from 80ºC to 95ºC. The temperature change had little impact on the gas generation quantity or rate. Since these perturbations had little effect on the gas generation, it is unlikely that any metallic uranium particles were somehow shielded (e.g., suffered mass transfer resistances from coating of corrosion products) from participation in the measured corrosion reactions.

The gas generation rate profile for the test conducted at 60ºC shows that the induction period was about 205 hours (~9 days), and that after 26 days, the reaction was near the end of the linear region. Subsequent heating at 95ºC after 145 days at 60ºC produced only about 5% additional gas. In the linear region at 60ºC, gas was generated at a rate of 440 ml total gas (at STP) per kg of settled sludge-day. In the linear region, the composition of the gas samples was 96% H_2 and 4% CO_2. The H_2 generation rate in the linear region at 60ºC was about a factor of 3 less than the rate obtained in the linear region at 80ºC.

At 40ºC, the reaction induction period was about 1340 hours (~56 days). About 80 ml total gas (at STP) per kg of settled sludge-day were generated in the linear region. Analysis of the gas collected in the linear region showed approximately 1% CO_2 and 99% H_2.

After about 150 days at 40ºC, the reaction vessel temperature was increased to 95ºC. Within several hours, a linear range of gas generation was established at 95ºC. The total gas generation rate at 95ºC was about 4600 ml total gas (at STP) per kg settled sludge-day, and the gas composition was about 98% H_2 and 2% CO_2.

Using the hydrogen gas generation rate data collected during the linear region at 40ºC, 60ºC, 80ºC, and 95ºC, the activation energy was calculated for the reaction:

$$U + 2\ H_2O \rightarrow UO_2 + 2\ H_2$$

The activation energy for uranium metal corrosion was 15.1 kcal/mole (63 kJ/mole). This is near the value for uranium metal corrosion in H_2-saturated water of 16.1 kcal/mole (67 kJ/mole), as derived from a review of the technical literature (Pajunen 1999).

The corrosion of uranium metal could be established not only by the observed evolution of hydrogen gas but also by the appearance, in the correct proportions, of krypton and xenon gases of the appropriate isotopic compositions. Furthermore, methane, ethane, and other hydrocarbons in the correct concentrations were observed in the evolved gases from the reaction of uranium carbide traces in the metallic fuel.

Small-Scale Gas Generation Testing with Floor Sludge (KC-4 P250, KC-4 M250, KC-5 P250 and KC-5 M250) and Canister Sludge (KC-2/3 M250) at 80ºC and 95ºC

The rates of gas generation from the tests with KC-4 and KC-5 and KC-2/3 M250 sludge conducted at 80ºC were very low compared with the 80ºC test with KC-2/3 P250 sludge. After 18 days, the gas generation rates were between 4 ml and 25 ml total gas (at STP) per kg of settled sludge-day. Of the gas generated, more than 90% was CO_2.

The finding that KC-2/3 M250 had low reactivity was unanticipated. Its counterpart, KC-2/3 P250, was found to be quite reactive. Furthermore, other data show that the dry particle density of KC-2/3 M250 is much greater than that of KC-2/3 P250 (7.57 g/cm^3 for M250 and 2.23 to 6.91 g/cm^3 for P250), which suggests a higher concentration of dense uranium metal. The total uranium (of all chemical forms) also is higher for the wet sludge M250 fraction, 40 wt% versus 18 wt% for the P250 fraction. The knowledge that uranium metal particles in the canister sludge are generally confined to sludge particles greater than 250 μm will eliminate regions of concern on thermal stability maps generated from modeling efforts.

The reaction vessels were agitated with a high-energy vibrator for 5 minutes each to determine if the sludge reactions with water are inhibited by coatings, films, or other mass transfer resistances surrounding the uranium metal particles. After agitation, the rate of gas generation initially increased and then appeared to return to a rate similar to that exhibited before agitation. Although the magnitudes of the gas generation rate increases are rather small, the gas generation mechanism(s) instigated by the agitation are unknown.

Large-Scale Gas Generation Testing at Ambient Temperature (~32ºC)

Gas samples were collected and analyzed from three large-scale tests: KC-4, KC-4 duplicate, and KC-5. The rates of gas generation from these tests were very low, less than 0.05 ml total gas (at STP) per kg settled sludge-day. The primary gases were CO_2 (63% to 92%) and H_2.

While the total moles of gas generated were nearly identical for KC-4 and KC-4 Dup, the compositions initially varied significantly: 45% H_2 for KC-4 and ~1% H_2 for KC-4 Dup. The compositions became closer with longer reaction time and subsequent gas sampling with neon purging. Although both systems were purged with neon gas multiple times before beginning the run, KC-4 Dup contained about seven times more residual air than KC-4. Oxygen in the system strongly affects the controlling mechanism for uranium metal/water reactions.

The overall gas generation rate of the KC-2/3 P250 large-scale test run at the hot cell temperature was almost 40 times higher (~0.9 ml/kg settled sludge-day) than the rates observed for the KC-4 and KC-5 tests. The gas collected after about 19 days of reaction was about 92% CO_2; about 95% CO_2 was

observed over the 195-day test duration. The KC-2/3 P250 large-scale test evidently has not transitioned to the hydrogen-mediated uranium corrosion mechanism even after 195 days of testing at the 32ºC hot cell temperature. The longer induction time at 32ºC likely is because of the larger vapor/sludge volume ratio in this large-scale test (~10) compared with the small-scale test (~1). This test is still underway, and will continue into FY2001.

Uranium Metal Content in Sludge

From the gas generation data and the projected corrosion reactions, the quantities of metallic uranium initially present in the sludge from each test were calculated. The KC-2/3 P250 sludge contained 7.4±0.9 wt% metallic uranium (on a settled-sludge basis). [This projected uranium metal content is consistent with results obtained from dissolution enthalpy (calorimetry) testing performed on KC-2/3 P250 (Bredt et al. 1999).] All other sludges evaluated in the gas generation testing were estimated to contain less than 0.2 wt% metallic uranium (settled-sludge basis).

Canister sludge sample KC-2/3 was split into two fractions using a 250-μm sieve. Approximately 25% of the original sample was made up of particles greater than 250 μm. Therefore, the projected uranium metal content in the original KC-2/3 canister sludge sample was: 1.9±0.2 wt% [(0.25x7.4±0.9) + (0.75x0.0485)]. [Note sample KC-2/3 M250 was estimated to contain 0.0485 wt% metallic uranium.]

Fission Product Gases

The existence of the krypton and xenon fission gases in the product gas gives evidence of the corrosion of uranium metal, because until corrosion occurs, the fission gases remain trapped within the uranium metal matrix. The krypton and xenon isotope ratios observed in the product gas are similar to the ratios that are expected based on burn-up calculations by the ORIGEN code, which provides a general confirmation to the uranium metal content in the sludges calculated from the gas generation data.

Hydrocarbon Evolution

Methane (CH_4), ethane (C_2H_6), and higher hydrocarbons were found in gases generated during all tests. Methane, ethane, and other hydrocarbons also have been observed in H_2-rich gases evolved at hot cell temperature from canister sludges 96-05, 96-06, 96-13, and 96-15 taken from the KE Basin (Appendix B of Makenas et al. 1997). The hydrocarbons and some hydrogen arise from the reaction of water with carbide carbon in the uranium metal fuel. The measured quantities of total carbon in the hydrocarbon gas products for KC-2/3 P250 tests indicate a total carbon concentration in the uranium fuel particles of about 780 ppm. This value is in general agreement with the reported carbon content of the metallic uranium fuels stored in the K Basins [i.e., nominal carbon content ranges from 365 to 735 ppm (Weakley 1979)]. This agreement provides additional confirmation of the sludge uranium metal content calculated from the gas generation data.

Carbon Dioxide Evolution

Significant quantities of CO_2 were found in gases generated during all large- and small-scale gas generation tests. Carbon dioxide was also observed in H_2-rich gases evolved at hot cell temperature from canister sludges 96-05, 96-06, 96-13, and 96-15 taken from the KE Basin (Makenas et al. 1997). The CO_2 found in all tests may be explained by the reaction in water of schoepite, $(UO_2)_8O_2(OH)_{12}(H_2O)_{12}$ (or $4UO_3{\cdot}9H_2O$), with calcite, $CaCO_3$, to form the more stable uranium phase, becquerelite, $Ca(UO_2)_6O_4(OH)_6(H_2O)_8$ (or $CaU_6O_{19}{\cdot}11H_2O$) and carbonic acid (H_2CO_3):

$$3\ (UO_2)_8O_2(OH)_{12}(H_2O)_{12} + 4\ CaCO_3 \rightarrow 4\ Ca(UO_2)_6O_4(OH)_6(H_2O)_8 + 4\ H_2CO_3 + 6\ H_2O$$
$$\rightarrow 4\ Ca(UO_2)_6O_4(OH)_6(H_2O)_8 + 10\ H_2O + 4\ CO_2\uparrow$$

Carbon dioxide generation will need to be taken into account for designing sludge retrieval, transportation, and storage systems. However, the exothermic contribution of this reaction is small with respect to that of the uranium metal corrosion reaction, and can probably be neglected in sludge thermal stability modeling efforts.

Comparison of Results with Gas Generation Data from KE Basin Canister Sludge Collected in 1996

Limited gas generation rate data were collected over short time intervals (up to several days) in 1996 from KE canister sludge samples held at ambient hot cell temperatures (35ºC). Gas was generated from some of these whole (i.e., unsieved) samples at rates ranging from 0 to 150 ml/kg settled sludge-day. The average gas generation rates from several measurements from two of the 1996 samples (96-05 and 96-06) were 27 and 59 ml/kg settled sludge-day. In comparison, the gas generation rate from KC-2/3 P250 at 40ºC during the linear period was about 80 ml/kg settled sludge-day. The composition of the gas from the 1996 samples (mostly H_2) was similar to that from KC-2/3 P250 at 40ºC during the linear period. On a whole sample basis, for a period of time (several days), the 96-05 and 96-06 canister sludge samples generated gas at rates 2 to 11 times greater than the projected rate at 35°C for the KC-2/3 sludge (accounting for the relatively unreactive M250 fraction of the KC-2/3 material). While the individual samples 96-05 and 96-06 exhibited a higher apparent reactivity (during short-term observations) than KC-2/3 canister sludge, several of the other canister samples collected in 1996 generated little or no gas. The KC-2/3 canister material was a fairly large composite (~ 3 kg) created from sludge collected from 10 sampling locations, and its gas generation behavior was monitored for more than 3000 hours. The gas generation behavior of KC-2/3 is expected to best represent nominal canister sludge collected from canisters containing moderately and severely damaged fuel. A review of the overall gas generation of the nine canister sludge samples collected in 1996, including those observations where samples generated little or no gas, indicates that a "composite" of the 1996 samples would likely exhibit a gas generation rate comparable to that of the KC-2/3 composite.

The 1996 samples did not appear to experience an induction period. In comparison, the current large-scale test with KC-2/3 P250 sludge at ambient hot cell temperatures (~32ºC) is still in an induction phase after a year of testing and has exhibited a maximum gas generation rate of only 2.4 ml/kg settled sludge-day. Sample handling and the large ratio of gas headspace volume to sludge ratio for the KC-2/3 P250 large-scale test may have contributed to the long induction time.

Evaluation of Reaction Surface Area of Uranium Particles in KC-2/3 P250

The rate at which uranium metal reacts with water depends on the available surface area of the uranium particles. An initial evaluation of the uranium metal reaction surface area per unit mass of settled sludge was performed using the results from the gas generation testing with sample KC-2/3 P250 (at 80ºC). Results from the preliminary evaluation indicate that the uranium metal surface area calculated from the gas generation data agrees reasonably well with theoretical predictions using the rate equation given in the Spent Nuclear Fuel Project Technical Databook (Reilly 1998). [Note: The rate equation in Reilly (1998) is being used within the thermal stability models for sludge transportation and storage.]

The uranium metal corrosion in the KC-2/3 P250 sludge sample appears to be well modeled as spheres or cubes of about 800-μm axial dimension (based on the rate equation in Reilly 1998). Use of a reaction rate enhancement factor with the rate equation in Reilly (1998) is probably not necessary.

Evaluation of Radiolysis as a Source of Hydrogen Production in K Basin Sludge

Based on an analysis of KE canister sludge performed in 1997, radiolysis does not appear to be a significant source of hydrogen generation in K Basin sludge.

References

Bredt, P. R., C. H. Delegard, A. J. Schmidt, and K. L. Silvers. 1999. *Testing and Analysis of Consolidated Sludge Sample from 105K East Basin Floor and Canisters.* PNNL-13341, Pacific Northwest National Laboratory, Richland, Washington.

Makenas, B. J., T. L. Welsh, R. B. Baker, E. W. Hoppe, A. J. Schmidt, J. Abrefah, J. M. Tingey, P. R. Bredt, and G. R. Golcar. 1997. *Analysis of Sludge from Hanford K East Basin Canisters.* HNF-SP-1201, DE&S Hanford, Inc., Richland, Washington.

Pajunen, A. L. 1999. *Uranium Oxidation Rate Summary for the Spent Nuclear Fuel Project.* HNF-4165, Rev. 0, DE&S Hanford, Inc., Richland, Washington.

Pearce, K. L., and S. C. Klimper. 2000. *105-K Basin Material Design Basis Feed Description for Spent Nuclear Fuel Project Facilities, Volume 2, Sludge.* HNF-SD-SNF-TI-009, Rev. 3, Fluor Hanford, Inc., Richland, Washington.

Reilly, M. A. 1998. *Spent Nuclear Fuel Project Technical Databook.* HNF-SD-SNF-TI-015, Rev. 6, DE&S Hanford, Inc., Richland, Washington.

Weakley, E. A. 1979. *Fuels Engineering Technical Handbook.* UNI-M-61, UNC Nuclear Industries, Richland, Washington.

Contents

Contents (continued)

Figures

Figures (continued)

Tables

Tables (continued)

1.0 Introduction

Two water-filled concrete pools [K East (KE) and K West (KW) Basins] in the 100K Area of the Hanford Site contain over 2100 metric tons of N Reactor fuel elements stored in aluminum or stainless steel canisters. During the time the fuel has been stored, approximately 52 m^3 of heterogeneous solid material (sludge) have accumulated in the canisters, as well as on the floor and in the associated pits. This sludge consists of various proportions of fuel, structural corrosion products, windblown material, and miscellaneous constituents such as ion exchange material (both organic and inorganic) and paint chips (Makenas et al. 1996-99). The inventory and compositions of all K Basin sludge materials are described in detail by Pearce and Klimper (2000). The baseline sludge management plan calls for the sludge to be packaged, shipped, and stored at T Plant in the Hanford 200 Area until final processing at a future date.

Because the sludge produces gas from chemical and, possibly, radiolytic reactions, gas generation must be considered when developing designs and determining costs for sludge retrieval, transportation, and storage systems. The work discussed in this report is being conducted by Pacific Northwest National Laboratory (PNNL) on actual sludge samples to better understand the reactions and assess the reaction rates. The work is being performed for the Spent Nuclear Fuel Sludge Handling Project managed by Fluor Hanford, Inc. This report is the first in a series of three. The sludge samples used for the tests described here were collected in March and April 1999 by Duke Engineering & Services Hanford from the KE Basin floor and fuel canisters (consolidated sludge samples). The second and third gas generation reports will describe tests conducted with other K Basin sludge samples and fragments from spent nuclear fuel.

This report provides the results of gas generation testing and analyses from August 1999 through June 2000. The overall goals for this testing were to collect gas generation rate and composition data to better understand the quantity and reactivity of the metallic uranium present in the K Basin sludge. The following specific objectives were included:

1. Determine the chemical reactivity of KE floor sludge compared with KE canister sludge.
2. Determine the quantity of uranium metal present in each sludge type.
3. Determine the reactivity of the uranium metal in KE canister sludge.
4. Determine how reactivity varies with particle size for the various KE sludges.
5. Provide data for input into sludge thermal stability models for safe sludge handling practices (e.g., uranium metal content, reaction rates).
6. Provide gas generation data that can be used as design input into sludge transportation and storage systems.
7. Estimate the uranium metal surface area per unit mass of sludge (combined with sludge calorimetry and particle size distribution data).
8. Determine if the oxidation rate measured for uranium in actual sludge agrees with the baseline project-accepted kinetic model for uranium oxidation in water (Reilly 1998).

Section 2.0 describes the experimental methods and materials, with Section 3.0 presenting the data derived from the testing. During the tests, hydrogen; fission gas products, krypton and xenon; methane and higher hydrocarbons; and carbon dioxide were generated. At the same time, oxygen and nitrogen in the test vessels were consumed (depleted). Section 4.0 details the chemistry of the gas generating (and consuming) reactions and interprets and discusses the test results. Appendix A contains data from work to verify the reliability and performance of the gas generation test system; Appendix B summarizes the

gas composition and generation rates from the gas sampling; Appendix C is an evaluation of radiolysis as a source of hydrogen production from KE canister sludge; Appendix D describes the derivation of surface-area-dependent rate laws; and Appendix E discusses the particle sizes of disintegrated spent nuclear fuel samples that underwent TGA oxidation testing in moist helium in another PNNL study.

An extensive technical data package (~3000 pages) containing the laboratory bench sheets and raw data (i.e., test instructions, laboratory record book pages, calibrations, temperature and pressure data, gas analysis data, etc.) is available from Fluor Hanford, Inc. (R. B. Baker).

2.0 Experimental Methods for Gas Measurements

The sludge used for these tests was collected by Duke Engineering & Services Hanford from the KE Basin floor and fuel canisters in March and April 1999 using a consolidated sampling technique (Pitner 1999a); i.e., material from several locations was combined to form "consolidated samples." For the gas generation testing, three sludge samples were used: fuel canister sludge (KC-2/3), floor sludge collected from between slotted fuel canisters containing highly damaged fuel (KC-4), and floor sludge collected away from fuel canisters and away from areas known to contain high concentrations of organic ion exchange resin (KC-5). The canister sludge used in this testing (KC-2/3) was a composite prepared by combining two consolidated sludge samples (KC-2, collected from canisters containing highly damaged fuel, and KC-3, collected from canisters containing moderately damaged fuel). Some of the original sludge samples have been sieved to generate subsamples consisting of particles greater than or less than 250 µm. The subsample fractions are designated as either P250 (i.e., plus, or greater than, 250 µm) or M250 (i.e., minus, or less than, 250 µm). Distinguishing the particle size mimics the separation operations planned for the retrieval of certain K Basin sludge types and helps gain a better understanding of how uranium metal is distributed in the sludge. Fine uranium metal particles have a high surface area and will react rapidly. Larger uranium metal particles will react with water at a slower rate, since their surface area per unit mass of sludge is lower.

Table 2.1 contains the general matrix for the gas generation testing. These tests were conducted as outlined in the PNNL test plans TP-30890-03 (Large-Scale Testing) and TP-30890-08 (Small-Scale Testing) at PNNL's High-Level Radiochemistry Facility in the 325 Building (325A HLRF), 300 Area. Three types of experiments were performed:

1. small-scale tests (~30-ml capacity vessels) at 40°C, 60°C, and 80ºC – KC-2/3 P250
2. small-scale tests at 80°C – KC-2/3 M250, KC-4 M250, KC-4 P250, KC-5 M250, and KC-5 P250
3. large-scale tests (~ 850-ml capacity vessels) conducted at ambient hot cell temperature (~32ºC) – KC-4, KC-4 Dup, KC-5, and KC-2/3.

Table 2.1. Experimental Matrix for Large- and Small-Scale Gas Generation Tests

Temperature and Test Scale	KC-2/3		KC-4		KC-5	
	M250 µm	**P250 µm**	**M250 µm**	**P250 µm**	**M250 µm**	**P250 µm**
40ºC-small		X[(a)]				
60ºC-small		X[(a)]				
80ºC-small	X[(a)]	X[(a)]	X[(a)]	X[(a)]	X[(a)]	X[(a)]
Ambient (~32ºC)-large		X	X X (Dup)		X	

Note: Large-scale tests at ambient temperatures (~32ºC) are being conducted with the >250 µm fraction of KC-2/3 Composite and the intact (before sieving) samples from KC-4, KC-4 Dup, and KC-5.
(a) Tests completed at 95°C.

The large-scale reactor vessel tests began in August 1999, with two sets of gas samples collected from KC-4, KC-4 Dup, and KC-5 and four samples from KC-2/3 P250. The small-scale tests were initiated in October 1999 with very significant gas generation observed in the vessels containing KC-2/3 P250 sludge at 40°C, 60°C, and 80ºC. After 95 to 145 days of reaction, the temperature in these three small-scale

KC-2/3 P250 tests was elevated to 95°C for 16 to 77 days to force the reactions to completion. Twelve, 8, and 10 gas samples, respectively, were collected from these tests. The remaining five small-scale tests were run at 80°C for about 100 days, and then elevated to 95°C for about 32 days. These vessels were each sampled five times. Table 2.2 provides information on the gas generation test materials, temperatures, and details on the gas sampling events.

The equipment, procedures, and test conditions are described in Section 2.1, and the K Basin sludge sample material is described in Section 2.2. Details on the verification of the reliability and performance of the gas generation test system are provided in Appendix A.

2.1 Experimental Conditions and Equipment

The reaction vessels (Sections 2.1.1 and 2.1.2) and the gas manifold system (Figure 2.1) used for the gas generation tests are similar to those described in earlier studies with simulated Hanford tank waste (Bryan and Pederson 1995) and in work with actual Hanford tank waste (Bryan et al. 1996; King et al. 1997). Each vessel has a separate pressure transducer on the gas manifold line. The entire surface of the reaction system exposed to the sludge sample is stainless steel, except for a gold-plated copper gasket sealing the flange at the top of the reaction vessel. Temperatures and pressures were recorded every 10 seconds on a Campbell Scientific CR10 datalogger; the data were averaged every 20 minutes and saved in a computer file. Temperature and pressure data were also manually logged once each day.

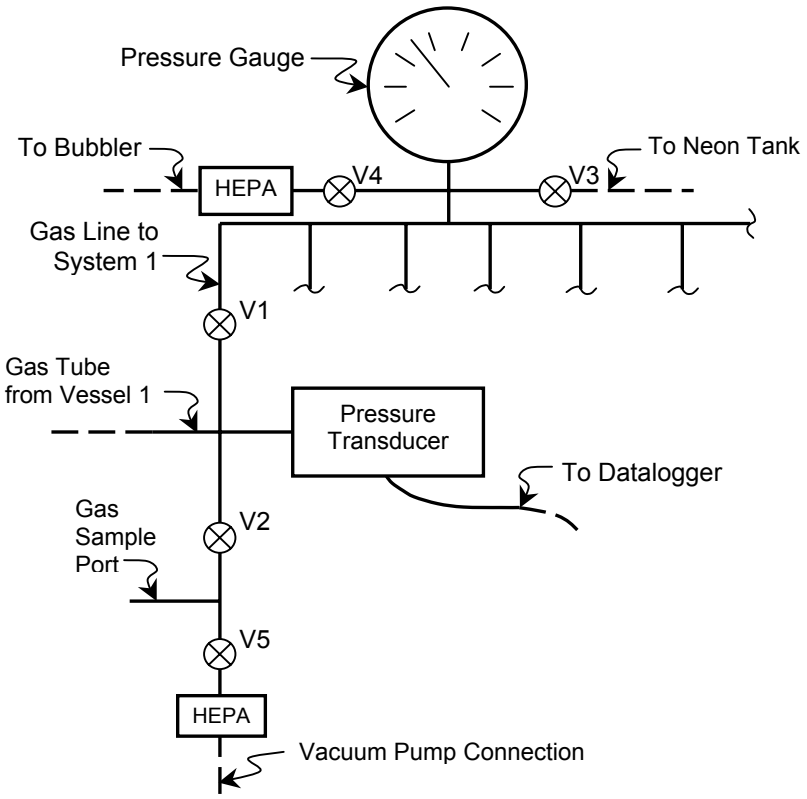

Figure 2.1. Pressure Manifold System Used in Gas Generation Tests

Table 2.2. K Basin Test Material Masses and Gas Sampling

Test Identification	Settled Sludge Mass, g	Test Temp., ºC	Start Date	Sample Date	Time at Temperature, h	
					Run Interval	Total
Small-Scale Gas Generation Tests						
KC-2/3 P250-40	23.69	40	10/7/99	10/25/99	1. 425	1. 425
		40	10/25/99	11/11/99	2. 344	2. 770
		40	11/11/99	11/29/99	3. 425	3. 1195
		40	11/29/99	12/17/99	4. 382	4. 1577
		40	12/17/99	1/31/00	5. 810	5. 2387
		40	1/31/00	3/3/00	6. 759	6. 3146
		40	3/3/00	3/20/00	7. 411	7. 3556
		95	3/20/00	3/21/00	8. 18.3	8. 3575
		95	3/21/00	3/24/00	9. 10.7	9. 3585
		95	3/24/00	3/30/00	10. 20.0	10. 3605
		95	3/30/00	4/5/00	11. 57.0	11. 3662
		95	4/5/00	4/19/00	12. 289	12. 3951
KC-2/3 P250-60	18.66	60	10/7/99	10/22/99	1. 353	1. 353
		60	10/22/99	11/2/99	2. 259	2. 612
		60	11/2/99	11/11/99	3. 151	3. 762
		60	11/11/99	11/19/99	4. 184	4. 946
		60	11/19/99	11/29/99	5. 235	5. 1181
		60	11/29/99	12/17/99	6. 382	6. 1563
		60	12/17/99	1/31/00	7. 798	7. 2361
		60	1/31/00	3/20/00[a]	1173 at 60°C	3534
		95	3/20/00	4/19/00	8. 671 at 95°C	8. 4205
KC-2/3 P250-80	13.71	80	10/8/99	10/12/99	1. 89	1. 89
		80	10/12/99	10/14/99	2. 41	2. 130
		80	10/14/99	10/19/99	3. 90	3. 219
		80	10/19/99	10/22/99	4. 89	4. 309
		80	10/22/99	10/25/99	5. 67	5. 376
		80	10/25/99	11/11/99	6. 352	6. 728
		80	11/11/99	11/29/99	7. 395	7. 1123
		80	11/29/99	12/17/99	8. 377	8. 1500
		80	12/17/99	1/31/00	9. 765	9. 2265
		80	3/6/00	3/20/00[a]	335 at 80°C	2600
		95	3/20/00	4/19/00	10. 733 at 95°C	10. 3333
KC-2/3 M250-80	17.56	80	10/7/99	10/25/99	1. 425	1. 425
		80	10/25/99	11/11/99	2. 296	2. 721
		80	11/11/99	12/17/99	3. 814	3. 1535
		80	12/17/99	1/31/00	4. 802	4. 2338
		80	1/31/00	2/17/00[a]	403 at 80°C	2741
		~32	2/17/00	5/5/00[a]	2088 at 32°C	--
		95	5/5/00	6/6/00	5. 769 at 95°C	5. 3510

Table 2.2. K Basin Test Material Masses and Gas Sampling

Test Identification	Settled Sludge Mass, g	Test Temp., ºC	Start Date	Sample Date	Time at Temperature, h	
					Run Interval	Total
KC-4 M250-80	15.14	80	10/7/99	10/25/99	1. 425	1. 425
		80	10/25/99	11/11/99	2. 296	2. 721
		80	11/11/99	12/17/99	3. 812	3. 1533
		80	12/17/99	1/31/00	4. 802	4. 2336
		80	1/31/00	2/17/00[(a)]	403 at 80°C	2739
		~32	2/17/00	5/5/00[(a)]	2088 at 32°C	--
		95	5/5/00	6/6/00	5. 769 at 95°C	5. 3508
KC-4 P250-80	7.82	80	10/7/99	10/25/99	1. 425	1. 425
		80	10/25/99	11/11/99	2. 295	2. 721
		80	11/11/99	12/17/99	3. 814	3. 1534
		80	12/17/99	1/31/00	4. 802	4. 2337
		80	1/31/00	2/17/00[(a)]	403 at 80°C	2740
		~32	2/17/00	5/5/00[(a)]	2088 at 32°C	--
		95	5/5/00	6/6/00	5. 769 at 95°C	5. 3509
KC-5 M250-80	13.86	80	10/7/99	10/25/99	1. 425	1. 425
		80	10/25/99	11/11/99	2. 296	2. 722
		80	11/11/99	12/17/99	3. 814	3. 1535
		80	12/17/99	1/31/00	4. 802	4. 2338
		80	1/31/00	2/17/00[(a)]	403 at 80°C	2741
		~32	2/17/00	5/5/00[(a)]	2088 at 32°C	--
		95	5/5/00	6/6/00	5. 769 at 95°C	5. 3510
KC-5 P250-80	16.23	80	10/7/99	10/25/99	1. 425	1. 425
		80	10/25/99	11/11/99	2. 296	2. 722
		80	11/11/99	12/17/99	3. 814	3. 1535
		80	12/17/99	1/31/00	4. 802	4. 2337
		80	1/31/00	2/17/00[(a)]	403 at 80°C	2740
		~32	2/17/00	5/5/00[(a)]	2088 at 32°C	--
		95	5/5/00	6/6/00	5. 769 at 95°C	5. 3509
Large-Scale Gas Generation Tests						
KC-4-L	421.51	~32	8/5/99	10/6/99	1. 1483	1. 1483
			10/6/99	3/13/00	2. 3788	2. 5271
KC-4-L Dup	378.25	~32	8/5/99	10/6/99	1. 1484	1. 1484
			10/6/99	3/13/00	2. 3788	2. 5271
KC-5-L	439.45	~32	8/5/99	10/6/99	1. 1484	1. 1484
			10/6/99	3/13/00	2. 3788	2. 5272
KC-2/3 P250-L	65.98	~32	10/7/99	10/25/99	1. 454	1. 454
			10/6/99	3/13/00	2. 3332	2. 3786
			3/13/00	4/19/00	3. 885	3. 4671
			4/19/00	6/20/00	4. 1486	4. 6160

(a) Dates of temperature transitions without sampling.

2.1.1 Small-Scale Reaction Vessels

Figure 2.2 illustrates the small-scale reaction vessel and shows where the thermocouples are placed inside and outside the vessel. The reaction vessels are 304 stainless steel cylinders, each internally ~1.75 cm diameter and 14 cm high (internal volume ~33 cm^3). For the gas generation testing, each vessel was wrapped in heating tape and insulated. Two thermocouples were attached to the external body, one for temperature control and one for over-temperature protection. Two thermocouples were inserted through the flange. The thermocouple centered in the lower half of the vessel monitored the temperature of the liquid phase; the one centered in the upper half monitored the gas phase temperature within the reaction vessel. The reaction vessels were placed in a hot cell and connected by a thin (0.0058-cm inside diameter) stainless steel tube to the gas manifold outside the hot cell. A stainless steel filter (60-µm pore size, Nupro) protected the tubing and manifold from contamination. A thermocouple was attached to this filter as well.

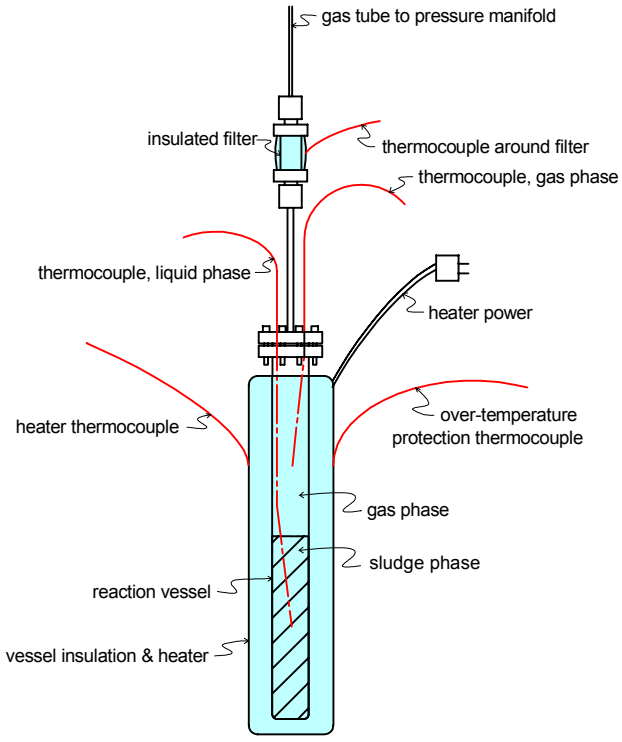

Figure 2.2. Reaction Vessel Used in Small-Scale Gas Generation Tests

2.1.2 Large-Scale Reaction Vessels

Figure 2.3 shows the large-scale reaction vessel and the thermocouple locations. These reaction vessels are 304 stainless steel cylinders with a reaction volume of approximately 800 to 850 ml. For the tests, the vessels were configured similar to the small-scale reaction vessels. Two thermocouples were inserted

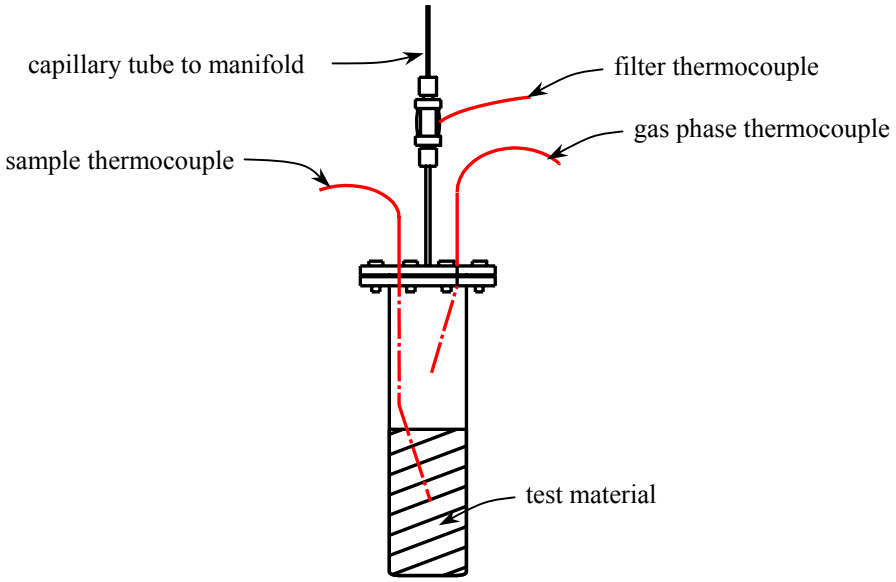

Figure 2.3. Reaction Vessel Used in Large-Scale Gas Generation Tests

through the lid. The thermocouple centered in the lower half of the vessel monitored the temperature of the sample; the one centered in the upper half monitored the gas phase temperature within the vessel. The reaction vessels were placed in a hot cell and connected by a thin tube (0.0058-cm inside diameter) to the gas manifold outside the hot cell. Again, a stainless steel filter (2-μm pore size, Nupro) was added to protect the tubing and manifold from contamination, and a thermocouple was attached to the filter. If the sludge were to have risen in the vessels from a buildup of gas beneath it, as has been observed in KE canister sludge in other studies (Makenas et al. 1997), the filter may have plugged. Consequently, a wedge and a plate (Figure 2.4) were added to the vessel. With this technique, if the sludge had risen in the vessel, the wedge would have created a channel for the gas to escape. If that failed, the plate suspended from the lid would have stopped any sludge migration.

Like the small-scale vessels, the large-scale vessels were equipped with heating tape and two external thermocouples (one for control, and one for over-temperature protection). While the large-scale gas generation tests were conducted at ambient cell temperature, if other temperatures were required, the test temperature could have been elevated.

2.1.3 Volume Determinations of System Components

The total moles of gas in the system were calculated using the Ideal Gas Law from the pressure, temperature, and volume of the parts of the apparatus having different gas phase temperatures: $moles_{total} = moles_{vessel} + moles_{filter} + moles_{manifold\ and\ tubing}$. The manifold and filter volumes were determined from pressure/volume relationships using a calibrated gas manifold system. The manifold volume (the pressure sensor, valves, and miscellaneous fittings) was 3.99 ml; the filter volume was 1.34 ml; and the tubing volume was 1.715 ml (by calculation). The cap stem (the tube from vessel to filter) had a volume of 0.20 ml; half of that was added to the filter volume, giving 1.44 ml, and half was added to the vessel volumes. The volume of each vessel was determined gravimetrically by filling it with water. These volumes are recorded in Table 2.3, along with the mass of settled sludge added to each vessel and the gas

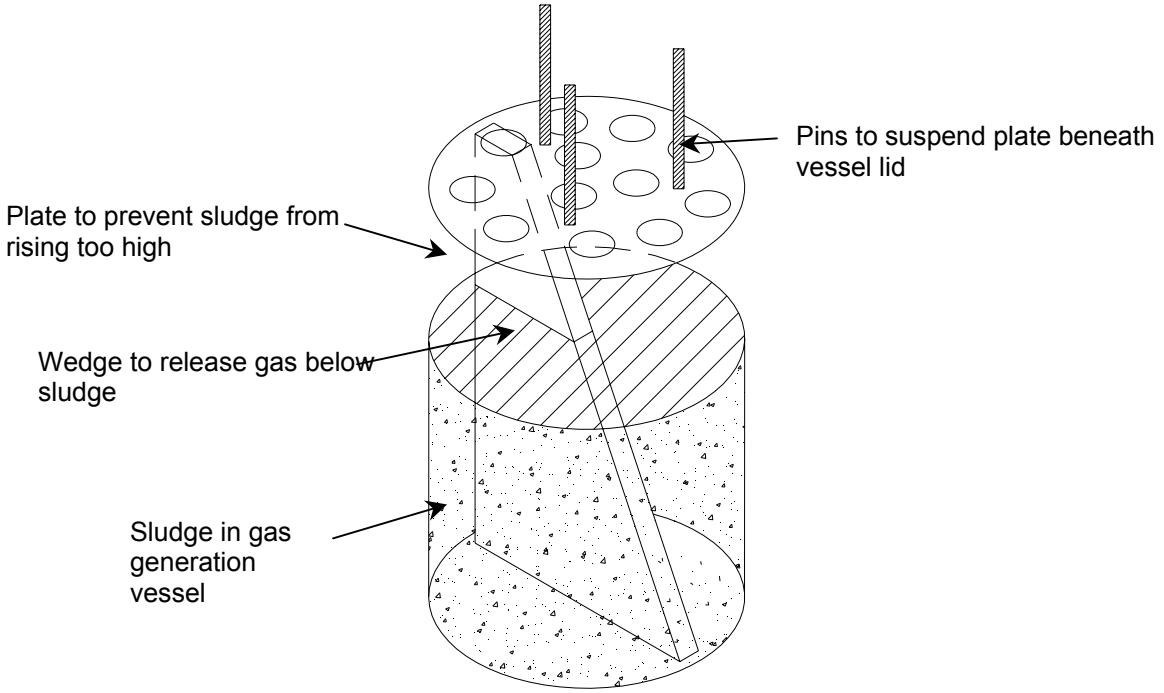

Figure 2.4. Wedge and Plate Added to Large-Scale Gas Generation Vessel to Release Gas Formed Beneath Sludge

Table 2.3. Masses of Settled Sludge and Vessel Volumes Used in Gas Generation Tests

System	**KC-4-L[(a)]**	**KC-4-L[(a)] Dup**	**KC-5-L[(a)]**	**KC-2/3-L[(a)]**	**KC-4 P250**	**KC-4 M250**
Temperature	~32°C	~32°C	~32°C	~32°C	80°C	80°C
Sample mass, g	421.51	378.25	439.45	65.98	7.82	15.14
Vessel volumes						
Gas phase, ml	425.79	455.64	425.1	646.47	18.53	16.50
Total, ml	810.3	809.3	806.9	834.6	32.68	32.83
System	**KC-5 P250**	**KC-5 M250**	**KC-2/3 P250**	**KC-2/3 P250**	**KC-2/3 P250**	**KC-2/3 M250**
Temperature	80°C	80°C	40°C	60°C	80°C	80°C
Sample mass, g	16.23	13.86	23.69	18.66	13.71	17.56
Vessel volumes						
Gas phase, ml	14.29	17.33	14.80	18.61	19.49	18.68
Total, ml	32.69	32.79	32.96	32.71	32.72	32.78

(a) "-L" indicates that test was conducted in a large-scale (850-ml) reactor vessel. All other tests were conducted in 30-ml reactor vessels.

phase volume in the vessel after the sample was added. The reproducibility of the molar gas determination using this manifold system has been established experimentally, and a detailed discussion can be found in Appendix A. The relative standard deviation for quantitative gas phase measurements conducted over a time frame similar to that of the gas generation tests is typically less than 2%.

An atmospheric pressure gauge was attached to the datalogger. The pressure in each system was the sum of atmospheric pressure and the differential pressure between the system internal and external (atmospheric) pressures. An inert cover gas was required to identify product gases and understand the chemical reactions occurring in the settled sludge. Because neon leaks more slowly than helium from the system, it was used as a cover gas. Argon was not used because it served as an indicator of atmospheric contamination. Nitrogen, as will be discussed later, can react with sludge and thus was not a suitable cover gas. The neon was analyzed independently by mass spectrometry and determined to contain no impurities in concentrations significant enough to warrant correction.

2.1.4 System Startup

At the start of each run, each system was purged by at least eight cycles of pressurizing with neon at 45 psi (310 kPa) and venting to the atmosphere. The systems were at atmospheric pressure, about 745 mm Hg (99.3 kPa), when sealed. The sample portion of the manifold was isolated (valves V1 and V2 closed; see Figure 2.1) for the remainder of the run. The vessels then were heated, and the temperature set points were adjusted to keep the material within 1°C of the desired liquid phase temperatures. For the reactions that were heated, the gas phase temperatures were measured to be 5°C to 25°C lower than those of the sample liquid phase.

2.1.5 Gas Sampling and Analysis

As necessary during the testing and at the end of each reaction sequence, the vessels were allowed to cool to ambient temperature and then a sample of the gas was taken for mass spectrometry analysis. Gases in the reaction system were assumed to be well mixed. The metal gas collection bottles were equipped with a valve and had a volume of approximately 75 ml (about four times the gas phase volume of the small-scale gas reaction system). After the bottle was evacuated overnight at high vacuum, it was attached to the gas sample port. Air was removed from the region between valves V2 and V5 (Figure 2.1) using a vacuum pump, then the gas sample was taken. After the collection bottle was removed, the bottle and sample port were surveyed for radioactive contamination. No contamination was found during these experiments. The reaction vessel was purged again with neon after each sampling event and before the next reaction sequence.

The composition of the gas phase of each reaction vessel during gas sampling was analyzed by staff of the PNNL Mass Spectrometry Facility using analytical procedure PNNL-MA-599 ALO-284 Rev. 1. The amount of a specific gas formed during heating is given by the mole percent of each gas multiplied by the total moles of gas present in a system. The measured amount of argon in gas samples is an indicator of how much nitrogen and oxygen from air has leaked into the system (the N_2:Ar ratio in air is 83.6:1; the O_2:Ar ratio is 22.4:1). The nitrogen produced or consumed in the vessel is the total nitrogen minus atmospheric nitrogen. A similar calculation is used to correct for oxygen production or consumption.

2.2 K Basin Sludge Test Material

Between May 7 and 13, 1999, six KE Basin consolidated samples were transferred from the Postirradiation Testing Laboratory (327 Building) to the 325A HLRF. These samples were collected in March and April 1999 by applying a vacuum and drawing sludge into 10.3-L sample containers (stainless steel vessels). Sludge was trapped in the container, while the excess water was returned to the basin through a 5-μm stainless steel filter. With this consolidated sampling technique, much larger volumes of sludge from several different sampling locations were collected in the same sample container. Facility records show that the KE Basin water pH ranged from 5.3 to 5.7 and averaged 5.44 during the sampling period. The temperature ranged from 13ºC to 17ºC. A detailed description of the sampling equipment and the consolidated sludge sampling campaign is provided by Pitner (1999a).

Table 2.4 provides sampling information for the material used in the gas generation testing. In addition to sludge, the balance of the 10.3-L consolidated sample container was filled with K Basin water. Work conducted on these samples is documented in instructions and Battelle Northwest Laboratory Record Book 56479. Additional information concerning chain of custody and sample receipt information can be found in Bredt et al. (1999a).

Table 2.4. Sampling Information for Consolidated Samples Shipped from the 327 Building to the 325A HLRF

Container	Material Type	Sampling Locations	Barrel Type	Barrel Material
KC-2	Canister Sludge from Highly Damaged Fuel	668E & W 2229E 4571E 6071W	Mark 0 Mark 0 Modified Co-Product Mark 0	Aluminum
KC-3	Canister Sludge from Moderately Damaged Fuel	4850W 4869E 3125W 2905E 450E 455W	Mark 0 Mark 0 Mark 0 Mark 0 Mark 0 Mark 0	Aluminum
KC-4[(a)]	Floor Sludge from Between Slotted Canister Barrels Containing Highly Damaged Fuel	0549 4573 5465	Modified Co-Product Modified Co-Product Modified Co-Product	Aluminum
KC-5[(b)]	Floor Sludge from Areas of Deep Sludge Typically Away from Highly Corroded Fuel and Areas with High Concentrations of Ion Exchange Material Beads	4648 3133 0548	Mark II Mark 0 Modified Co-Product	Stainless Steel Aluminum Aluminum

(a) Sample KC-4 was collected from the floor of the basin; however, the sampling locations were near Modified Co-Product barrels.

(b) Sample KC-5 was collected from the basin floor, but barrels were previously in these locations.

The sample containers were inspected upon receipt at 325A HLRF for indications of excessive gas generation during shipment from the 327 Building to the 325 Building. No explicit evidence was found to indicate gas generation occurred in the sludge during the transport.

For the gas generation testing, three sludge samples were used: fuel canister sludge (KC-2/3), floor sludge collected from between canisters with screened bottoms or slotted sides containing highly damaged fuel (KC-4), and floor sludge collected away from fuel canisters and away from areas known to contain high concentrations of organic ion exchange resin (KC-5). The canister sludge used in this testing (KC-2/3) was a composite prepared by combining two consolidated sludge samples (KC-2, containing ~2,200 grams of sludge collected from four different canisters containing highly damaged fuel, and KC-3, containing ~950 grams of sludge collected from six different canisters containing moderately damaged fuel). Therefore, the KC-2/3 composite was 70 wt% sludge from canisters containing severely damaged fuel, and 30 wt% sludge from canisters containing moderately damaged fuel. In comparison, KE canister sludge, on a whole, is projected to be made up as follows: 20 vol% from canisters containing intact fuel, 50 vol% from canisters containing moderately damaged fuel, and 30 vol% from canisters containing severely damaged fuel (Pitner 1999b). The KC-2/3 composite contains a significantly higher fraction of sludge from canisters containing the highly damaged fuel.

Subsamples of KC-4, KC-5, and KC-2/3 were wet-sieved through a Tyler 60-mesh screen (250-μm openings) to separate the P250 and M250 fractions. A portion of sludge was placed on top of the Tyler 60 sieve. The loaded sieve was then raised and lowered repeatedly into a pan filled with supernatant KE Basin water taken from the respective sample container. As the sieve was raised, particles smaller than 250 μm drained into the pan. The solids on the Tyler-60 sieve were immediately transferred to a large vessel filled with clean supernatant to keep the sludge wet at all times. Table 2.5 shows how the initial samples were split based on particle size.

The chemical compositions of the settled-sludge samples are shown in Table 2.6. The weight percent solids were determined by drying aliquots at 104-106°C according to procedure PNL-ALO-504. Dried aliquots of the sludge samples were prepared for analysis by fusion in KNO_3/KOH and subsequent dilution according to analytical procedure PNL-ALO-115. The uranium concentrations were measured by a kinetic phosphorescence technique using procedure PNL-ALO-4014. Elemental concentrations, including uranium, were measured by inductively coupled plasma emission spectroscopy according to the procedure PNL-ALO-211. The radiochemical compositions of the sludges are listed in Table 2.6. The concentrations of ^{60}Co, ^{137}Cs, ^{154}Eu, and ^{241}Am were determined by gamma ray spectrometry (procedure PNL-ALO-450), and the plutonium isotopic concentrations by plutonium extraction (procedure PNL-ALO-417) followed by alpha spectrometry (PNL-ALO-422). Sludge sample pHs were measured in the hot cell using a wand-type pH meter. For each set of measurements, the meter accuracy was verified, and the pH values corrected, based on measurements of calibrated buffer solutions. Measurement accuracy is estimated to be ±0.1-0.2 pH units.

Table 2.5. Particle Distribution of Consolidated Sludge Samples (Bredt et al. 1999)

Sludge Sample	Particle Distribution; Wet Basis, wt%		Particle Distribution; Dry Basis, wt%	
	P250	M250	P250	M250
KC-2/3	22	78	28	72
KC-3	37	63	48	52
KC-4	10	90	16	84
KC-5	36	64	64	36

Table 2.6. Chemical Compositions of Sludge Materials

Concentration, dry basis					
Analyte, wt%	**KC-2/3 P250**	**KC-2/3 M250**	**KC-4**	**KC-4 Dup**	**KC-5**
Al	13.5	1.92	6.87	6.77	15.3
Ca	0.23	0.096	1.04	1.03	0.481
Fe	2.91	1.43	24.1	24.4	16.1
Mg	0.088	0.030	0.311	0.349	0.177
Na	0.301	0.216	0.347	0.372	0.374
Si	1.94	0.29	5.01	4.81	5.46
U	35.4	69.2	18.1	17.6	6.47
U, phos.	35.2	68.3	16.7	16.5	6.36
Analyte, µCi/g					
^{60}Co	0.451	0.452	1.07	1.10	1.10
^{137}Cs	2040	414	1660	1690	1320
^{154}Eu	6.32	9.10	2.62	2.57	1.11
^{241}Am	75.5	99.4	29.4	29.1	13.1
^{238}Pu	13.0	17.4	4.53	5.28	1.99
^{239,240}Pu	90.3	123	39.3	39.1	13.1
Concentration, wet basis					
Analyte, wt%	**KC-2/3 P250**	**KC-2/3 M250**	**KC-4**	**KC-4 Dup**	**KC-5**
Al	6.90	1.13	2.22	2.17	5.36
Ca	0.118	0.057	0.336	0.330	0.168
Fe	1.49	0.842	7.78	7.81	5.64
Mg	0.045	0.018	0.100	0.112	0.062
Na	0.154	0.127	0.112	0.119	0.131
Si	0.99	0.17	1.62	1.54	1.91
U	18.1	40.8	5.85	5.63	2.26
U, phos.	18.0	40.2	5.39	5.28	2.23
Solids	51.1	58.9	32.3	32.0	35.0
Analyte, µCi/g					
^{60}Co	0.230	0.266	0.346	0.352	0.385
^{137}Cs	1042	244	536	541	462
^{154}Eu	3.23	5.36	0.846	0.822	0.389
^{241}Am	38.6	58.5	9.50	9.31	4.59
^{238}Pu	6.64	10.2	1.46	1.69	0.697
^{239,240}Pu	46.1	72.4	12.7	12.5	4.59

The crystalline phases present in the KC-2/3 P250 and KC-5 P250 sludges were determined by X-ray diffractometry (XRD) according to procedure PNNL-RPG-268. For each sludge, XRD was performed on samples that both had and had not undergone 80-95°C heating in the small-scale testing. Results of the XRD analyses are given in Table 2.7. The relative XRD peak intensities of the heated and unheated materials were compared to identify the in-growth and disappearance of phases. Three $Al(OH)_3$ phases (gibbsite, bayerite, and nordstrandite) were found in all samples, but boehmite (AlOOH), formed by the dehydration of the $Al(OH)_3$, was found only in the heated samples. Uraninite ($UO_{2.25}$) was found only in the uranium-rich KC-2/3 P250 samples but was the most prominent phase; goethite (FeOOH) was only present in the KC-5 samples. The uranium oxidation product schoepite (described as $UO_3 \cdot 2H_2O$ in the Powder Diffraction File, PDF) was found in all samples except the heated KC-2/3 P250 material. Becquerelite [$Ca(UO_2)_6O_4(OH)_6 \cdot 8H_2O$] was found conclusively in the KC-5 P250 samples only and was prominent in the heated material. Though found in other K Basin sludges (Makenas et al. 1996), no calcite ($CaCO_3$) was found in any of the four test samples. The only Hanford soil mineral found was the quartz (SiO_2) present in the unheated KC-5 P250 material.

Table 2.7. Crystalline Phases Identified by X-ray Diffractometry in Selected KE Basin Sludges With and Without Heating During Small-Scale Testing

Crystalline Phase Name and Formula	PDF #	Prominence in Sludge[(a)]			
		KC-2/3 P250		KC-5 P250	
		Not Heated	Heated	Not Heated	Heated
Uraninite, $UO_{2.25}$	20-1344	H	H	N	N
Schoepite, $UO_3 \cdot 2H_2O$	29-1376	M	N	L-	L
Becquerelite, $Ca(UO_2)_6O_4(OH)_6 \cdot 8H_2O$	29-389	?	N	L-	M
Gibbsite, $Al(OH)_3$	33-18	M	M	M	M
Bayerite, $Al(OH)_3$	20-11	M	M	M	H
Nordstrandite, $Al(OH)_3$	24-6	L	L	L	L
Boehmite, AlOOH	5-190	N	M	N	M
Goethite, FeOOH	29-713	N	N	M	M
Quartz, SiO_2	46-1045	N	N	H	N

(a) H – high; M – medium; L – low; N – not observed; ? – possible.

3.0 Gas Generation from K Basin Samples

In each gas generation test, gas-tight reaction vessels were loaded with selected KE Basin materials, the gas space purged with neon, and the loaded vessels heated to the selected temperature. Gas samples were taken from the vessels periodically and at the end of each run sequence in accordance with the test plan. After each gas sample was taken, the vessel was purged to remove previously generated gases before testing resumed. Gas generation rates were determined for each gas sample based on the heating time, the gas composition, the total gas quantity in the system from which the sample was taken, and from the sludge mass present in each reaction vessel.

Section 3.1 presents the results from the variable temperature study (40°C to 95°C) of the KC-2/3 P250 canister composite sludge. Section 3.2 contains the gas generation results at 80°C for the P250 and M250 fractions of samples KC-5 and KC-4, and the M250 fraction of sample KC-2/3. Results of the large-scale, ambient temperature gas generation studies of KC-4 (in duplicate), KC-5, and KC-2/3 P250 are presented in Section 3.3.

3.1 Gas Generation Results (Small-Scale) from KC-2/3 P250 Canister Composite Sludge at 40°C, 60°C, 80°C, and 95°C

This section presents the gas generation and pH data from tests of KC-2/3 P250 sludge heated at 40°C, 60°C, and 80°C. In each of these tests, near the end of the run, the temperature in the reaction vessels was increased to 95°C. This final heating step was undertaken to force the reactions to completion and to derive the quantity of uranium metal present in the initial sludge. The total amounts of gas produced (i.e., H_2, CO_2, CH_4, etc.) versus heating time are plotted in Figure 3.1. The gas generation rates increase with increasing temperature. An induction period is observed before onset of gas generation in all tests. This induction period prior to gas generation has been observed in the corrosion of uranium in aerated waters (Montenyohl 1960). The induction time encompasses the period in which the protective uranium oxide (UO_2) layer is lost and an initial uranium hydride layer (required for evolution of hydrogen gas by the reaction of uranium with water in anoxic media) is created.

The induction times for the 40ºC, 60ºC, and 80ºC tests are ~1340, 205, and 26.9 hours, respectively. These times were taken to be the points of intersection of the low initial rates and the linear regions of the high gas generation rates. Note in Figure 3.1 that agitation of the 80ºC test had no effect on gas generation, either in inducing a step-increase in gas release, or in instigating an enhanced reaction rate (caused, for example, by exposing fresh surfaces to reaction).

Once the hydride layer is established, a linear gas generation rate is observed at intermediate times. For the 80°C system, the gas generation rate is constant from ~80 to 120 hours; for the 60°C system, the gas generation rate is constant from ~350 to ~700 hours. The linear regions correspond to the periods between the first and second gas samplings for 60ºC and 80ºC tests (about 10-30% of full reaction; see Figure 3.1). The linear region occurs around 1900-3000 hours of reaction time for the 40ºC test.

Figure 3.1 shows that little further reaction occurred at 95°C for the test started at 80°C and that about 5% additional gas was generated in the test begun at 60°C. The gas generating reactions in the 40°C test had proceeded only to about 40% completion when the temperature was increased to 95°C. Therefore, another period of linear gas generation rate could be ascertained for the initial few hours of reaction at

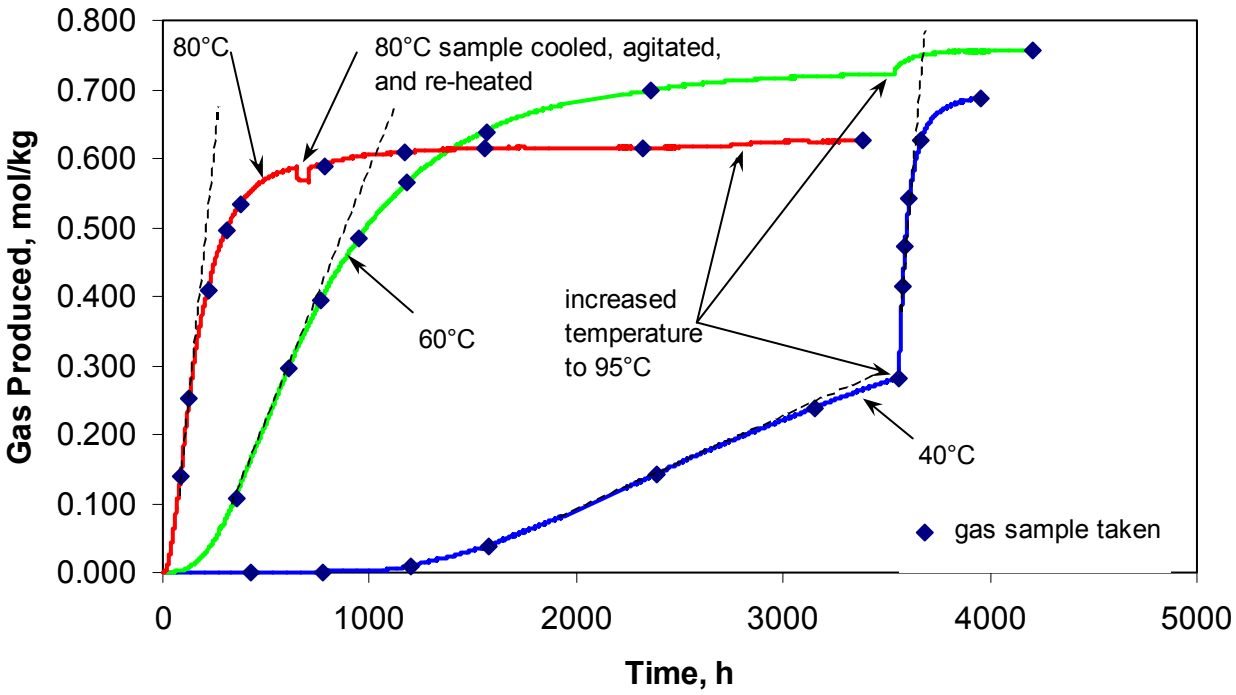

Figure 3.1. Total Gas Generation from KC-2/3 P250 Material in Small-Scale Reaction Vessels at 40°C, 60°C, and 80°C and Completed at 95°C (dashed lines indicate rates at linear gas generation)

95°C in the test begun at 40°C. It is seen that at completion, the three tests produced from 0.62 to 0.75 moles of gas per kilogram of settled KC-2/3 P250 sludge.

The gas sample compositions from the 40°C, 60°C, and 80°C tests are given in Tables B.1, B.2, and B.3 (Appendix B), respectively. Gas samples were analyzed by mass spectrometry. The compositions of the generated gases, derived from the compositions of sampled gas by excluding the neon cover gas, argon, and trace nitrogen and oxygen from atmospheric contamination, also are presented and are indicated by shading. For example, if analysis found 80% neon, 5% carbon dioxide, and 15% hydrogen, the composition of gas formed by excluding neon would be 25% CO_2 and 75% H_2. The uncertainties in all the entries in these tables are approximately plus or minus 1 in the last digit.

The presence of argon indicates atmospheric contamination, because it is not present in the cover gas and is not produced by the sludge. Nitrogen could have been generated or consumed by the sludge or could have come from atmospheric contamination. The percent nitrogen actually generated or consumed is given by the percent nitrogen found minus 83.6 times the percent argon in the sample (the ratio of nitrogen to argon in dry air is 83.6). The percent oxygen actually generated or consumed in the samples may be calculated in a method similar to nitrogen. The sum of all percents for a run in Tables B.1, B.2, and B.3 may not be exactly 100%, because the values were rounded.

Individual gas generation rates may be calculated based on the total moles of gas produced (Figure 3.1) and the generated gas compositions (Tables B.1, B.2, and B.3). Tables B.4, B.5, and B.6 show the gas generation rates derived in this manner for KC-2/3 P250 sludge in the 40°C, 60°C, and 80°C tests.

The KE Basin water pH ranged from 5.3 to 5.7 when the sludge samples were retrieved in March and April 1999 (Section 2.2). The pHs of the sludge samples then were measured after storage and testing in the hot cell. The pH of a sample of KC-2/3 P250 slurry that had not undergone testing in the small-scale vessels was measured in May 2000 after ~13 months at hot cell temperature (~32°C). The pH was 5.4, virtually unchanged from that of the initial KE Basin water. The pHs of the KC-2/3 P250 small-scale test materials were measured July 20-27, 2000, about 3 months after completion of the final 95°C heating but while the vessels remained closed and not exposed to air. The pHs for the 40°C, 60°C, and 80°C test slurries were 6.4, 5.4, and 5.1, respectively. The pHs decreased to 4.4, 5.0, and 4.1, respectively, when re-measured on August 30, 2000, about 5 weeks after the test vessels had been opened and the slurries exposed to air. The pH data for the KC-2/3 materials are summarized with pH data for other small-scale test materials in Table 3.1 (see Section 3.2).

3.2 Gas Generation Results (Small-Scale) for the KE Floor Sludge Samples (P250 and M250 from KC-4 and KC-5) and the M250 Canister Sludge Sample (KC-2/3)

This section contains gas generation and pH data from the tests with the M250 samples of KC-4, KC-5, and KC-2/3 and the P250 samples of KC-4 and KC-5 in small-scale reaction vessels. In these tests, power to the heaters was terminated after 97 days at 80°C. The vessels remained sealed and at ambient hot cell temperature (~32°C) for 87 days, and negligible gas generation was observed. The vessels then were heated to 95°C for 32 days to force the completion of the reactions. Data on the total amount of gas produced versus heating time measured for the P250 samples (KC-4 and KC-5) are shown in Figure 3.2. The M250 material (KC-4, KC-5, and KC2/3) total gas generated data are shown in Figure 3.3. Unlike the KC-2/3 P250 material discussed in Section 3.1, no induction period to gas generation was observed.

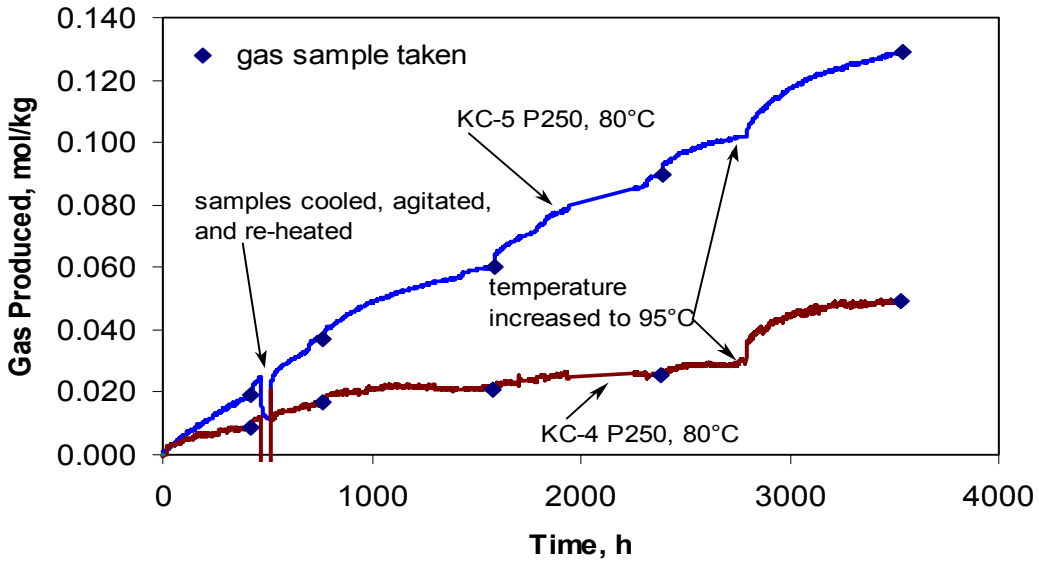

Figure 3.2. Total Gas Generation from KC-4 P250 and KC-5 P250 at 80°C, Left at ~32°C for 87 Days (time not plotted) and Completed at 95°C (small-scale tests)

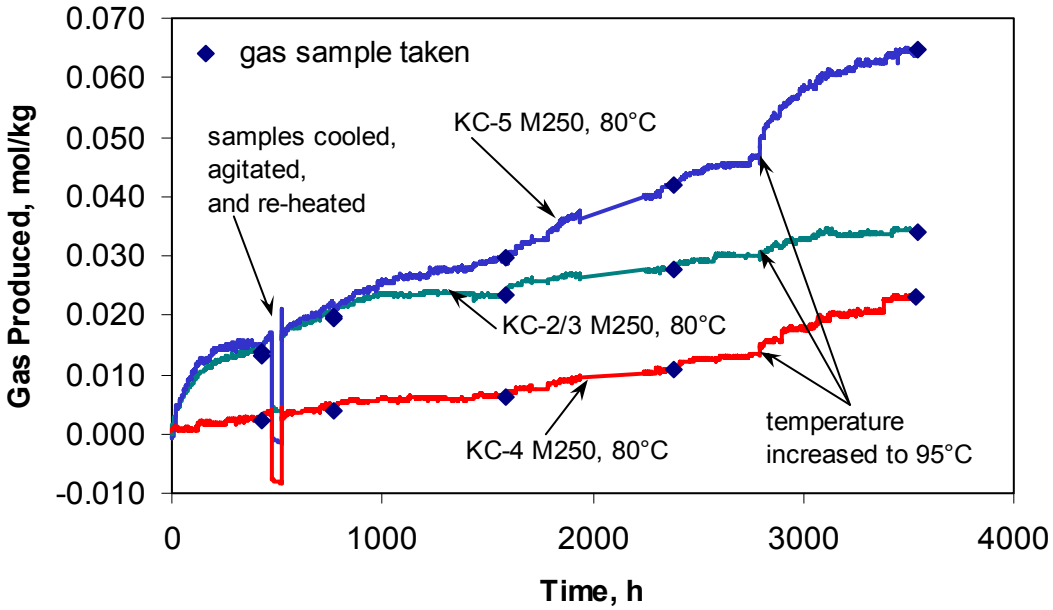

Figure 3.3. Total Gas Generation from KC-4 M250, KC-5 M250, and KC-2/3 M250 at 80°C, Left at ~32°C for 87 Days (time not plotted) and Completed at 95°C (small-scale tests)

Gas samples were analyzed by mass spectrometry; their compositions are given in Tables B.7 through B.11. Of more interest are the generated gas compositions presented in shading below each entry. Argon again was used to indicate atmospheric contamination and as a basis to correct for nitrogen and oxygen consumed or generated by the sludge reactions (see Section 3.1). The sum of all percents in Tables B.7 through B.11 for a gas sample may not be exactly 100%, because again the values were rounded.

The individual gas generation rates are calculated based on the total moles of gas produced (Figures 3.2 and 3.3) and the gas compositions (Tables B.7 through B.11). Tables B.12 through B.16 display the gas generation rates for M250 samples of KC-4, KC-5, and KC-2/3 material and the P250 samples of KC-4 and KC-5 material at 80°C, respectively. The gas generation rates at 80°C for these samples are 30 to 100 times lower than that of the KC-2/3 P250 sample, reacted at 80°C, discussed in Section 3.1. The rate of CO_2 production also is lower but only by about a factor of 10. As a result, the proportion of CO_2 in the product gas is much higher.

The samples cooled from 80°C were agitated with a high-energy vibrator ~500 hours into the reaction, and reheated (see Figures 3.2 and 3.3). Gas generation rates increased immediately after the agitation; similar increases also were observed after most of the gas sampling events. Although the magnitudes of the gas generation changes were small, the reason for the increase in gas generation by these perturbations is not known and may simply be due to absorption of CO_2 at the lower temperature and its release upon agitation and heating (see Section 4.3).

The pHs of samples of the KC-2/3 M250 and the non-sieved KC-4 and KC-5 materials were measured in May 2000, ~13 months after sampling and being stored at hot cell temperature. The pHs of samples of the small-scale test materials derived from these sludges (KC-2/3 M250, and the M250 and P250 fractions of KC-4 and KC-5) were measured immediately after opening the small-scale test vessels. These measurements, taken July 20-27, 2000, were about 2 months after completion of the reactions at 95°C. The small-scale test samples then were re-measured on August 30, 2000, after 5 weeks of exposure

to the hot cell atmosphere. The pH values found for all the small-scale test materials, including the KC-2/3 P250 small-scale test materials, at the various sampling and measurement times, are shown in Table 3.1.

Table 3.1 KE Basin Sludge pH for Materials Used in the Small-Scale Tests

Sludge and Small-Scale Test Temperature[a]	Sludge Sample pH		
	In Hot Cell 13 Months After Sampling[b]	Upon Opening the Reactor	Five Weeks After Opening the Reactor
KC-2/3 M250, 80°C	5.0	6.7	5.2
KC-2/3 P250, 40°C	5.4	6.4	4.4
KC-2/3 P250, 60°C		5.4	5.0
KC-2/3 P250, 80°C		5.1	4.1
KC-4 M250, 80°C	7.8[c]	6.7	7.4
KC-4 P250, 80°C		7.0	7.3
KC-5 M250, 80°C	7.2[c]	6.7	6.2
KC-5 P250, 80°C		6.7	6.6

(a) Heating in all tests completed at 95°C.
(b) KE Basin pH at the time of sampling ranged from 5.3 to 5.7 and was 5.44 on average.
(c) pH values for the respective unsieved KC-4 and KC-5 materials.

It is seen that the pHs of the KC-2/3 materials stored in the hot cell were similar to those of the KE Basin waters at the time of sampling. The KC-2/3 pHs were near the starting values or had increased when measured immediately after opening the small-scale test vessels. The pHs decreased significantly, however, after 5 weeks of exposure to air to be near or below the initial pHs of the KC-2/3 sludges. In contrast, after the 13-month storage in the hot cell, the KC-4 and KC-5 pHs rose to about 2 units above the KE Basin pH. The pHs of the KC-4 and KC-5 sludges then decreased as much as 1 pH unit after 80°C/95°C heating and subsequent air exposure.

3.3 Gas Generation Results from KC-4, KC-4 Dup, KC-5, and KC-2/3 P250 Large-Scale Samples at Hot Cell Temperature

Thermal gas generation and pH data measured from large-scale tests of KC-4 (in duplicate), KC-5, and KC-2/3 P250 sludge at hot cell temperature are presented here. The total amounts of gas produced versus reaction time were measured for each large-scale test, and the results are shown in Figure 3.4. To obtain rates for each gas present, gas samples were analyzed by mass spectroscopy. The mole percent composition of the gases sampled in these systems is given in Tables B.17 through B.20, respectively. The compositions of generated gas are presented (in shaded areas) below the entry for each run.

The generation rates of individual gases are calculated based on the total moles of gas produced and the composition of the gas generated (Tables B.17 through B.20). Tables B.21 through B.24 present the gas generation rates for KC-4, KC-4 Dup, KC-5, and KC-2/3 P250 large-scale tests, respectively.

The gas generation rates for these samples are ~35 to 2500 times lower than the rate found for the KC-2/3 P250 composite sample at 40°C discussed in Section 3.1. The KC-2/3 P250 test has run for about 1 year and is continuing; the remaining tests were terminated after 220 days.

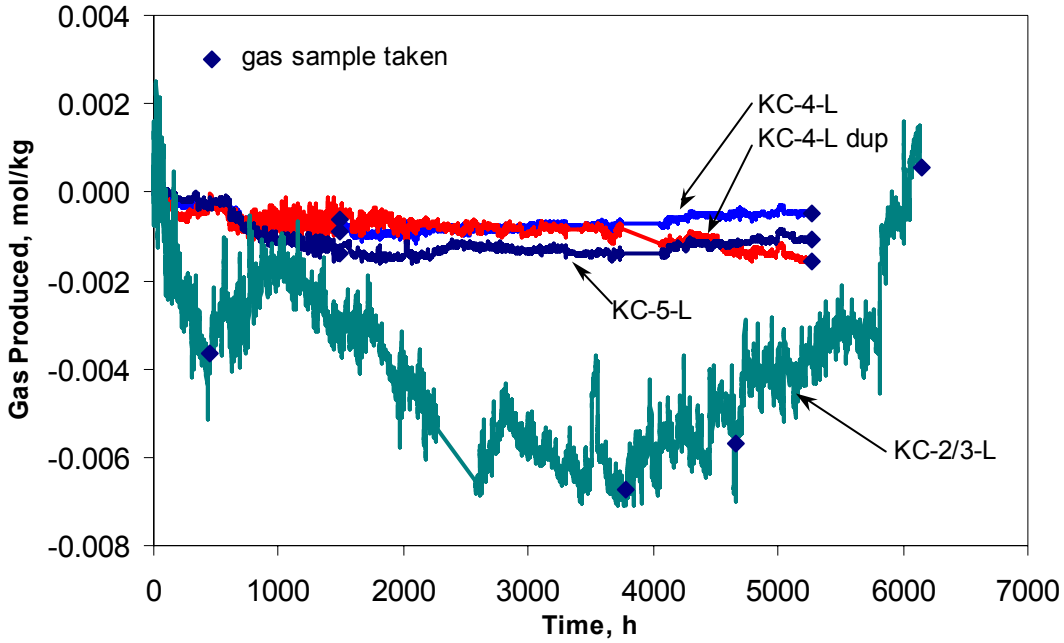

Figure 3.4. Total Gas Generation from KC-2/3-L, KC-4-L, KC-4-L Dup, and KC-5-L at ~32°C (large-scale tests)

As might be expected, the changes in pH in the large-scale tests performed at hot cell temperature were less than those experienced by the small-scale tests completed at 95°C. The pHs of the KC-4 and KC-5 materials confined in the large-scale tests were unchanged or decreased a few tenths of a pH unit after almost 11 months (Table 3.2). The pH of the KC-2/3 P250 large-scale test sludge has not been measured because the test is still underway.

Table 3.2. KE Basin Sludge pH for Materials Used in the Large-Scale Tests

Sludge	Sludge Sample pH		
	In Hot Cell 13 Months After Sampling[(a)]	Upon Opening the Reactor	Five Weeks After Opening the Reactor
KC-2/3 P250	5.4	Reactor still closed	
KC-4	7.8	7.5	7.8
KC-4 Dup		6.9	7.5
KC-5	7.2	7.0	6.9

(a) KE Basin pH at the time of sampling ranged from 5.3 to 5.7 and was 5.44 on average.

4.0 Results and Discussion of Gas Generation from KE Basin Sludge

The evaluation of results from the gas generation tests performed at various temperatures on samples KC-2/3, KC-4, and KC-5 is presented in this section. Section 4.1 describes the chemical reactions postulated to be responsible for the observed gas generation and consumption phenomena. Section 4.2 examines in more detail the observations found for the KC-2/3 P250 small-scale tests. The results of the other small-scale tests conducted at 80ºC and completed at 95ºC for samples KC-4 P250, KC-5 P250, KC-4 M250, KC-5 M250, and KC-2/3 M250 are examined in Section 4.3. Section 4.4 discusses the results from the large-scale tests. Gas generation results from KE canister samples collected in 1996 are included as Section 4.5 for comparison. An evaluation of the surface area and initial size of the uranium metal particles in KC-2/3 P250 material, using gas generation data, is given in Section 4.6. The kinetics of carbon dioxide evolution in the small-scale tests (not including KC-2/3 P250) is evaluated in Section 4.7. An evaluation of radiolysis as a potential source of hydrogen production from the sludge is provided in Appendix C. Appendix D presents mathematical derivations of the dependencies of surface-area-dependent corrosion rates on particle shapes.

While the best available gas generation rate and compositional data were collected for this study, factors beyond the bounds of the testing (listed below) may have affected the absolute gas generation rates for the K Basin sludge. Additional factors may be identified in the future.

- A portion of the uranium metal originally present in the sludge may have reacted before the gas generation tests were initiated. That is, sludge handling during retrieval, sample recovery, sample sieving, and gas vessel loading may have exposed fresh uranium metal surfaces to air and initiated subsequent uranium metal oxidation. The sludge samples also were held at temperatures (~32ºC) significantly greater than those of the KE Basin (~13ºC to 17ºC) for several months before testing commenced. This storage may have altered the original composition and reactivity of the sludge.

- Potential reactions occurring in the test vessels may be more complex than those described in the next section. For example, some technical studies would suggest that 2% to 9% of the uranium metal reacted could convert to uranium hydride.

4.1 Gas Generating (and Gas Consuming) Reactions

The hydrogen (H_2), isotopes of the fission product gases krypton (Kr) and xenon (Xe), methane (CH_4) and higher hydrocarbons, and carbon dioxide (CO_2) produced in the current tests were also observed in the 1996 gas collection tests associated with KE canister sludge (Makenas et al. 1997; see Section 4.5 of this report). Furthermore, in nearly all cases, oxygen (O_2) and nitrogen (N_2) from the atmosphere were consumed. The absolute and relative rates of the appearance and disappearance of these gases give evidence of the underlying chemical reactions thought to be occurring in the sludge. These reactions affect the behavior of the sludge in retrieval, transport, and storage conditions.

4.1.1 Uranium Corrosion and the Roles of Hydrogen, Oxygen, and Nitrogen

The oxidation of metallic uranium under conditions relevant to K Basin sludge occurs by several reactions. The reactions involve the production and depletion of gases.

$$U + 2\ H_2O \rightarrow UO_2 + 2\ H_2 \quad (1)$$

$$U + O_2 \rightarrow UO_2 \quad (2)$$

$$U + 0.875\ N_2 \rightarrow UN_{1.75} \quad (3)$$

In aerated waters (such as those present in the KE Basin), uranium metal corrosion occurs largely by Reactions 2 (Montenyohl 1960) and 3.[(a)] However, if the system becomes isolated from the atmosphere (as is the case for the sealed test vessels), the direct reaction of uranium with water is dominant and hydrogen gas is evolved (Reaction 1). Significantly, though both Reactions 1 and 2 occur in water to produce UO_2, the rate of Reaction 2 (in the presence of dissolved oxygen) is about 30 times slower than that of the anoxic Reaction 1 (Johnson et al. 1994). In other words, dissolved oxygen inhibits uranium metal corrosion in water.

Hydrogen accelerates the corrosion of uranium metal in water through the formation of the poorly adherent intermediate corrosion product, uranium hydride, UH_3 (Montenyohl 1960). Indeed, UH_3 has been observed by XRD in a sludge sample taken from one of the closed canisters from the KW Basin (Makenas et al. 1998). The UH_3 intermediate is unstable in water, forming UO_2 and hydrogen atoms; the hydrogen atoms then may combine to form H_2 gas. Alternatively, the hydrogen radicals (and the H_2), especially if occluded, can interact with the underlying bulk uranium metal to form more UH_3 and continue the corrosion cycle.

Evidence for the transition from corrosion in the presence of oxygen and nitrogen (Reactions 2 and 3) to corrosion by water mediated by hydride formation (Reaction 1) is found in data from the KC-2/3 P250 test conducted at 60ºC (see Figure 3.1 and Table B.5). During the initial ~100 hours of the 60ºC test, essentially zero net gas is produced (Figure 3.1). This reflects the offsetting consumption of O_2 and N_2, generation of H_2, and likely uptake of some portion of the generated H_2 by uranium metal. Data for the first sampling (335 hours) of the 60ºC test in Table B.5 show that the H_2 produced is about six times the total amount of O_2 and N_2 consumed. By the time of the second sampling (612 hours), this factor is over 1000, and corrosion is occurring overwhelmingly by Reaction 1.

The UH_3-mediated corrosion mechanism is established during this induction time. Evidence for hydrogen uptake into the corroding metal is found in the lower observed ratios of H_2 to other gases formed during uranium metal corrosion (e.g., hydrocarbons, Kr, Xe) at the beginning of the KC-2/3 P250 tests compared with the higher ratios found later (see Section 4.2.2). The early H_2 shortfall evidently is a result of hydride formation during the induction time.

4.1.2 Release of Fission Product Gases

The existence of the Kr and Xe fission products in the generated gases gives qualitative evidence of the corrosion of irradiated uranium metal. This assertion is based on two reasonable suppositions: 1) that until corrosion occurs, the fission gases remain trapped within the uranium metal matrix and 2) that the metal corrosion products (UO_2, UH_3) cannot react with, and thus retain (except through physical

(a) No explicit mention of the reaction of uranium metal with N_2 in aqueous systems was found in the technical literature. The postulated Reaction 3 is based on the observed depletion of N_2 from the gas phase in the present tests and the observation of a non-stoichiometric $UN_{1.75}$ product from reaction of uranium metal with N_2 at 200-300ºC (Cordfunke 1969).

entrapment), the inert Kr and Xe gases. According to burn-up calculations by the ORIGEN code, the Kr and Xe concentrations in irradiated N Reactor metal fuel increase almost linearly with exposure (Figure 4.1), whereas their isotopic ratios and the total Kr/total Xe ratios remain relatively unaffected by exposure (Table 4.1). Thus, with knowledge of burn-up and measurements of Kr and Xe quantities released by uranium metal corrosion, the quantity of uranium metal can be calculated. Conversely, with knowledge of uranium metal quantity, the burn-up can be calculated by measuring Kr and Xe quantities released by the corroding metal. Equations for both types of calculations are given in Figure 4.1.

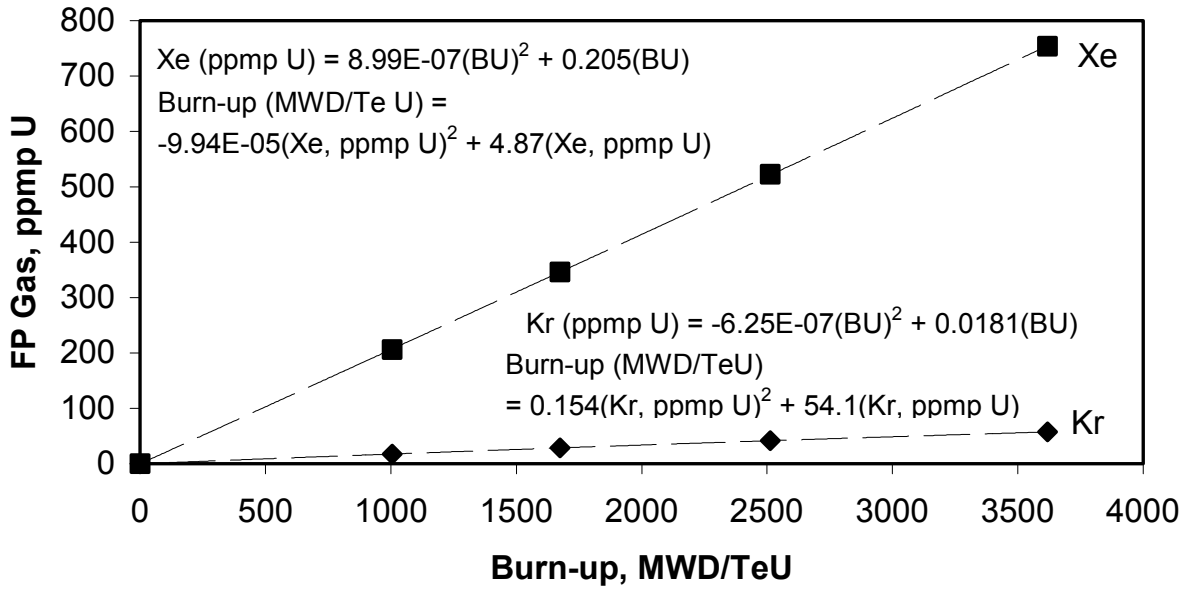

Figure 4.1. Growth of Kr and Xe Gas Concentration with Irradiation Exposure (ORIGEN)

Table 4.1. Fission Product Gas Isotopic and Elemental Ratios Based on ORIGEN

Isotope	Isotope Distribution, in %, Discharge at Various Irradiation Exposures			
	1005 MWD/TeU	1675 MWD/TeU	2519 MWD/TeU	3619 MWD/TeU
^{83}Kr	13.76	13.61	13.43	13.18
^{84}Kr	27.12	27.44	27.81	28.31
^{85}Kr(a)	6.91	6.89	6.84	6.78
^{86}Kr	52.19	52.03	51.87	51.73
ΣKr, g/TeU	17.7	28.6	41.6	57.5
^{130}Xe	0.01	0.02	0.04	0.05
^{131}Xe	10.94	10.92	10.77	10.53
^{132}Xe	16.86	17.14	17.47	17.89
^{134}Xe	28.72	28.48	28.29	28.08
^{136}Xe	43.47	43.43	43.43	43.43
ΣXe, g/TeU	206	346	523	754
ΣXe/ΣKr	11.6	12.1	12.6	13.1

(a) $t_{½}$ = 10.76 years.

In practice, applying this technique to determine uranium metal quantities in a sludge sample is imprecise for at least two reasons. First, the sludge can be generated by a number of different fuel elements, each of which may have suffered different exposure. At best, a uranium metal concentration based on an "average" irradiation exposure of the collected metallic fuel particles is obtained. Second, the irradiation exposure within any given fuel element differs spatially according to its radial location (e.g., near the cladding versus deep within the fuel element). Uranium metal sloughed by corrosion and radiation embrittlement from near the cladding (and water and graphite moderators) will have experienced higher thermal neutron flux and thus higher exposure.

4.1.3 Creation and Release of Hydrocarbons

Methane, ethane, and higher hydrocarbons, as well as hydrogen, arise from the reaction of water with carbide carbon in the uranium metal fuel. The carbon content nominally ranges from 365 to 735 ppm in the metallic uranium fuels stored in the K Basins (Weakley 1979). At these low carbon concentrations in the uranium-carbon system, the expected disposition of carbon is as the compound UC (uranium monocarbide) dispersed within metallic uranium (Wilkinson 1962). Uranium carbide inclusions, which appear as rectangles or parallelograms about 20 μm on a side, are observed and photomicrographed in irradiated N Reactor fuel (Marschman et al. 1997).

Hydrogen, methane, ethane, propane, butane, pentane, and hexane have been observed in the reaction of uranium metal-monocarbide mixtures with water at 80ºC. Carbon concentrations were 19,900 to 50,400 ppm parts uranium, equivalent to U:C mole ratios of 1:0.39 to 1:1 (Bradley and Ferris 1962, 1964).[(a)] In these prior studies, the fractions of the higher hydrocarbons decreased with increase in carbon concentration, and all carbon reported to the gas phase as hydrocarbons. A summary of the gas product distributions observed for the Bradley and Ferris (1962, 1964) tests is given in Table 4.2, and is compared with the total H_2 and hydrocarbon gases found at the end of the KC-2/3 P250 80ºC test.

Table 4.2. Gas Product Distributions Observed for Reactions of UC and UC/U Mixtures at 80ºC

[C], ppm parts U	Refs.[(a)]	Gas Composition, vol%				C Present as CH_4, Atom Fraction
		H_2	CH_4	C_2H_6	Higher Hydrocarbons	
50400 (pure UC)	1	11.1	86.0	1.84	1.05	0.921
49200	2	13	84	1.76	0.99	0.921
41800	1	36.3	59.9	1.95	1.72	0.855
41800	2	37	60	1.78	1.26	0.926
19900	2	79	18	1.14	1.25	0.712
Nominally 550	KC-2/3 P250, 80ºC	99.219	0.615	0.088	0.078	0.591

(a) 1 - Bradley and Ferris (1962); 2 - Bradley and Ferris (1964).

Because the carbon content of the N Reactor uranium metal fuel averages only 550 ppm, the statistical likelihood of carbon radicals combining to form ethane might be expected to be lower than observed for materials with carbon concentrations of 19,900 to 50,400 ppm parts uranium. The atom fraction of carbon present as methane thus would be higher than found in the earlier tests. This is not the case, however, and methane consistently represents about 59 atom% of the gaseous hydrocarbon carbon in the present 80°C tests (see data in Section 4.2.3). The start of this trend of decreasing atom fraction methane

(a) Tests performed at higher carbon concentrations; i.e., UC with $UC_{1.85\pm0.03}$ or pure $UC_{1.85\pm0.03}$; left wax and graphite residues (Bradley and Ferris 1962, 1964).

with decreasing carbon concentration is shown in Bradley and Ferris (1962, 1964). The carbon present as methane decreases from about 92 atom% at ~40,000-50,000 ppm to about 71 atom% at ~20,000 ppm.

For the KC-2/3 P250 80°C test, Reaction 4 rationalizes the observed hydrocarbon product distribution that arises when the UC contained in the fuel reacts with water:

$$UC + 2\ H_2O \rightarrow UO_2 + 0.591\ CH_4 + 0.085\ C_2H_6 + 0.060\ C_3H_8 + 0.015\ C_4H_{10} + 0.248\ H_2 \quad (4)$$

The C_3 and higher hydrocarbons could not be discriminated by mass spectrometry in the present tests. They were projected to be $C_{3.2}H_{8.4}$ on average, based on the observations of Bradley and Ferris (1962, 1964), and are represented in Reaction 4 by propane and butane in that proportion. The projected 0.248 moles of hydrogen arising per mole of UC is a significant contributor to the total gas generated from UC reaction with H_2O. However, this quantity is a negligible (~0.14%) addition to the hydrogen generated by reaction of uranium metal with water (Reaction 1) in nominal 550 ppm carbon fuel, as shown in Table 4.2.

4.1.4 Carbon Dioxide Generation

Significant quantities of CO_2 were found in gases generated during all large- and small-scale gas generation tests. One possible explanation for evolution of CO_2 in all tests is the reaction in water of schoepite, $(UO_2)_8O_2(OH)_{12}(H_2O)_{12}$ (or $4UO_3 \cdot 9H_2O$), with calcite, $CaCO_3$, to form the more stable uranium phase, becquerelite, $Ca(UO_2)_6O_4(OH)_6(H_2O)_8$ (or $CaU_6O_{19} \cdot 11H_2O$) and carbonic acid (H_2CO_3):

$$3\ (UO_2)_8O_2(OH)_{12}(H_2O)_{12} + 4\ CaCO_3 \rightarrow 4\ Ca(UO_2)_6O_4(OH)_6(H_2O)_8 + 4\ H_2CO_3 + 6\ H_2O$$
$$\rightarrow 4\ Ca(UO_2)_6O_4(OH)_6(H_2O)_8 + 10\ H_2O + 4\ CO_2\uparrow \quad (5)$$

Calcite and a calcium uranium oxide hydrate, $CaU_6O_{19} \cdot 12H_2O$, have been observed by XRD in floor sludge from the KE Basin (Makenas et al. 1996); schoepite and metaschoepite [$(UO_2)_8O_2(OH)_{12}(H_2O)_{10}$] have been found in canister sludge from the KE Basin (Makenas et al. 1997).

Becquerelite is the thermodynamically stable uranium solid phase for uranium(VI)-bearing ground waters in equilibrium with calcite and atmospheric carbon dioxide ($10^{-3.5}$ atm), and schoepite forms becquerelite under those conditions (Finch 1997; Finch and Murakami 1999). The transformation of schoepite to becquerelite has been attributed to a charge-balanced exchange reaction of calcium ions from solution with interlayer hydronium ions within the layered schoepite structure. The hydronium ions released by this exchange report to solution and lower the pH (Finch and Ewing 1991).

Laboratory tests in 25ºC 1 M $CaCl_2$ solution show schoepite converts to becquerelite within 3 months, although the reaction requires an additional 6 months to reach equilibrium according to pH and uranium concentration data (Sandino et al. 1994). In related tests run at 60ºC, schoepite reacts with $CaCl_2$ solution (concentration not specified) to form becquerelite within 1 week (Vochten and Van Haverbeke 1990).

Under conditions very similar to those of the present tests (initially pH 5.45 solution at 90ºC in sealed vessels), schoepite was reacted with distilled water, with 0.01 M Ca solution, with 0.01 M Ca/0.001 M Si, and with 0.001 M Ca/0.001 M Si (Sowder et al. 1996). The calcium was introduced as $Ca(NO_3)_2$ and the silicon as Na_2SiO_3. In the absence of calcium, schoepite remained unchanged. In the presence of calcium, becquerelite (as determined by XRD) formed after 1 to 30 days (Table 4.3). Dissolved silica apparently slowed this reaction. Significantly, no silicon-bearing solid phase was identified by either

Table 4.3. Solid Phases Produced by the Reaction of Schoepite with Various Solutions (Sowder et al. 1996)

Solution	Solid Phases Observed	
	1 day	30 days
Distilled water	Schoepite	Schoepite
0.01 M $Ca(NO_3)_2$	Becquerelite	Becquerelite
0.01 M $Ca(NO_3)_2$ / 0.001 M Na_2SiO_3	Schoepite	Becquerelite
0.001 M $Ca(NO_3)_2$ / 0.001 M Na_2SiO_3	Schoepite	Becquerelite/schoepite

XRD or scanning electron microscopy/energy dispersive spectrometry in the tests of Sowder et al. (1996), despite the prediction of uranophane $\{Ca[(UO_2)(SiO_3OH)]_2(H_2O)_5\}$ or soddyite $\{[(UO_2)_2(SiO_4)]_2(H_2O)_2\}$ as the thermodynamically favored solid phases in such systems (Finch 1997 and Chen et al. 1999) and their observation in oxic groundwater corrosion of UO_2 at 90°C (Wronkiewicz et al. 1996).

In more recent tests, (meta)schoepite $[(UO_2)_8O_2(OH)_{12}(H_2O)_{10}$, but prepared in the same way as the schoepite in the work of Sowder et al. (1996)], was reacted with 0.01 M $Ca(NO_3)_2$ in a pH 5.5 buffer at 60°C (Sowder et al. 1999). Using XRD to characterize the solid phase, the reaction to form becquerelite was found to be about half-complete at 2 days and complete at 3 days. At 0.001 M $Ca(NO_3)_2$ and 70°C, no transformation of the metaschoepite could be discerned by XRD even after 28 days.

A paragenetic sequence of mineralization was observed in aerated reaction of unirradiated UO_2 with simulated groundwater at 90°C (Wronkiewicz et al. 1996). The UO_2 was observed to transform to $UO_{2.25}$ and then to schoepite, becquerelite, and compreignacite[(a)] (at ~1 to 3 years) followed by soddyite (~3 years), and uranophane and other alkali and alkaline earth uranyl silicates (4 to 7 years). Decreases in pH and alkali, alkaline earth, and silicon solution concentrations also were observed.

The KE Basin sludges contain quartz (SiO_2) from Hanford soils and are expected to be at saturation in amorphous silica (~$10^{-2.7}$ M Si). The KE Basin sludges also contain calcite, and the calcium concentrations in waters associated with the sludges are about 8.5×10^{-6} M (derived from Makenas et al. 1997). Thus, the silicon solution concentrations established in the present tests are similar to those indicated in the silica-bearing solutions in Table 4.3, but the calcium concentrations are much lower. Based on the findings of Wronkiewicz et al. (1996) and Sowder et al. (1996, 1999), a becquerelite solid phase may form under the conditions of the present tests and generate CO_2.

Indirect evidence for the occurrence of Reaction 5 at hot cell temperature also was found in recent chemical processing tests run for a composite canister KE Basin sludge (Schmidt et al. 1999). In these tests, the amount of CO_2 that evolved by the reaction of the sludge with nitric acid was much lower than expected based on organic and inorganic carbon analyses, conducted about 2 years earlier, of the starting sludge materials. Subsequent measurements (reported in Schmidt et al. 1999) showed the pH of the sludge slurry to be 5.10±0.10, substantially lower than the 6.38 and 6.68 values found for the original sludge supernatant solutions (p. D-33 of Makenas et al. 1997). At pH 5.1, calcium carbonate is unstable and dissolves to saturate the solution with CO_2 gas and produce carbonic acid. The lowered pH and loss of inorganic carbon are consistent with the postulated reaction of schoepite with calcite to produce becquerelite.

(a) Compreignacite is $K_2(UO_2)_6O_4(OH)_6(H_2O)_8$.

4.1.5 Reaction Enthalpies and Free Energies

The enthalpy (ΔH_{298}) and Gibbs free energy (ΔG_{298}) of the predominant gas-forming reactions [uranium corrosion by water to produce UO_2 and H_2 in Reaction 1 and schoepite forming becquerelite and CO_2 by Reaction 5] may be estimated if the standard enthalpies and Gibbs free energies of formation ($\Delta H^0_{f,298}$ and $\Delta G^0_{f,298}$) of the respective reactant and product compounds are known. The reaction of enthalpy and Gibbs free energy values may then be compared and combined to determine the energy available to self-heat the stored sludge.

The relevant enthalpies and free energies of formation and derived reaction enthalpies and free energies are summarized in Table 4.4. A measured value for the $\Delta H^0_{f,298}$ of becquerelite could not be found in the technical literature. This value was estimated using the technique described by Chen et al. (1999). According to calculation, Reaction 5 (as written) has a Gibbs free energy of -834.2 kJ, or -34.8 kJ/mole uranium. The reaction enthalpy is -452.6 kJ, or -18.9 kJ/mole uranium. The corresponding values for uranium reaction with water are -557.4 kJ/mole uranium Gibbs free energy and -513.2 kJ/mole enthalpy. The uranium corrosion thus has a Gibbs free energy about 16 times higher (per mole uranium) than the schoepite conversion to becquerelite; the enthalpy is about 27 times higher.

Table 4.4. Thermodynamic Analyses of Schoepite and Uranium Metal Gas-Forming Reactions

Compound		Thermodynamic Value, kJ/mole		Refs.[(a)]
Formula	**Name**	**$\Delta H^0_{f,298}$**	**$\Delta G^0_{f,298}$**	
Schoepite Reaction (5) 3 $(UO_2)_8O_2(OH)_{12}(H_2O)_{12}$ + 4 $CaCO_3$ → 4 $Ca(UO_2)_6O_4(OH)_6(H_2O)_8$ + 10 H_2O + 4 CO_2				
Reactants				
$(UO_2)_8O_2(OH)_{12}(H_2O)_{12}$ (s)	schoepite	-14908.7	-13299.4	1
$CaCO_3$ (s)	calcite	-1206.92	-1128.79	2
Products				
$Ca(UO_2)_6O_4(OH)_6(H_2O)_8$ (s)	becquerelite	-11393.5	-10324.7	3; 1
H_2O (l)	water	-285.830	-237.129	2
CO_2 (g)	carbon dioxide	-393.509	-394.359	2
Net Reaction as Written, kJ		ΔH_{298} = -452.6	ΔG_{298} = -834.2	calc.
Net Reaction per Mole of Uranium, kJ		ΔH^0_{298} = -18.9	ΔG^0_{298} = -34.8	calc.
Net Reaction per kg Stoichiometric Sludge, kJ		ΔH_{298} = -55.1	ΔG_{298} = -101.4	calc.
Uranium Metal Reaction (1) U + 2 H_2O → UO_2 + 2 H_2				
Reactants				
U (s)	uranium metal	0	0	2
H_2O (l)	water	-285.830	-237.129	2
Products				
UO_2 (s)	uranium dioxide	-1084.9	-1031.7	2
H_2 (g)	hydrogen	0	0	2
Net Reaction as Written, kJ		ΔH_{298} = -513.2	ΔG_{298} = -557.4	calc.
Net Reaction per Mole of Uranium, kJ		ΔH^0_{298} = -513.2	ΔG^0_{298} = -557.4	calc.
Net Reaction per kg Stoichiometric Sludge, kJ		ΔH_{298} = -1873	ΔG_{298} = -2034	calc.

(a) 1 - Finch and Murakami (1999); 2 - Wagman et al. (1982); 3 - Chen et al. (1999); s = solid, l = liquid, g = gas.

The total reaction energy in the sludge depends on the quantities of limiting reactant(s) available for Reactions 1 and 5. Because the specific mineral quantities present in the sludge are unknown, the limiting reagent to produce becquerelite, which has a 6:1 U:Ca mole ratio, could be either schoepite or calcite (or another source of free calcium). The total U:Ca mole ratios for the sludges (Table 2.6) are much greater than 6 for the KC-2/3 sludge (i.e., possibly calcite or free calcium limited) and are about 3 and 2.2 for KC-4 and KC-5 (i.e., possibly schoepite limited). Given the large quantities of water in the sludge, the limiting reagent in uranium metal corrosion reaction 1 is uranium metal.

The enthalpies and Gibbs free energies of Reactions 1 and 5 also may be compared on a per-kilogram basis for hypothetical stoichiometric reaction mixtures (Table 4.4). For Reaction 1, the stoichiometric mixture is about 86.9 wt% uranium metal and 13.1 wt% water and would evolve almost 1900 kJ (enthalpy) and 7.3 moles of non-condensable H_2 gas per kilogram sludge. This is enough heat to convert about 730 grams of 20°C water to 100°C vapor. The sludge mixture stoichiometric for Reaction 5 contains about 69.4 wt% uranium (in about 95.1 wt% schoepite) and 1.94 wt% calcium (as 4.9 wt% calcite).[(a)] Complete reaction of the dry components would produce about 55 kJ of heat and 0.5 moles of non-condensable CO_2 gas per kilogram. This is enough to heat the same quantity of water (730 grams) from 20°C to only about 38°C. Though the schoepite reaction produces gas and heat, the gas evolution and energetics are distinctly more pronounced for the uranium metal corrosion reaction.

4.2 Gas Analysis for the KC-2/3 P250 Small-Scale Tests

The KC-2/3 P250 tests at 40°C, 60°C, and 80ºC produced the highest gas generation rates observed in the present tests. Each test underwent a final period at 95°C to ensure completion of reactions. The observed gas generation as a function of time was shown in Figure 3.1. In each of the three tests, gas production occurred under three regimes:

- an initial induction period in which little or no net gas was generated
- a region of linear gas generation rate between about 10% and 30% of total gas production
- a region of slowly decreasing rate of gas generation with gas generation nearly complete after about 1000 hours at 80°C and 3000 hours at 60°C.

During the induction period, the quantity of gases generated by the various reactions discussed in Section 4.1 evidently were offset by the consumption of atmospheric N_2 and O_2 in reaction with uranium metal. Some uptake of H_2 into the uranium metal to form hydrides also may have occurred. In the linear (maximum) region of the 80°C test, the gas generation rate (at standard temperature and pressure) is about 1600 ml/kg settled sludge-day. The rate observed in the linear region of the 60ºC test was about 440 ml/kg settled sludge-day; the rate at 40°C was about 82 ml/kg settled sludge-day; and the rate at 95°C, in the test initially at 40°C, was about 4600 ml/kg settled sludge-day. The rate decrease to essentially zero gas production after extended times for the 60°C and 80°C tests suggested, but did not prove, that the gas generating reactions had proceeded to almost complete consumption of reactants. The subsequent temperature increase to 95°C for these tests and lack of substantial effect (Figure 3.1) demonstrated that the reactions were, in fact, nearly complete. The maximum gas generation rates are shown in Table 4.5.

(a) In fact, the reaction also requires water to dissolve the calcite and solvate the H^+ released from the schoepite in forming becquerelite.

Table 4.5. Maximum Gas Generation Rates for KC-2/3 P250 Small-Scale Tests

Gas	Gas Generation Rates for KC-2/3 P250, ml/kg settled sludge-day, at temperature			
	40°C	60°C	80°C	95°C
H_2	80	410	1250	3200
CO_2	1.46	22	350	1350
∑ fission gases	0.046	0.18	0.67	1.3
∑ hydrocarbon gases	0.17	1.4	4.7	36
Total gas	82	440	1600	4600

4.2.1 Activation Energy Analysis

Hydrogen is the primary gas produced by the KC-2/3 P250 sludge at 40°C, 60°C, 80°C, and 95°C. Hydrogen gas generation rates were determined from the linear regions of the respective plots of specific gas formed (moles gas per kg sludge) for the tests run at 40°C, 60°C, and 80°C, and in the linear 95°C region of the test begun at 40°C. Because of the induction period and the S-shaped kinetics curves, the linear regions necessarily correspond to times of highest reaction (gas production) rate. The induction times encompass periods when atmospheric O_2 and N_2 are being consumed by low rate reactions with uranium metal, and the hydride-mediated uranium metal corrosion by water is low because the free hydrogen necessary for UH_3 mediation is at low concentration and the metal is covered by a protective oxide, not hydride, film.

$$U + 1.5\ H_2 \rightarrow UH_3\ (+\ 2\ H_2O) \rightarrow UO_2 + 3.5\ H_2$$

Activation energies may be derived from the maximum gas generation rate and inverse induction time data by use of the Arrhenius equation. The rate data are presented in Table 4.6. The Arrhenius plots derived from these data are presented in Figure 4.2. The corrosion rate of uranium metal in H_2-saturated water, as measured by uranium metal weight loss and based on a survey of data in the technical literature (Pajunen 1999), is shown in Figure 4.2 for comparison. The activation energies derived from the Arrhenius plots are also displayed in Figure 4.2.

Measurement of total gas generation rates and gas compositions also permitted calculation of the evolution rates of CO_2. The maximum CO_2 gas generation rates occurred near the beginning of the reactions and also seemed to require an induction time (perhaps to saturate the solution with CO_2).

Table 4.6. Reaction Rates for KC-2/3 P250 in Small-Scale Tests

Temp., °C	1/T, K^{-1}	Rate, moles/kg-day[(a)]		(Induction Time)$^{-1}$, h^{-1}	ln rate H_2	ln rate CO_2	ln (ind. time)$^{-1}$
		H_2	CO_2				
40	0.003197	3.23E-3	6.07E-5	7.46E-4	-5.74	-9.71	-7.20
60	0.002999	1.71E-2	9.12E-4	4.88E-3	-4.07	-7.00	-5.32
80	0.002834	5.19E-2	1.46E-2	3.72E-2	-2.96	-4.23	-3.29
95	0.002717	1.27E-1	5.61E-2	--	-2.06	-2.88	--

(a) Maximum rates taken from Tables B.4, B.5, and B.6.

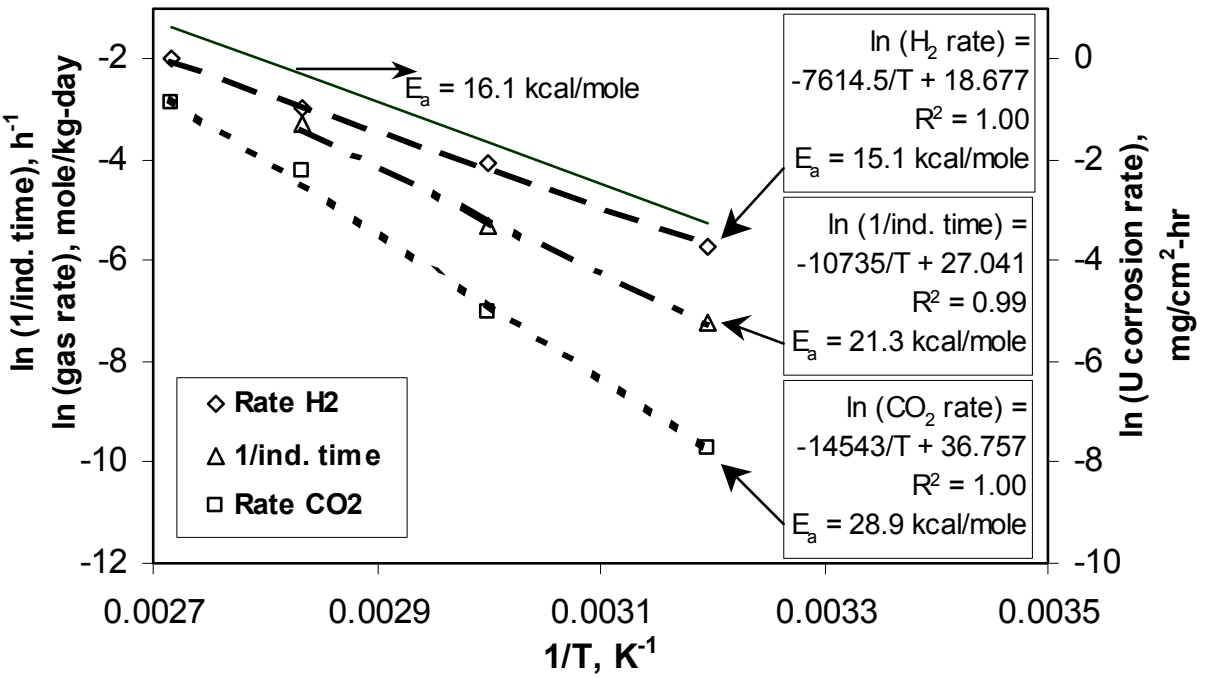

Figure 4.2. Arrhenius Plots for Inverse Induction Time to Onset of H_2 Generation, H_2 and CO_2 Gas Generation Rates in KC-2/3 P250 Sludge, and U Metal Corrosion in H_2-Saturated Water (derived from Pajunen 1999)

As shown in Figure 4.2, the activation energy (E_a) for CO_2 formation (□ symbols) is 28.9 kcal/mole, equivalent to 121 kJ/mole. The activation energy derived from the inverse induction time for onset of H_2 generation (i.e., conclusion of oxidation by atmospheric oxygen and establishment of the non-protective UH_3 layer next to the uranium metal; Δ symbols) was 21.3 kcal/mole (89 kJ/mole). Comparative values for the activation energies of these reactions could not be found in the technical literature.

The E_a for H_2 formation from uranium metal corrosion (◊) was 15.1 kcal/mole (63 kJ/mole). This value is near the E_a for uranium metal corrosion in H_2-saturated water of 16.1 kcal/mole or 67 kJ/mole, as derived from a review of the technical literature (Pajunen 1999).

4.2.2 Uranium Corrosion and the Roles of Hydrogen, Oxygen, and Nitrogen

The net and cumulative quantities of gas produced in each of the samplings in the 40°C, 60°C, and 80°C tests of the KC-2/3 sludge are presented in Tables 4.7 through 4.9, respectively. The total amount of H_2 evolved in the KC-2/3 P250 test at 80°C (and completed at 95°C) over the 3333 hours of reaction is 0.00729 moles (Table 4.9). The final heating at 95°C for 733 hours provided less than 1% of the total evolved H_2. The test at 60°C produced 0.0123 moles of H_2 over 4205 hours with an estimated 5% produced in the 671 hours of 95°C heating (Table 4.8). The test begun at 40°C produced 0.0152 moles of H_2 over 3951 hours. About 56% of this total was produced during the 377 hours of 95°C heating (Table 4.7). The early initial uptake of H_2 (postulated in the formation of UH_3) and its subsequent release as the uranium metal is consumed and the hydride exposed to water is seen in the H_2/C mole ratio plots in Figures 4.3 through 4.5 for the tests at 40°C, 60°C, and 80°C, respectively. The H_2 release occurs later as the reaction temperature decreases. For example, in the first sampling of the 80°C test, a relatively low

Table 4.7. Net and Cumulative Quantities of Gas Evolved for KC-2/3 P250 at 40ºC

Gas	Gas Quantities, moles, at Sampling Times											
	425.33 hr	**769.66 hr**	**1195.00 hr**	**1577.33 hr**	**2387.00 hr**	**3145.67 hr**	**3556.33 hr**	**3574.67 hr (at 95ºC)**	**3585.34 hr (at 95ºC)**	**3605.33 hr (at 95ºC)**	**3662.34 hr (at 95ºC)**	**3951.00 hr (at 95ºC)**
CO_2	6.62E-06	2.77E-06	5.32E-06	6.60E-06	1.09E-05	2.56E-05	2.46E-05	9.67E-04	6.64E-04	4.76E-04	3.94E-04	2.92E-04
Cumulative	6.62E-06	9.39E-06	1.47E-05	2.13E-05	3.22E-05	5.78E-05	8.24E-05	1.05E-03	1.71E-03	2.19E-03	2.58E-03	2.87E-03
H_2	2.12E-07	1.68E-06	1.76E-04	6.72E-04	2.64E-03	2.24E-03	1.02E-03	2.42E-03	1.33E-03	1.55E-03	1.77E-03	1.41E-03
Cumulative	2.12E-07	1.89E-06	1.78E-04	8.50E-04	3.49E-03	5.73E-03	6.75E-03	9.18E-03	1.05E-02	1.20E-02	1.38E-02	1.52E-02
N_2	-7.01E-06	-3.63E-06	2.00E-07	-4.21E-07	2.66E-07	1.83E-06	2.11E-06	-6.90E-07	9.91E-07	2.16E-06	1.17E-06	-5.01E-07
Cumulative	-7.01E-06	-1.06E-05	-1.04E-05	-1.09E-05	-1.06E-05	-8.76E-06	-6.64E-06	-7.33E-06	-6.34E-06	-4.18E-06	-3.00E-06	-3.50E-06
O_2	-3.83E-06	-1.60E-06	-6.98E-08	-1.81E-07	-5.90E-07	-4.61E-07	-1.46E-07	-1.67E-06	-3.80E-07	-4.74E-07	-2.08E-07	-6.29E-07
Cumulative	-3.83E-06	-5.43E-06	-5.49E-06	-5.68E-06	-6.27E-06	-6.73E-06	-6.87E-06	-8.55E-06	-8.93E-06	-9.40E-06	-9.61E-06	-1.02E-05
CH_4	7.82E-07	1.57E-06	2.59E-06	1.57E-06	3.16E-06	2.01E-06	9.45E-07	2.36E-05	1.41E-05	1.18E-05	6.13E-06	4.76E-06
Cumulative	7.82E-07	2.35E-06	4.94E-06	6.51E-06	9.67E-06	1.17E-05	1.26E-05	3.62E-05	5.03E-05	6.21E-05	6.82E-05	7.30E-05
C_2H_x	1.84E-08	2.77E-08	1.84E-07	1.74E-07	3.59E-07	2.88E-07	1.18E-07	2.77E-06	1.59E-06	1.41E-06	1.00E-06	1.05E-06
Cumulative	1.84E-08	4.61E-08	2.31E-07	4.05E-07	7.64E-07	1.05E-06	1.17E-06	3.94E-06	5.53E-06	6.94E-06	7.94E-06	8.99E-06
$\geq C_3H_x$			9.77E-08	9.49E-08	1.08E-07	9.59E-08	3.94E-08	6.81E-07	3.98E-07	3.99E-07	3.55E-07	4.68E-07
Cumulative	0.00E+00	0.00E+00	9.77E-08	1.93E-07	3.00E-07	3.96E-07	4.36E-07	1.12E-06	1.51E-06	1.91E-06	2.27E-06	2.74E-06
Σ C_yH_x C	8.19E-07	1.62E-06	3.27E-06	2.22E-06	4.22E-06	2.89E-06	1.31E-06	3.13E-05	1.85E-05	1.59E-05	9.26E-06	8.33E-06
Cumulative	8.19E-07	2.44E-06	5.72E-06	7.93E-06	1.22E-05	1.50E-05	1.64E-05	4.76E-05	6.62E-05	8.21E-05	9.13E-05	9.97E-05
^{83}Kr	4.60E-09	6.46E-09	1.30E-08	9.49E-09	2.16E-08	1.60E-08	7.88E-09	1.82E-08	1.22E-08	1.23E-08	1.61E-08	1.65E-08
Cumulative	4.60E-09	1.11E-08	2.41E-08	3.36E-08	5.51E-08	7.11E-08	7.90E-08	9.71E-08	1.09E-07	1.22E-07	1.38E-07	1.54E-07
^{84}Kr	9.20E-09	1.29E-08	2.50E-08	1.90E-08	4.31E-08	2.88E-08	1.38E-08	3.63E-08	2.45E-08	2.15E-08	2.91E-08	3.03E-08
Cumulative	9.20E-09	2.21E-08	4.71E-08	6.61E-08	1.09E-07	1.38E-07	1.52E-07	1.88E-07	2.13E-07	2.34E-07	2.63E-07	2.93E-07
^{85}Kr	4.60E-10	6.46E-10	8.68E-10	9.49E-10								
Cumulative	4.60E-10	1.11E-09	1.97E-09	2.92E-09	2.92E-09	2.92E-09	2.92E-09	2.92E-09	2.92E-09	2.92E-09	2.92E-09	2.92E-09
^{86}Kr	1.47E-08	2.21E-08	4.67E-08	3.64E-08	7.19E-08	5.43E-08	2.36E-08	5.45E-08	3.37E-08	3.38E-08	5.16E-08	4.68E-08
Cumulative	1.47E-08	3.69E-08	8.35E-08	1.20E-07	1.92E-07	2.46E-07	2.70E-07	3.24E-07	3.58E-07	3.92E-07	4.43E-07	4.90E-07
Σ Kr	2.90E-08	4.22E-08	8.55E-08	6.58E-08	1.37E-07	9.91E-08	4.53E-08	1.09E-07	7.04E-08	6.76E-08	9.68E-08	9.36E-08
Cumulative	2.90E-08	7.12E-08	1.57E-07	2.22E-07	3.59E-07	4.58E-07	5.03E-07	6.12E-07	6.83E-07	7.50E-07	8.47E-07	9.41E-07
^{130}Xe	8.28E-11	1.85E-10	2.17E-10	1.42E-10			9.84E-11	4.54E-09	1.84E-10	2.15E-10		2.75E-10
Cumulative	8.28E-11	2.67E-10	4.84E-10	6.27E-10	6.27E-10	6.27E-10	7.25E-10	5.26E-09	5.45E-09	5.66E-09	5.66E-09	5.94E-09
^{131}Xe	3.04E-08	3.69E-08	7.92E-08	6.01E-08	1.26E-07	9.27E-08	4.13E-08	9.53E-08	5.81E-08	6.76E-08	9.04E-08	8.81E-08
Cumulative	3.04E-08	6.73E-08	1.47E-07	2.07E-07	3.32E-07	4.25E-07	4.66E-07	5.62E-07	6.20E-07	6.87E-07	7.78E-07	8.66E-07
^{132}Xe	4.97E-08	5.91E-08	1.28E-07	9.65E-08	2.05E-07	1.50E-07	6.89E-08	1.59E-07	9.18E-08	1.08E-07	1.42E-07	1.49E-07
Cumulative	4.97E-08	1.09E-07	2.37E-07	3.33E-07	5.38E-07	6.88E-07	7.57E-07	9.16E-07	1.01E-06	1.12E-06	1.26E-06	1.41E-06
^{134}Xe	8.19E-08	1.02E-07	2.11E-07	1.61E-07	3.41E-07	2.49E-07	1.14E-07	2.77E-07	1.53E-07	1.81E-07	2.36E-07	2.39E-07
Cumulative	8.19E-08	1.83E-07	3.94E-07	5.55E-07	8.97E-07	1.15E-06	1.26E-06	1.54E-06	1.69E-06	1.87E-06	2.11E-06	2.35E-06
^{136}Xe	1.13E-07	1.38E-07	2.89E-07	2.20E-07	4.71E-07	3.42E-07	1.58E-07	3.77E-07	2.14E-07	2.52E-07	3.29E-07	3.47E-07
Cumulative	1.13E-07	2.52E-07	5.40E-07	7.60E-07	1.23E-06	1.57E-06	1.73E-06	2.11E-06	2.32E-06	2.57E-06	2.90E-06	3.25E-06
Σ Xe	2.75E-07	3.36E-07	7.07E-07	5.38E-07	1.14E-06	8.34E-07	3.82E-07	9.12E-07	5.17E-07	6.09E-07	7.97E-07	8.23E-07
Cumulative	2.75E-07	6.11E-07	1.32E-06	1.86E-06	3.00E-06	3.83E-06	4.22E-06	5.13E-06	5.64E-06	6.25E-06	7.05E-06	7.87E-06

Table 4.8. Net and Cumulative Quantities of Gas Evolved for KC-2/3 P250 at 60°C

Gas	Gas Quantities, moles, at Sampling Times							
	353.00 hr	**611.67 hr**	**762.33 hr**	**946.00 hr**	**1181.00 hr**	**1562.99 hr**	**2361.33 hr**	**4205.32 hr (at 60ºC and 95ºC)**
CO_2	4.42E-05	1.36E-04	1.07E-04	1.16E-04	1.08E-04	8.93E-05	9.99E-05	6.12E-04
Cumulative	4.42E-05	1.80E-04	2.87E-04	4.03E-04	5.11E-04	6.00E-04	7.00E-04	1.31E-03
H_2	8.19E-04	3.44E-03	1.80E-03	1.62E-03	1.45E-03	1.37E-03	1.06E-03	7.19E-04
Cumulative	8.19E-04	4.26E-03	6.06E-03	7.68E-03	9.13E-03	1.05E-02	1.16E-02	1.23E-02
N_2	-1.15E-04	-1.56E-06	1.76E-07	-6.15E-07	4.02E-07	6.39E-07	3.37E-06	2.04E-06
Cumulative	-1.15E-04	-1.16E-04	-1.16E-04	-1.17E-04	-1.16E-04	-1.16E-04	-1.12E-04	-1.10E-04
O_2	-3.67E-05	-9.48E-07	3.90E-06	-4.39E-07	-4.02E-07	-3.38E-07	-2.61E-07	-6.26E-07
Cumulative	-3.67E-05	-3.77E-05	-3.38E-05	-3.42E-05	-3.46E-05	-3.50E-05	-3.52E-05	-3.58E-05
CH_4	5.69E-06	7.70E-06	5.75E-06	7.18E-06	7.17E-06	7.45E-06	4.78E-06	4.59E-06
Cumulative	5.69E-06	1.34E-05	1.91E-05	2.63E-05	3.35E-05	4.09E-05	4.57E-05	5.03E-05
C_2H_x	6.95E-07	1.02E-06	7.31E-07	7.97E-07	8.34E-07	8.31E-07	6.17E-07	1.21E-06
Cumulative	6.95E-07	1.72E-06	2.45E-06	3.24E-06	4.08E-06	4.91E-06	5.53E-06	6.73E-06
$\geq C_3H_x$	5.06E-07	9.28E-07	6.09E-07	6.55E-07	6.26E-07	5.03E-07	2.29E-07	6.30E-07
Cumulative	5.06E-07	1.43E-06	2.04E-06	2.70E-06	3.32E-06	3.83E-06	4.06E-06	4.69E-06
Σ C_yH_x C	8.68E-06	1.27E-05	9.14E-06	1.08E-05	1.08E-05	1.07E-05	6.74E-06	9.01E-06
Cumulative	8.68E-06	2.14E-05	3.05E-05	4.14E-05	5.22E-05	6.29E-05	6.96E-05	7.86E-05
^{83}Kr	1.90E-08	2.32E-08	1.22E-08	1.14E-08	1.04E-08	1.01E-08	9.15E-09	7.88E-09
Cumulative	1.90E-08	4.22E-08	5.43E-08	6.57E-08	7.62E-08	8.62E-08	9.54E-08	1.03E-07
^{84}Kr	3.48E-08	4.64E-08	2.44E-08	2.28E-08	2.09E-08	2.01E-08	1.83E-08	1.84E-08
Cumulative	3.48E-08	8.12E-08	1.06E-07	1.28E-07	1.49E-07	1.69E-07	1.88E-07	2.06E-07
^{85}Kr	1.90E-09	2.32E-09	2.44E-09		2.61E-09	1.01E-09		
Cumulative	1.90E-09	4.22E-09	6.65E-09	6.65E-09	9.26E-09	1.03E-08	1.03E-08	1.03E-08
^{86}Kr	6.32E-08	8.82E-08	4.26E-08	3.70E-08	3.39E-08	3.52E-08	3.20E-08	2.36E-08
Cumulative	6.32E-08	1.51E-07	1.94E-07	2.31E-07	2.65E-07	3.00E-07	3.32E-07	3.56E-07
Σ Kr	1.19E-07	1.60E-07	8.16E-08	7.12E-08	6.78E-08	6.64E-08	5.95E-08	4.99E-08
Cumulative	1.19E-07	2.79E-07	3.60E-07	4.32E-07	4.99E-07	5.66E-07	6.25E-07	6.75E-07
^{130}Xe	2.53E-10	3.71E-10		1.71E-10	1.56E-10	1.76E-10	1.83E-10	2.10E-10
Cumulative	2.53E-10	6.24E-10	6.24E-10	7.95E-10	9.51E-10	1.13E-09	1.31E-09	1.52E-09
^{131}Xe	1.04E-07	1.44E-07	6.70E-08	6.55E-08	6.00E-08	5.79E-08	5.72E-08	5.25E-08
Cumulative	1.04E-07	2.48E-07	3.15E-07	3.81E-07	4.41E-07	4.98E-07	5.56E-07	6.08E-07
^{132}Xe	1.64E-07	2.37E-07	1.13E-07	1.05E-07	9.39E-08	9.56E-08	9.60E-08	8.66E-08
Cumulative	1.64E-07	4.01E-07	5.14E-07	6.19E-07	7.13E-07	8.08E-07	9.05E-07	9.91E-07
^{134}Xe	2.75E-07	3.85E-07	1.83E-07	1.74E-07	1.56E-07	1.56E-07	1.55E-07	1.44E-07
Cumulative	2.75E-07	6.60E-07	8.43E-07	1.02E-06	1.17E-06	1.33E-06	1.48E-06	1.63E-06
^{136}Xe	3.79E-07	5.57E-07	2.53E-07	2.42E-07	2.19E-07	2.21E-07	2.20E-07	2.15E-07
Cumulative	3.79E-07	9.36E-07	1.19E-06	1.43E-06	1.65E-06	1.87E-06	2.09E-06	2.31E-06
Σ Xe	9.23E-07	1.32E-06	6.15E-07	5.87E-07	5.29E-07	5.31E-07	5.28E-07	4.99E-07
Cumulative	9.23E-07	2.25E-06	2.86E-06	3.45E-06	3.98E-06	4.51E-06	5.04E-06	5.54E-06

Table 4.9. Net and Cumulative Quantities of Gas Evolved for KC-2/3 P250 at 80°C

Gas	Gas Quantities, moles, at Sampling Times									
	88.67 hr	**129.67 hr**	**219.33 hr**	**308.67 hr**	**375.67 hr**	**728.00 hr**	**1123.00 hr**	**1500.00 hr**	**2265.33 hr**	**3333.34 hr (at 80°C and 95°C)**
CO_2	4.21E-04	3.42E-04	3.69E-04	2.68E-04	1.52E-04	1.60E-04	1.11E-04	7.30E-05	8.74E-05	1.60E-04
Cumulative	4.21E-04	7.63E-04	1.13E-03	1.40E-03	1.55E-03	1.71E-03	1.82E-03	1.90E-03	1.98E-03	2.14E-03
H_2	1.43E-03	1.22E-03	2.00E-03	1.06E-03	4.80E-04	7.41E-04	2.04E-04	5.85E-05	4.64E-05	5.37E-05
Cumulative	1.43E-03	2.64E-03	4.65E-03	5.71E-03	6.19E-03	6.93E-03	7.13E-03	7.19E-03	7.24E-03	7.29E-03
N_2	-3.68E-06	1.55E-07	-9.63E-07	1.06E-07	4.62E-07	-1.19E-06	-9.05E-07	3.28E-07	-1.86E-06	-1.60E-06
Cumulative	-3.68E-06	-3.53E-06	-4.49E-06	-4.38E-06	-3.92E-06	-5.11E-06	-6.01E-06	-5.69E-06	-7.55E-06	-9.15E-06
O_2	-3.21E-06	-4.31E-07	-5.26E-07	-1.66E-07	6.52E-08	-6.09E-07	-8.01E-07	-6.01E-09	-1.32E-06	-1.39E-06
Cumulative	-3.21E-06	-3.65E-06	-4.17E-06	-4.34E-06	-4.27E-06	-4.88E-06	-5.68E-06	-5.69E-06	-7.01E-06	-8.40E-06
CH_4	1.06E-05	3.45E-06	8.51E-06	5.43E-06	2.75E-06	8.44E-06	3.79E-06	1.07E-06	6.16E-07	5.17E-07
Cumulative	1.06E-05	1.41E-05	2.26E-05	2.80E-05	3.08E-05	3.92E-05	4.30E-05	4.41E-05	4.47E-05	4.52E-05
C_2H_x	1.50E-06	5.05E-07	1.05E-06	7.07E-07	3.55E-07	1.01E-06	5.10E-07	1.82E-07	2.29E-07	3.83E-07
Cumulative	1.50E-06	2.01E-06	3.06E-06	3.77E-06	4.12E-06	5.14E-06	5.65E-06	5.83E-06	6.06E-06	6.44E-06
$\geq C_3H_x$	1.41E-06	5.28E-07	1.05E-06	6.56E-07	3.42E-07	8.23E-07	4.30E-07	1.54E-07	1.29E-07	2.00E-07
Cumulative	1.41E-06	1.94E-06	3.00E-06	3.65E-06	3.99E-06	4.82E-06	5.25E-06	5.40E-06	5.53E-06	5.73E-06
Σ C_yH_x C	1.81E-05	6.13E-06	1.40E-05	8.92E-06	4.54E-06	1.31E-05	6.17E-06	1.92E-06	1.48E-06	1.92E-06
Cumulative	1.81E-05	2.42E-05	3.82E-05	4.71E-05	5.17E-05	6.48E-05	7.09E-05	7.28E-05	7.43E-05	7.62E-05
^{83}Kr	3.24E-08	1.30E-08	2.11E-08	1.01E-08	4.42E-09	8.44E-09	3.18E-09	8.42E-10	1.43E-09	1.67E-09
Cumulative	3.24E-08	4.54E-08	6.65E-08	7.66E-08	8.10E-08	8.94E-08	9.26E-08	9.34E-08	9.49E-08	9.65E-08
^{84}Kr	5.30E-08	2.33E-08	3.16E-08	2.02E-08	8.85E-09	1.69E-08	6.37E-09	1.40E-09	1.43E-09	1.67E-09
Cumulative	5.30E-08	7.64E-08	1.08E-07	1.28E-07	1.37E-07	1.54E-07	1.60E-07	1.62E-07	1.63E-07	1.65E-07
^{85}Kr	1.77E-09	2.59E-09	3.52E-09	5.05E-09		2.11E-09	1.27E-09	8.42E-11	7.17E-11	8.33E-11
Cumulative	1.77E-09	4.36E-09	7.88E-09	1.29E-08	1.29E-08	1.50E-08	1.63E-08	1.64E-08	1.65E-08	1.65E-08
^{86}Kr	8.84E-08	3.89E-08	4.92E-08	3.28E-08	1.44E-08	2.96E-08	9.55E-09	1.40E-09	1.43E-09	1.67E-09
Cumulative	8.84E-08	1.27E-07	1.76E-07	2.09E-07	2.24E-07	2.53E-07	2.63E-07	2.64E-07	2.66E-07	2.67E-07
Σ Kr	1.76E-07	7.78E-08	1.05E-07	6.81E-08	2.76E-08	5.70E-08	2.04E-08	3.73E-09	4.37E-09	5.08E-09
Cumulative	1.76E-07	2.53E-07	3.59E-07	4.27E-07	4.55E-07	5.12E-07	5.32E-07	5.36E-07	5.40E-07	5.45E-07
^{130}Xe	3.24E-10	1.82E-10	2.46E-10	1.51E-10		1.69E-10	4.78E-11	1.40E-11	5.73E-11	3.33E-11
Cumulative	3.24E-10	5.06E-10	7.52E-10	9.03E-10	9.03E-10	1.07E-09	1.12E-09	1.13E-09	1.19E-09	1.22E-09
^{131}Xe	1.41E-07	6.23E-08	9.14E-08	5.55E-08	2.52E-08	4.86E-08	1.43E-08	4.21E-09	2.87E-09	1.67E-09
Cumulative	1.41E-07	2.04E-07	2.95E-07	3.51E-07	3.76E-07	4.24E-07	4.39E-07	4.43E-07	4.46E-07	4.47E-07
^{132}Xe	2.33E-07	1.01E-07	1.51E-07	9.09E-08	4.13E-08	8.44E-08	2.39E-08	7.02E-09	4.30E-09	3.33E-09
Cumulative	2.33E-07	3.34E-07	4.85E-07	5.76E-07	6.17E-07	7.02E-07	7.25E-07	7.32E-07	7.37E-07	7.40E-07
^{134}Xe	3.89E-07	1.63E-07	2.43E-07	1.46E-07	6.82E-08	1.35E-07	3.98E-08	1.12E-08	5.73E-09	6.67E-09
Cumulative	3.89E-07	5.52E-07	7.95E-07	9.41E-07	1.01E-06	1.14E-06	1.18E-06	1.20E-06	1.20E-06	1.21E-06
^{136}Xe	5.39E-07	2.20E-07	3.37E-07	2.07E-07	9.69E-08	1.94E-07	5.73E-08	1.68E-08	8.60E-09	8.33E-09
Cumulative	5.39E-07	7.59E-07	1.10E-06	1.30E-06	1.40E-06	1.60E-06	1.65E-06	1.67E-06	1.68E-06	1.69E-06
Σ Xe	1.30E-06	5.48E-07	8.23E-07	5.00E-07	2.32E-07	4.63E-07	1.35E-07	3.93E-08	2.16E-08	2.00E-08
Cumulative	1.30E-06	1.85E-06	2.67E-06	3.17E-06	3.40E-06	3.87E-06	4.00E-06	4.04E-06	4.06E-06	4.08E-06

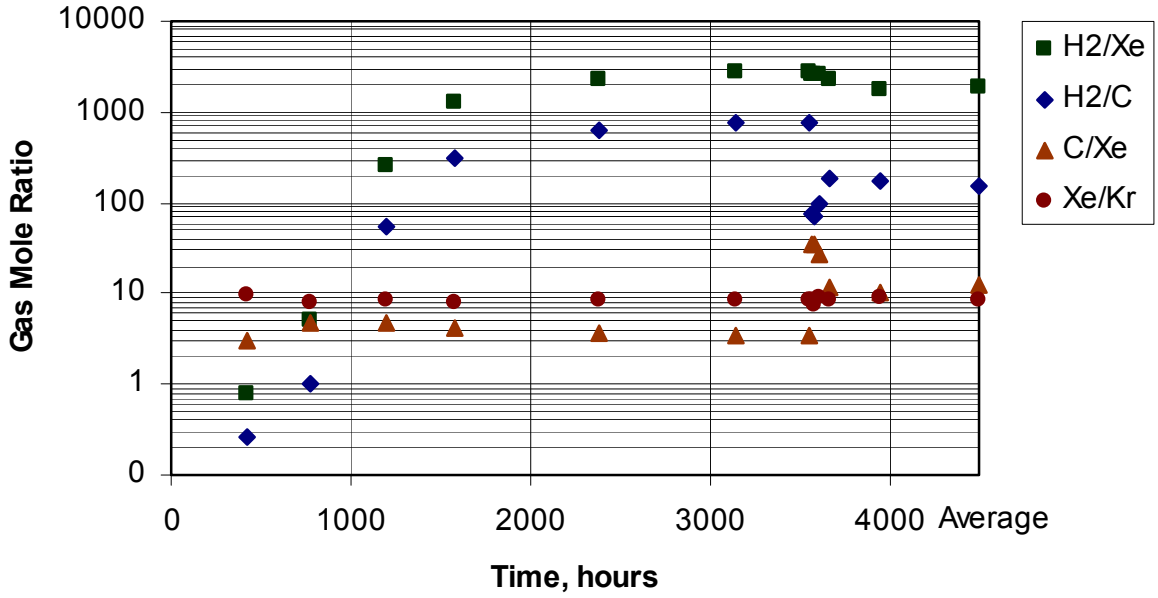

Figure 4.3. Mole Ratios of Gases Generated from Corrosion of Uranium Metal in KC-2/3 P250 at 40°C. Temperature Increased to 95°C at 3557 Hours.

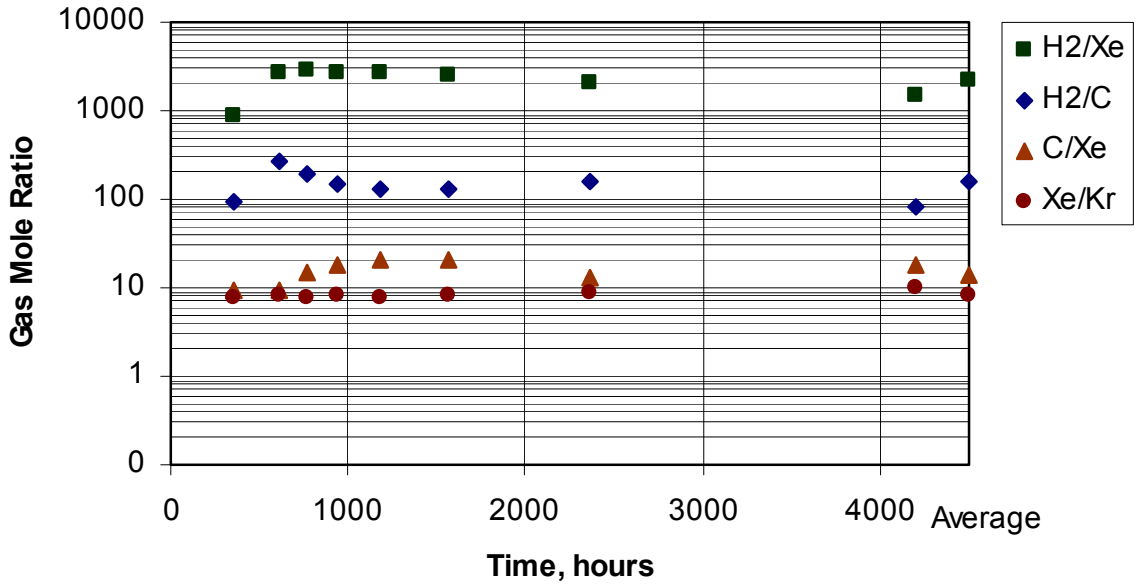

Figure 4.4. Mole Ratios of Gases Generated from Corrosion of Uranium Metal in KC-2/3 P250 at 60°C. Temperature Increased to 95°C at 3534 Hours.

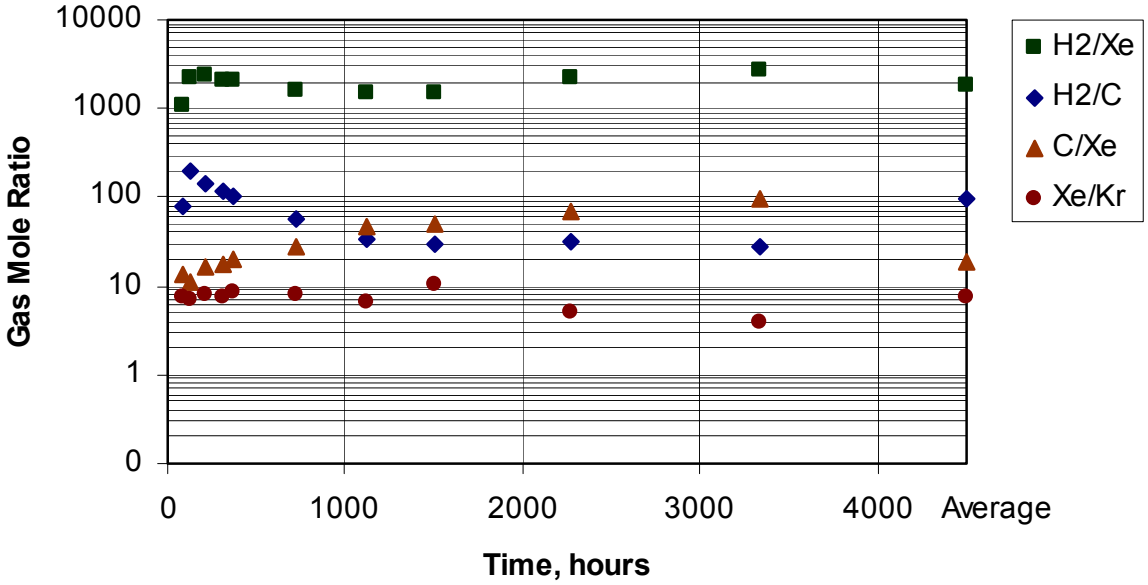

Figure 4.5. Mole Ratios of Gases Generated from Corrosion of Uranium Metal in KC-2/3 P250 at 80°C. Temperature Increased to 95°C at 2600 Hours.

H_2/C ratio of about 80:1 is observed, reflecting hydrogen uptake (hydride formation) in the metal. In the second sampling, the ratio becomes about 200:1 (hydrogen released) and then decreases in further samplings to around 30:1. Over the entire reaction, a ratio of 96:1 is observed. Similar trends, though not as pronounced, are seen for the H_2/Xe ratios at the three test temperatures.

According to Reaction 1, the 0.00729 moles of H_2 produced by the 80°C test correspond to 0.00364 moles of uranium metal reacted. The quantities of uranium metal reacted with O_2 and N_2 according to Reactions 2 and 3 are 0.0000084 and 0.0000105 moles, respectively, and are small in comparison with the uranium corroded by water by Reaction 1. Given the initial 13.71 gram mass of KC-2/3 P250 settled sludge used in this test (Table 2.3), the uranium mass fraction is estimated to be 0.0636, or 6.36 wt%. Similar evaluations may be made for the KC-2/3 P250 tests run at 60°C and 40°C and completed at 95°C (Table 4.10). The estimated uranium metal concentrations in these tests are 8.04 wt% and 7.66 wt%, respectively, or 7.4±0.9 wt% on average. This value is consistent with, but has much better precision than, the 4.0 wt% (±4.8 wt%) uranium metal estimated for the same wet sludge materials by reaction calorimetry (Bredt et al. 1999).

4.2.3 Fission Product Gases

The Kr and Xe isotope ratios observed in the product gas are similar to the ratios that are expected based on burn-up calculations by the ORIGEN code (Table 4.11). The lower relative quantity of ^{85}Kr found in the present tests can be attributed to radioactive decay. The decrease in ^{85}Kr abundance indicates a cooling time since discharge ranging from about 12 to 26 years. N Reactor was last at power 14 years ago (1986). The Xe:Kr mole ratio remains fairly constant with progress of the reaction (Tables 4.7 through 4.9; Figures 4.3 through 4.5) and is about 8.0:1 overall, corresponding to a mass ratio of 12.7:1.

Table 4.10. Metallic Uranium Reacted Calculated from Gas Generation and Consumption Reactions in KC-2/3 P250 Small-Scale Tests

Reaction	U Reacted Based on Various Reactions, moles		
	40°C	**60°C**	**80°C**
Reaction 1 $U + 2\ H_2O \rightarrow UO_2 + 2\ H_2$	7.61E-3	6.14E-3	3.65E-3
Reaction 2 $U + O_2 \rightarrow UO_2$	1.02E-5	3.58E-5	8.40E-6
Reaction 3 $U + 0.875\ N_2 \rightarrow UN_{1.75}$	4.00E-6	1.26E-4	1.05E-5
Total Moles U (Σ Equations 1-3)	7.63E-3	6.30E-3	3.66E-3
Settled Sludge Mass in Test, g	23.69	18.66	13.71
U metal, wt% settled sludge	7.66	8.04	6.36

Table 4.11. Isotope Ratios for KC-2/3 P250 Small-Scale Tests

Gas	Isotopic Composition, Atom%			ORIGEN[(a)]
	40°C Test[(b)]	**60°C Test**	**80°C Test**	
^{83}Kr	15.1	15.2	17.7	13.3
^{84}Kr	29.7	29.9	30.2	28.3
^{85}Kr	1.3	2.3	3.2	6.8
^{86}Kr	53.9	53.0	48.8	51.5
^{130}Xe	0.080	0.027	0.032	0.05
^{131}Xe	11.0	11.0	11.0	10.7
^{132}Xe	17.9	17.9	18.1	18.0
^{134}Xe	29.8	29.4	29.6	28.0
^{136}Xe	41.3	41.7	41.3	43.2
Xe:Kr	8.37	8.20	7.49	8.2

(a) ORIGEN2 calculation for N Reactor MkIV fuel at 2921 MWD/TeU; ratios change <3% relative at lower burn-ups; ^{85}Kr has a 10.76-year half-life.
(b) Kr isotopic data for the first four samples having quantifiable ^{85}Kr.

The expected atom ratio according to ORIGEN calculations (Table 4.11) is about 8.2:1, with a mass ratio of 13:1.

The fission product gas quantities can be used to cross check the amount of uranium reacted or to estimate the "average" burn-up of the uranium metal being corroded. Using the estimated amount of uranium reacted based on hydrogen evolution and an estimated 2900 MWD/TeU burn-up of the uranium fuel represented by the samples (see Section 4.1), the Kr and Xe gas concentrations can be calculated and compared with those observed. According to the ORIGEN code (and inferred from the equations presented in Figure 4.1), burn-up of 2900 MWD/TeU produces 47.2 μg Kr/gram uranium (or 0.0132 mole%Kr/mole U) and 602 μg Xe/gram uranium (0.106 mole% Xe/mole U). With 2 moles of H_2 being produced per mole of uranium corroded (U metal corrosion by N_2 and O_2 is negligible), the expected product gas ratios become 0.0068 mole%Kr/mole H_2 and 0.053 mole%Xe/mole H_2. The

observed ratios for the three KC-2/3 P250 small-scale tests average 0.0064 mole%Kr/mole H_2 and 0.051 mole%Xe/mole H_2 and, given the nearly linear rate of Kr and Xe growth with irradiation exposure, indicate an "average" burn-up of ~2800 MWD/TeU.

4.2.4 Hydrocarbons

Methane, ethane, and higher hydrocarbons were found in gases generated during the KC-2/3 P250 small-scale tests. The concentrations of carbon in the uranium metal fuel can be determined by comparing the quantity of total carbon in the hydrocarbon gas products (Tables 4.7 through 4.9) with the hydrogen (which was generated almost solely by the reaction of water with uranium). The carbon concentration in the uranium metal, based on the cumulative hydrogen and hydrocarbon gases generated for the 40°C, 60°C, and 80°C tests are 659, 630, and 1050 ppm parts uranium, respectively. These values are consistent with the expected carbon concentration in uranium metal fuel of 365-735 ppm parts uranium (Weakley 1979).

The methane fraction of the total hydrocarbon carbon increases with decreasing reaction temperature. The fractions of carbon found as methane are 0.59, 0.64, and 0.73, respectively, at 80°C, 60°C, and 40°C. The ratios of gaseous carbon from hydrocarbon sources to the Xe fission product gas in the KC-2/3 small-scale tests are shown in Figures 4.3 through 4.5. The relatively constant ratios during the period of rapid uranium metal corrosion in the 80°C test indicate that the hydrocarbon gases from carbide carbon are generated and released at the same relative rates as the fission product Xe. This constancy supports the assumption that the carbide carbon and fission product gases are distributed homogeneously in the uranium metal matrix, at least on the scale of the sludge particles in the present sample. However, the ratio rises steadily at longer reaction times. The increase may indicate that the hydrocarbon is slowly being released from the sludge with time (i.e., that the hydrocarbons are retained in the moist sludge better than is the Xe). The enhanced C/Xe ratios observed when the 40°C and 60°C test temperatures are increased to 95°C (if caused by thermal exsolution of the hydrocarbons) support this explanation.

4.2.5 Carbon Dioxide

Carbon dioxide comprises about 15%, 9.5%, and 22% of the total gas generated during the tests with KC-2/3 P250 at 40°C, 60°C, and 80ºC, respectively. It is likely that calcium ion (from calcite or other sources) rather than schoepite is the limiting reagent in these tests, given the high uranium and low calcium concentrations in the KC-2/3 P250 material (Table 2.6). Nevertheless, the relative schoepite and calcite quantities are unknown.

Provided schoepite is not the limiting reagent, an upper bound on the inorganic carbon concentrations in the sludge may be projected if the amount of CO_2 is known. The total amount of CO_2 produced is 0.00287 moles (Table 4.7) from the 23.69 grams (wet as-settled sludge basis) of KC-2/3 P250 in the 40°C test. This is equivalent to about 1460 ppm total inorganic carbon (TIC). The TIC concentrations determined in the same way for the 60°C and 80°C tests are 840 and 1880 ppm, respectively. The range of TIC observed in KE Basin floor and Weasel Pit as as-settled sludge was 5.36 to 1990 ppm (Makenas et al. 1996) and 155 to 9790 ppm in KE canister sludge (Makenas et al. 1997).

Data from pH and XRD measurements of the KC-2/3 P250 sludge may be used to find evidence of the reaction of schoepite and calcite to form becquerelite and release CO_2. The XRD analysis for the KC-2/3 P250 material stored in the hot cell for about 17 months showed schoepite and possibly becquerelite but no calcite. The XRD of the KC-2/3 P250 material reacted in the small-scale vessel at 80°C to 95°C did

not show any of these phases (Table 2.7). The XRD evidence thus did not confirm the occurrence of Reaction 5 in the KC-2/3 P250 material.

As shown in Table 3.1, the pH of the KC-2/3 P250 sludge stored in the hot cell was about 5.4, near that of the KE Basin waters at the time the sludge materials were retrieved. The pHs in the slurries upon opening the 40°C, 60°C, and 80°C test vessels were 6.4, 5.4, and 5.1, but decreased to 4.4, 5.0, and 4.1, respectively, after the slurries had been exposed to air for about 5 weeks. The relatively low (~5.4) starting pH of the KE Basin waters is consistent with the reaction of schoepite to form becquerelite (Reaction 5). The continued low pH of the sludges in the small-scale tests, and particularly the pH decrease after the sludges are exposed to air, also is consistent with the release of carbonic acid by Reaction 5.

4.3 Results of Other Small-Scale Tests at 80ºC

Small-scale tests conducted on KC-2/3 M250, KC-4 M250, KC-4 P250, KC-5 M250, and KC-5 P250 sludges were sampled four times during the 97 days of heating at 80°C. Heat to the vessels was discontinued 17 days after the fourth sampling (i.e., 114 days were spent at 80°C). The tests vessels remained sealed at hot cell temperature (~32°C) for 87 days, heated for 32 days at 95°C to force the reactions to completion, and then sampled for the fifth time.

Data for all five samplings are presented in Tables 4.12 through 4.16 for the five sludges. The five tests generated gas at maximum rates at 80°C ranging from 5 to 40 ml/kg settled sludge-day. The rates compare with the maximum 1600 ml/kg settled sludge-day rate observed at 80°C for the small-scale KC 2/3 P250 test (Table 4.17) and indicate that, aside from the KC-2/3 P250 sludge, the materials investigated in the small-scale tests are relatively benign.

The cumulative product gases after 97 days at 80°C are predominantly (92% to >99%) CO_2, with uranium metal corrosion manifested by O_2 and N_2 depletion, H_2 formation, and hydrocarbon and fission product gas generation (in most cases). As shown in Figures 3.2 and 3.3, rapid gas production generally occurred after each of the first four samplings. The surges are postulated to occur by the following mechanism during the gas sampling sequence. In gas sampling, the vessels first are cooled from 80°C to the ~32°C hot cell temperature. Because the CO_2 product gas has much higher solubility in solution at lower temperature, it partially dissolves in the moist sludge. After the vessel has reached hot cell temperature, the vapor space is sampled and the vapor space back-filled with neon. The vessels then are closed and reheated to 80°C. With heating, the CO_2 dissolved during the cooling phase is driven from solution to produce the gas surge.

With the 95°C heating, each system's behavior again was marked by an initial rapid gas surge (i.e., release of dissolved CO_2) followed by an extended period of gas evolution at steadily decreasing rates. The gas production kinetics at 95°C for the five small-scale tests are examined in more detail in Section 4.7. The gas compositions found in the fifth sampling generally were richer in CO_2 (96.6% to 99.4%) than were found cumulatively in the four samples taken during the 80°C testing. Gases still seemed to be evolving slowly from the KC-5 P250 test at the end of the 95°C heating; the other four tests were at or near exhaustion (Figures 3.2 and 3.3).

Except for the tests with KC-5 P250 and KC-5 M250, the overall quantities of H_2 generated (with respect to the uranium corrosion reactions) were much less than the quantities of O_2 and N_2 consumed. The

Table 4.12. Net and Cumulative Quantities of Gas Evolved for KC-2/3 M250 at 80°C

Gas	Gas Quantities, moles, at Sampling Times				
	425.33 hr	**721.01 hr**	**1535.34 hr**	**2337.68 hr**	**3489.34 hr (at 80°C, 32°C, and 95°C)**
CO_2	2.71E-04	1.58E-04	9.61E-05	8.97E-05	1.20E-04
Cumulative	2.71E-04	4.28E-04	5.24E-04	6.14E-04	7.34E-04
H_2	5.32E-07	6.86E-07	6.67E-07	6.50E-07	1.15E-06
Cumulative	5.32E-07	1.22E-06	1.89E-06	2.54E-06	3.69E-06
N_2	-9.01E-06	-9.17E-07	-1.88E-06	-2.20E-06	-8.78E-06
Cumulative	-9.01E-06	-9.93E-06	-1.18E-05	-1.40E-05	-2.28E-05
O_2	-4.03E-06	-7.79E-09	-3.77E-07	-5.35E-07	-2.94E-06
Cumulative	-4.03E-06	-4.04E-06	-4.41E-06	-4.95E-06	-7.89E-06
CH_4	5.91E-08	2.74E-08	5.34E-08	5.20E-08	1.17E-07
Cumulative	5.91E-08	8.66E-08	1.40E-07	1.92E-07	3.09E-07
C_2H_x	2.96E-08				2.92E-08
Cumulative	2.96E-08	2.96E-08	2.96E-08	2.96E-08	5.88E-08
$\geq C_3H_x$	2.96E-08			1.30E-08	
Cumulative	2.96E-08	2.96E-08	2.96E-08	4.26E-08	4.26E-08
Σ C_yH_x C	2.12E-07	2.74E-08	5.34E-08	9.33E-08	
Cumulative	2.12E-07	2.39E-07	2.93E-07	3.86E-07	5.61E-07
^{83}Kr	2.96E-10	1.37E-10	6.67E-10	2.60E-10	8.76E-10
Cumulative	2.96E-10	4.33E-10	1.10E-09	1.36E-09	2.24E-09
^{84}Kr	7.39E-10	4.12E-10	1.20E-09	5.20E-10	1.31E-09
Cumulative	7.39E-10	1.15E-09	2.35E-09	2.87E-09	4.19E-09
^{85}Kr		4.12E-11	6.67E-11		
Cumulative	0.00E+00	4.12E-11	1.08E-10	1.08E-10	1.08E-10
^{86}Kr	1.33E-09	5.49E-10	2.67E-09	9.10E-10	2.92E-09
Cumulative	1.33E-09	1.88E-09	4.55E-09	5.46E-09	8.38E-09
Σ Kr	2.37E-09	1.14E-09	4.60E-09	1.69E-09	5.11E-09
Cumulative	2.37E-09	3.50E-09	8.11E-09	9.80E-09	1.49E-08
^{130}Xe					
Cumulative	0.00E+00	0.00E+00	0.00E+00	0.00E+00	0.00E+00
^{131}Xe	4.44E-09	1.37E-10	2.67E-09	2.60E-09	5.84E-09
Cumulative	4.44E-09	4.57E-09	7.24E-09	9.84E-09	1.57E-08
^{132}Xe	5.91E-09	2.74E-09	4.00E-09	3.90E-09	1.02E-08
Cumulative	5.91E-09	8.66E-09	1.27E-08	1.66E-08	2.68E-08
^{134}Xe	1.18E-08	4.12E-09	8.00E-09	6.50E-09	1.61E-08
Cumulative	1.18E-08	1.59E-08	2.40E-08	3.05E-08	4.65E-08
^{136}Xe	1.63E-08	6.86E-09	1.07E-08	7.80E-09	2.19E-08
Cumulative	1.63E-08	2.31E-08	3.38E-08	4.16E-08	6.35E-08
Σ Xe	3.84E-08	1.39E-08	2.53E-08	2.08E-08	5.40E-08
Cumulative	3.84E-08	5.23E-08	7.77E-08	9.85E-08	1.53E-07

Table 4.13. Net and Cumulative Quantities of Gas Evolved for KC-4 M250 at 80°C

Gas	Gas Quantities, moles, at Sampling Times				
	425.00 hr	**721.00 hr**	**1533.34 hr**	**2335.67 hr**	**3487.34 hr (at 80°C, 32°C, and 95°C)**
CO_2	4.49E-05	3.74E-05	4.07E-05	4.61E-05	1.61E-04
Cumulative	4.49E-05	8.22E-05	1.23E-04	1.69E-04	3.30E-04
H_2	1.04E-06	1.13E-06	1.95E-06	2.22E-06	5.52E-06
Cumulative	1.04E-06	2.17E-06	4.12E-06	6.34E-06	1.19E-05
N_2	-1.01E-05	-2.28E-07	-8.16E-07	-1.46E-06	-4.20E-06
Cumulative	-1.01E-05	-1.04E-05	-1.12E-05	-1.26E-05	-1.68E-05
O_2	-5.44E-06	-2.34E-07	-6.51E-07	-7.43E-07	-1.04E-06
Cumulative	-5.44E-06	-5.67E-06	-6.32E-06	-7.06E-06	-8.10E-06
CH_4	4.66E-08	2.31E-08	3.41E-08	4.66E-08	5.61E-08
Cumulative	4.66E-08	6.97E-08	1.04E-07	1.50E-07	2.07E-07
C_2H_x	3.50E-08	2.31E-08	3.41E-08	3.50E-08	4.21E-08
Cumulative	3.50E-08	5.80E-08	9.21E-08	1.27E-07	1.69E-07
$\geq C_3H_x$	4.66E-08	2.31E-08	4.55E-08	3.50E-08	2.80E-08
Cumulative	4.66E-08	6.97E-08	1.15E-07	1.50E-07	1.78E-07
Σ C_yH_x C	2.64E-07	1.42E-07	2.46E-07	2.28E-07	2.29E-07
Cumulative	2.64E-07	4.07E-07	6.53E-07	8.81E-07	1.11E-06
^{83}Kr					
Cumulative	0.00E+00	0.00E+00	0.00E+00	0.00E+00	0.00E+00
^{84}Kr					
Cumulative	0.00E+00	0.00E+00	0.00E+00	0.00E+00	0.00E+00
^{85}Kr					
Cumulative	0.00E+00	0.00E+00	0.00E+00	0.00E+00	0.00E+00
^{86}Kr					
Cumulative	0.00E+00	0.00E+00	0.00E+00	0.00E+00	0.00E+00
Σ Kr	0.00E+00	0.00E+00	0.00E+00	0.00E+00	0.00E+00
Cumulative	0.00E+00	0.00E+00	0.00E+00	0.00E+00	0.00E+00
^{130}Xe					
Cumulative	0.00E+00	0.00E+00	0.00E+00	0.00E+00	0.00E+00
^{131}Xe		3.46E-10		2.33E-10	
Cumulative	0.00E+00	3.46E-10	3.46E-10	5.79E-10	5.79E-10
^{132}Xe		4.61E-10		3.50E-10	
Cumulative	0.00E+00	4.61E-10	4.61E-10	8.11E-10	8.11E-10
^{134}Xe		6.92E-10		3.50E-10	
Cumulative	0.00E+00	6.92E-10	6.92E-10	1.04E-09	1.04E-09
^{136}Xe		9.23E-10		4.66E-10	
Cumulative	0.00E+00	9.23E-10	9.23E-10	1.39E-09	1.39E-09
Σ Xe	0.00E+00	2.42E-09	0.00E+00	1.40E-09	0.00E+00
Cumulative	0.00E+00	2.42E-09	2.42E-09	3.82E-09	3.82E-09

Table 4.14. Net and Cumulative Quantities of Gas Evolved for KC-4 P250 at 80°C

Gas	Gas Quantities, moles, at Sampling Times				
	425.33 hr	**720.67 hr**	**1534.33 hr**	**2336.67 hr**	**3483.00 hr (at 80°C, 32°C, and 95°C)**
CO_2	7.36E-05	6.86E-05	6.89E-05	6.69E-05	1.46E-04
Cumulative	7.36E-05	1.42E-04	2.11E-04	2.78E-04	4.24E-04
H_2	5.03E-07	6.60E-07	1.33E-06	1.72E-06	5.37E-06
Cumulative	5.03E-07	1.16E-06	2.49E-06	4.22E-06	9.58E-06
N_2	-9.88E-06	-1.91E-06	-5.00E-06	-3.05E-06	-1.19E-05
Cumulative	-9.88E-06	-1.18E-05	-1.68E-05	-1.98E-05	-3.17E-05
O_2	-3.85E-06	1.85E-07	-8.75E-08	-1.57E-06	-1.12E-06
Cumulative	-3.85E-06	-3.66E-06	-3.75E-06	-5.32E-06	-6.44E-06
CH_4	2.58E-08		1.28E-08	1.29E-08	3.04E-08
Cumulative	2.58E-08	2.58E-08	3.86E-08	5.14E-08	8.19E-08
C_2H_x	2.58E-08		1.28E-08		
Cumulative	2.58E-08	2.58E-08	3.86E-08	3.86E-08	3.86E-08
$\geq C_3H_x$	5.16E-08	1.29E-08	2.55E-08	1.29E-08	
Cumulative	5.16E-08	6.46E-08	9.01E-08	1.03E-07	1.03E-07
Σ C_yH_x C	2.41E-07	4.10E-08	1.19E-07	4.08E-08	#VALUE!
Cumulative	2.41E-07	2.82E-07	4.01E-07	4.55E-07	4.85E-07
^{83}Kr					
Cumulative	0.00E+00	0.00E+00	0.00E+00	0.00E+00	0.00E+00
^{84}Kr					
Cumulative	0.00E+00	0.00E+00	0.00E+00	0.00E+00	0.00E+00
^{85}Kr					
Cumulative	0.00E+00	0.00E+00	0.00E+00	0.00E+00	0.00E+00
^{86}Kr					
Cumulative	0.00E+00	0.00E+00	0.00E+00	0.00E+00	0.00E+00
Σ Kr	0.00E+00	0.00E+00	0.00E+00	0.00E+00	0.00E+00
Cumulative	0.00E+00	0.00E+00	0.00E+00	0.00E+00	0.00E+00
^{130}Xe					
Cumulative	0.00E+00	0.00E+00	0.00E+00	0.00E+00	0.00E+00
^{131}Xe		3.88E-10			
Cumulative	0.00E+00	3.88E-10	3.88E-10	3.88E-10	3.88E-10
^{132}Xe		2.59E-10			
Cumulative	0.00E+00	2.59E-10	2.59E-10	2.59E-10	2.59E-10
^{134}Xe		2.59E-10			
Cumulative	0.00E+00	2.59E-10	2.59E-10	2.59E-10	2.59E-10
^{136}Xe		3.88E-10			
Cumulative	0.00E+00	3.88E-10	3.88E-10	3.88E-10	3.88E-10
Σ Xe	0.00E+00	1.29E-09	0.00E+00	0.00E+00	0.00E+00
Cumulative	0.00E+00	1.29E-09	1.29E-09	1.29E-09	1.29E-09

Table 4.15. Net and Cumulative Quantities of Gas Evolved for KC-5 M250 at 80°C

Gas	Gas Quantities, moles, at Sampling Times				
	425.33 hr	**721.67 hr**	**1535.33 hr**	**2337.67 hr**	**3489.33 hr (at 80°C, 32°C, and 95°C)**
CO_2	1.28E-04	1.13E-04	1.32E-04	1.14E-04	2.57E-04
Cumulative	1.28E-04	2.40E-04	3.72E-04	4.86E-04	7.43E-04
H_2	5.69E-07	7.00E-07	1.57E-06	1.70E-06	5.86E-06
Cumulative	5.69E-07	1.27E-06	2.84E-06	4.54E-06	1.04E-05
N_2	-6.92E-06	-4.46E-07	4.30E-07	5.37E-06	-1.55E-06
Cumulative	-6.92E-06	-7.37E-06	-6.94E-06	-1.56E-06	-3.12E-06
O_2	6.73E-05	-8.36E-08	2.30E-08	-2.13E-07	-1.57E-07
Cumulative	6.73E-05	6.72E-05	6.72E-05	6.70E-05	6.68E-05
CH_4	4.61E-08	2.86E-08	4.39E-08	2.99E-08	5.39E-08
Cumulative	4.61E-08	7.47E-08	1.19E-07	1.48E-07	2.02E-07
C_2H_x	4.61E-08	4.28E-08	4.39E-08	2.99E-08	7.19E-08
Cumulative	4.61E-08	8.90E-08	1.33E-07	1.63E-07	2.35E-07
$\geq C_3H_x$	7.69E-08	5.71E-08	7.32E-08	2.99E-08	3.59E-08
Cumulative	7.69E-08	1.34E-07	2.07E-07	2.37E-07	2.73E-07
Σ C_yH_x C	3.82E-07	2.95E-07	3.64E-07	1.84E-07	3.12E-07
Cumulative	3.82E-07	6.77E-07	1.04E-06	1.23E-06	1.54E-06
^{83}Kr					
Cumulative	0.00E+00	0.00E+00	0.00E+00	0.00E+00	0.00E+00
^{84}Kr		4.28E-10			
Cumulative	0.00E+00	4.28E-10	4.28E-10	4.28E-10	4.28E-10
^{85}Kr					
Cumulative	0.00E+00	0.00E+00	0.00E+00	0.00E+00	0.00E+00
^{86}Kr		4.28E-10			
Cumulative	0.00E+00	4.28E-10	4.28E-10	4.28E-10	4.28E-10
Σ Kr	0.00E+00	8.57E-10	0.00E+00	0.00E+00	0.00E+00
Cumulative	0.00E+00	8.57E-10	8.57E-10	8.57E-10	8.57E-10
^{130}Xe					
Cumulative	0.00E+00	0.00E+00	0.00E+00	0.00E+00	0.00E+00
^{131}Xe		4.28E-10			
Cumulative	0.00E+00	4.28E-10	4.28E-10	4.28E-10	4.28E-10
^{132}Xe		5.71E-10			
Cumulative	0.00E+00	5.71E-10	5.71E-10	5.71E-10	5.71E-10
^{134}Xe		8.57E-10			
Cumulative	0.00E+00	8.57E-10	8.57E-10	8.57E-10	8.57E-10
^{136}Xe		1.14E-09			
Cumulative	0.00E+00	1.14E-09	1.14E-09	1.14E-09	1.14E-09
Σ Xe	0.00E+00	3.00E-09	0.00E+00	0.00E+00	0.00E+00
Cumulative	0.00E+00	3.00E-09	3.00E-09	3.00E-09	3.00E-09

Table 4.16. Net and Cumulative Quantities of Gas Evolved for KC-5 P250 at 80°C

Gas	Gas Quantities, moles, at Sampling Times (hours)				
	425.33 hr	**721.67 hr**	**1534.66 hr**	**2337.00 hr**	**3488.33 hr (at 80°C, 32°C, and 95°C)**
CO_2	2.73E-04	3.22E-04	3.99E-04	3.85E-04	6.86E-04
Cumulative	2.73E-04	5.96E-04	9.95E-04	1.38E-03	2.07E-03
H_2	2.35E-05	7.86E-06	2.75E-06	1.69E-06	3.99E-06
Cumulative	2.35E-05	3.14E-05	3.41E-05	3.58E-05	3.98E-05
N_2	-7.77E-06	4.25E-07	9.25E-08	4.13E-07	-2.13E-06
Cumulative	-7.77E-06	-7.34E-06	-7.25E-06	-6.84E-06	-8.96E-06
O_2	-5.12E-06	8.90E-08	1.24E-07	-1.04E-07	-3.42E-07
Cumulative	-5.12E-06	-5.03E-06	-4.90E-06	-5.01E-06	-5.35E-06
CH_4	2.86E-07	9.48E-08	5.78E-08	4.22E-08	5.49E-08
Cumulative	2.86E-07	3.80E-07	4.38E-07	4.80E-07	5.35E-07
C_2H_x	1.22E-07	5.42E-08	5.78E-08	5.62E-08	7.32E-08
Cumulative	1.22E-07	1.77E-07	2.34E-07	2.91E-07	3.64E-07
$\geq C_3H_x$	2.45E-07	1.08E-07	1.30E-07	4.22E-08	3.66E-08
Cumulative	2.45E-07	3.53E-07	4.83E-07	5.25E-07	5.62E-07
Σ C_yH_x C	1.31E-06	5.47E-07	5.86E-07	2.88E-07	3.17E-07
Cumulative	1.31E-06	1.85E-06	2.44E-06	2.73E-06	3.04E-06
^{83}Kr	9.52E-09				
Cumulative	9.52E-09	9.52E-09	9.52E-09	9.52E-09	9.52E-09
^{84}Kr	5.44E-09				
Cumulative	5.44E-09	5.44E-09	5.44E-09	5.44E-09	5.44E-09
^{85}Kr					
Cumulative	0.00E+00	0.00E+00	0.00E+00	0.00E+00	0.00E+00
^{86}Kr	1.36E-09				
Cumulative	1.36E-09	1.36E-09	1.36E-09	1.36E-09	1.36E-09
Σ Kr	1.63E-08	0.00E+00	0.00E+00	0.00E+00	0.00E+00
Cumulative	1.63E-08	1.63E-08	1.63E-08	1.63E-08	1.63E-08
^{130}Xe	4.08E-11	2.71E-11			
Cumulative	4.08E-11	6.79E-11	6.79E-11	6.79E-11	6.79E-11
^{131}Xe	2.72E-09	1.35E-09			
Cumulative	2.72E-09	4.07E-09	4.07E-09	4.07E-09	4.07E-09
^{132}Xe	4.08E-09	2.71E-09	1.45E-09	4.22E-10	
Cumulative	4.08E-09	6.79E-09	8.23E-09	8.66E-09	8.66E-09
^{134}Xe	6.80E-09	4.06E-09	2.89E-09	4.22E-10	
Cumulative	6.80E-09	1.09E-08	1.38E-08	1.42E-08	1.42E-08
^{136}Xe	9.52E-09	5.42E-09	2.89E-09	7.03E-10	
Cumulative	9.52E-09	1.49E-08	1.78E-08	1.85E-08	1.85E-08
Σ Xe	2.32E-08	1.36E-08	7.23E-09	1.55E-09	0.00E+00
Cumulative	2.32E-08	3.67E-08	4.40E-08	4.55E-08	4.55E-08

Table 4.17. Maximum Gas Generation Rates for Small-Scale Tests at 80°C

Gas	Maximum Gas Generation Rate for Small-Scale Tests at 80°C, ml/kg settled sludge-day					
	KC-2/3 M250	KC-2/3 P250	KC-4 M250	KC-4 P250	KC-5 M250	KC-5 P250
H_2	0.077	1250	0.15	0.17	0.088	2.0
CO_2	21	350	4.8	18	16	38
Total gas	21	1600	5	18	16	40

larger fraction of O_2 and N_2 consumption indicates that uranium metal corrosion in the KC-4 P250, KC-4 M250, and KC-2/3 M250 tests is dominated by Reactions 2 and 3. It is probable that all of the uranium metal initially present in the KC-2/3 M250, KC-4, and KC-5 sludges has been completely consumed in the 80°C and 95°C heating, because the five small-scale tests have had more extensive heating than the KC-2/3 P250 material at 80°C and 95°C. Assuming the uranium metal has been completely oxidized, the uranium metal concentrations present in the five sludges can be estimated based on the N_2 and O_2 consumed and the H_2 produced. The uranium metal concentrations (settled-sludge basis) range from 0.015% to 0.14%, much lower than the estimated 6.36% (7.4% on average for all three tests) in the KC-2/3 P250 materials reacted to completion under similar conditions (Table 4.18).

It is important to note that the uranium metal concentrations are higher for all sludges (KC-2/3, KC-4, and KC-5) in the coarser P250 fraction than in the M250 fraction. The lack of significant metallic uranium in the lower particle size regime, particularly for the KC-2/3 material, is unexpected. This phenomenon would occur, however, if the uranium oxide product adheres to the underlying uranium metal and the oxide/metal particles arise primarily from metal particles larger than 250 μm. Fuel fragments have been observed to fracture into millimeter-sized particles by moist thermal treatment (Appendix E). Metal particle size is considered in more detail in Section 4.6. Because the fission product gas concentrations in most of the small-scale tests are near the analytical detection limits, reliable estimates of the fuel burn-up are not possible.

Table 4.18. Metallic Uranium Reacted Calculated from Gas Generation and Consumption Reaction Small-Scale Tests at 80ºC and Completed at 95°C

Reaction	U Reacted Based on Various Reactions, moles					
	KC-2/3 M250	KC-2/3 P250	KC-4 M250	KC-4 P250	KC-5 M250	KC-5 P250
Reaction 1 $U + 2\ H_2O \rightarrow UO_2 + 2\ H_2$	1.84E-6	3.65E-3	5.93E-6	4.79E-6	5.20E-6	1.99E-5
Reaction 2 $U + O_2 \rightarrow UO_2$	7.89E-6	8.40E-6	8.10E-6	6.44E-6	0[(a)]	5.35E-6
Reaction 3 $U + 0.875\ N_2 \rightarrow UN_{1.75}$	2.60E-5	1.05E-5	1.92E-5	3.63E-5	3.56E-6	1.02E-5
Total Moles U (Σ Equations 1-3)	3.58E-5	3.66E-3	3.33E-5	4.75E-5	8.76E-6	3.55E-5
Settled Sludge Mass in Test, g	17.56	13.71	15.14	7.82	13.86	16.23
U metal, wt% settled sludge	0.0485	6.36	0.0524	0.145	0.0150	0.0521

(a) Negative oxidation value reported as zero.

The quantity of metallic uranium present in the consolidated sludge samples prior to sieving can be calculated from mass distributions found by sieving (Table 2.5) and the data on uranium metal concentrations in the sieved fractions (Tables 4.10 and 4.18). The estimated uranium metal content in KC-2/3 is 1.9±0.2 wt% (settled-sludge basis) [(0.25x7.4±0.9) + (0.75x0.0485)]. For floor sludge samples KC-4 and KC-5, the uranium metal contents are 0.062 wt% (settled-sludge basis) [(0.10x0.145) + (0.90x0.0524)] and 0.028 wt% [(0.36x0.0521) + (0.64x0.0150)], respectively.

The total amount of carbon from hydrocarbons found in the gas samples may be compared with the estimated uranium metal concentrations (Table 4.18) to determine carbide carbon concentrations in the initial metal fuel. The relevant material quantities, shown in Table 4.19, give reasonable to high values for carbon concentration in the KC-2/3 M250 and both KC-4 tests. The carbon concentrations in the uranium metal for the KC-5 tests are much higher than the 365-735 ppm expected from fuel specifications (Weakley 1979). The high concentrations of evolved hydrocarbon may reflect the fact that the KC-5 sludge contains visible amounts of organic ion exchange resin (Bredt et al. 1999). Thermal degradation of the resin may be the cause of the observed excess hydrocarbon gas.

Table 4.19. Hydrocarbon Carbon and TIC Concentrations Estimated for Small-Scale Tests

Sludge	[C], ppmp U	TIC, ppm
KC-2/3 M250	>790	500
KC-2/3 P250	1050	1880
KC-4 M250	1680	260
KC-4 P250	>520	650
KC-5 M250	8850	640
KC-5 P250	4330	1530

The CO_2 evolved from the five small-scale tests gives evidence of the reaction of schoepite with calcite to form becquerelite, and the CO_2 quantity may be used to determine a lower limit on the TIC present in the sludge materials. Based on the amounts of CO_2 evolved through the gas sampling, the TIC concentrations in the sludge samples range from about 260 to 1530 ppm in the as-settled sludge, as shown in Table 4.19 and are somewhat lower than the 1880 ppm concentration found for KC-2/3 P250.

Data from pH measurements of the sludges in the small-scale testing may be used to find evidence of Reaction 5. The pHs of the six sludges that underwent small-scale testing are compared in Table 3.2. The pHs of the KC-2/3 M250 and P250 materials after 13 months in the hot cell were 5.0 and 5.4, respectively, and remained similar to those of the starting KE Basin waters at the time of sampling. In contrast, the KC-4 and KC-5 pHs rose to 7.8 and 7.2, respectively, after 13 months. The higher uranium concentrations in the KC-2/3 settled canister sludges (~40 wt% and 18 wt% for the M250 and P250 fractions, respectively) compared with the KC-4 and KC-5 settled floor sludges (~5.5 wt% and 2.2 wt%, respectively) may be responsible for the lower pH in the canister sludge. The maintenance of low pH for the KC-2/3 canister sludges may be because $UO_{2.25}$ present in the canister sludge (as shown in the XRD of KC-2/3 P250) air-oxidized to form more schoepite for Reaction 5. In contrast, the KC-4 and KC-5 sludges, taken from the floor area, did not have a significant $UO_{2.25}$ reservoir (as shown by XRD for KC-5) to air-oxidize and form more schoepite.

The uranium metal-rich KC-2/3 P250 sludges generally maintained their relatively low pHs (5.1 to 6.4) at the completion of the small-scale vessel hydrothermal testing. The KC-2/3 M250 canister sludge pH was

5.0 without hydrothermal treatment but increased to 6.7 after heating to 80-95°C. The KC-2/3 M250 sludge, though rich in uranium, has much less uranium metal than the KC-2/3 P250 fraction. Upon air exposure, the pH of each hydrothermally treated KC-2/3 canister sludge decreased to range from 4.1 to 5.2, near or below the starting pH. Although the starting pHs of the KC-4 and KC-5 floor sludges were about 2 pH units higher than for the KC-2/3 P250 canister sludge, the floor sludge pHs also decreased with hydrothermal treatment and/or subsequent air exposure. The pH decreases found by hydrothermal treatment in the KC-4 and KC-5 floor sludge and air exposure for the KC-2/3 canister sludges are consistent with the progression of Reaction 5.

The KC-5 P250 sludge was analyzed by XRD for samples that had and had not undergone 80°C to 95°C heating in the small-scale tests. Both schoepite and becquerelite were observed at relatively small concentrations in the unheated material (Table 2.7). While quantitation is not possible by the XRD techniques used, the relative prominences of the schoepite and, particularly, the becquerelite patterns increased in the heated KC-5 P250 material. The XRD findings thus are consistent with the occurrence of Reaction 5.

4.4 Gas Analysis from KC-4, KC-4 Dup, KC-5, and KC-2/3 P250 Large-Scale Tests at Hot Cell Temperature

Gas samples were collected twice from the KC-4, KC-4 Dup, and KC-5 large-scale tests run at hot cell temperature; the later samplings were after about 220 days of contact. Values for the total quantities of gas produced in these tests are presented in Tables 4.20 through 4.22, respectively. The overall gas generation rates (mostly CO_2 and H_2) were low and remarkably similar for the KC-4 and KC-5 materials: about 0.024 ml/kg settled sludge-day for KC-4, 0.025 ml/kg settled sludge-day for KC-4 Dup, and 0.024 ml/kg settled sludge-day for KC-5. The gas compositions for the KC-4 and KC-4 Dup tests did not show good agreement in the first sampling (compare Tables 4.20 and 4.21). However, by the time of the second sampling at 220 days, CO_2 comprised about 36% of the KC-4 and about 52% of the KC-4 Dup gas product. The KC-5 gas product was about 71% CO_2. Most of the balance was H_2.

The overall gas generation rate of the KC-2/3 P250 large-scale test run at the hot cell temperature was almost 40 times higher (~0.9 ml/kg settled sludge-day) than the rates observed for the KC-4 and KC-5 tests. Gas quantity data from the three samplings of the KC-2/3 P250 large-scale test are shown in Table 4.23. The gas collected after about 19 days of reaction was about 92% CO_2; about 95% CO_2 was observed over the three samples taken the first 256 days. The maximum H_2 and CO_2 gas generation rates observed for the large-scale tests are compared in Table 4.24. The KC-2/3 P250 large-scale test may be transitioning to the hydrogen-mediated uranium corrosion mechanism after about 250 days of testing at the 32°C hot cell temperature. According to the Arrhenius plots of reactions of the same material in the small-scale tests (Figure 4.2), the induction time required at 32°C should be about 145 days. The longer induction time at 32°C likely is because of the larger vapor/sludge volume ratio in this large-scale test (~10) compared with the small-scale tests (~1). The H_2 concentration would be more dilute in the large-scale test and perhaps not yet sufficient to initiate the H_2-mediated corrosion. The large vapor space in the KC-2/3 P250 large-scale test is also reflected in the noisier gas production plot (Figure 3.4) when compared with the other large-scale tests conducted at vapor/sludge volume ratios of ~1.

The total gas generation rate over the last ~200 hours of reaction (plotted in Figure 3.4) is about $2x10^{-4}$ moles/kg-day. In contrast, the maximum H_2 gas generation rate based on the Arrhenius fit of the

Table 4.20. Net and Cumulative Quantities of Gas Evolved for KC-4 at Hot Cell Temperature (~32°C)

Gas	Gas Quantities, moles, at Sampling Times	
	1483.33 hr	**5271.33 hr**
CO_2	1.63E-05	1.77E-05
Cumulative	1.63E-05	3.40E-05
H_2	1.52E-05	4.40E-05
Cumulative	1.52E-05	5.92E-05
N_2	-3.00E-05	6.53E-07
Cumulative	-3.00E-05	-2.94E-05
O_2	-1.82E-05	-3.19E-07
Cumulative	-1.82E-05	-1.85E-05
CH_4	3.33E-07	
Cumulative	3.33E-07	3.33E-07
C_2H_x		
Cumulative	0.00E+00	0.00E+00
$\geq C_3H_x$		
Cumulative	0.00E+00	0.00E+00
Σ C_yH_x C	3.33E-07	
Cumulative	3.33E-07	3.33E-07
^{83}Kr		
Cumulative	0.00E+00	0.00E+00
^{84}Kr	3.33E-09	
Cumulative	3.33E-09	3.33E-09
^{85}Kr		
Cumulative	0.00E+00	0.00E+00
^{86}Kr	5.00E-09	
Cumulative	5.00E-09	5.00E-09
Σ Kr	8.33E-09	0.00E+00
Cumulative	8.33E-09	8.33E-09
^{130}Xe		
Cumulative	0.00E+00	0.00E+00
^{131}Xe	1.33E-08	5.16E-08
Cumulative	1.33E-08	6.49E-08
^{132}Xe	1.67E-08	5.16E-08
Cumulative	1.67E-08	6.83E-08
^{134}Xe	3.33E-08	8.60E-08
Cumulative	3.33E-08	1.19E-07
^{136}Xe	5.00E-08	1.03E-07
Cumulative	5.00E-08	1.53E-07
Σ Xe	1.13E-07	2.92E-07
Cumulative	1.13E-07	4.06E-07

Table 4.21. Net and Cumulative Quantities of Gas Evolved for KC-4 Dup at Hot Cell Temperature (~32°C)

Gas	Gas Quantities, moles, at Sampling Times	
	1483.67 hr	**5271.33 hr**
CO_2	2.36E-05	2.09E-05
Cumulative	2.36E-05	4.46E-05
H_2	1.80E-07	4.02E-05
Cumulative	1.80E-07	4.04E-05
N_2	1.48E-05	4.28E-05
Cumulative	1.48E-05	5.76E-05
O_2	-9.13E-05	-6.16E-05
Cumulative	-9.13E-05	-1.53E-04
CH_4	1.80E-07	3.81E-07
Cumulative	1.80E-07	5.61E-07
C_2H_x		
Cumulative	0.00E+00	0.00E+00
$\geq C_3H_x$		
Cumulative	0.00E+00	0.00E+00
Σ C_yH_x C	1.80E-07	3.81E-07
Cumulative	1.80E-07	5.61E-07
^{83}Kr	1.80E-09	
Cumulative	1.80E-09	1.80E-09
^{84}Kr	3.60E-09	
Cumulative	3.60E-09	3.60E-09
^{85}Kr		
Cumulative	0.00E+00	0.00E+00
^{86}Kr	5.41E-09	
Cumulative	5.41E-09	5.41E-09
Σ Kr	1.08E-08	0.00E+00
Cumulative	1.08E-08	1.08E-08
^{130}Xe		
Cumulative	0.00E+00	0.00E+00
^{131}Xe	1.44E-08	
Cumulative	1.44E-08	1.44E-08
^{132}Xe	1.80E-08	
Cumulative	1.80E-08	1.80E-08
^{134}Xe	3.60E-08	
Cumulative	3.60E-08	3.60E-08
^{136}Xe	5.41E-08	
Cumulative	5.41E-08	5.41E-08
Σ Xe	1.23E-07	0.00E+00
Cumulative	1.23E-07	1.23E-07

Table 4.22. Net and Cumulative Quantities of Gas Evolved for KC-5 at Hot Cell Temperature (~32°C)

Gas	Gas Quantities, moles, at Sampling Times	
	1484.00 hr	**5271.67 hr**
CO_2	3.22E-05	3.54E-05
Cumulative	3.22E-05	6.76E-05
H_2	1.97E-06	2.58E-05
Cumulative	1.97E-06	2.78E-05
N_2	-3.63E-05	7.97E-06
Cumulative	-3.63E-05	-2.83E-05
O_2	-2.20E-05	-6.15E-07
Cumulative	-2.20E-05	-2.26E-05
CH_4		1.79E-07
Cumulative	0.00E+00	1.79E-07
C_2H_x		
Cumulative	0.00E+00	0.00E+00
$\geq C_3H_x$		
Cumulative	0.00E+00	0.00E+00
Σ C_yH_x C		1.79E-07
Cumulative	0.00E+00	1.79E-07
^{83}Kr		
Cumulative	0.00E+00	0.00E+00
^{84}Kr		
Cumulative	0.00E+00	0.00E+00
^{85}Kr		
Cumulative	0.00E+00	0.00E+00
^{86}Kr		
Cumulative	0.00E+00	0.00E+00
Σ Kr	0.00E+00	0.00E+00
Cumulative	0.00E+00	0.00E+00
^{130}Xe		
Cumulative	0.00E+00	0.00E+00
^{131}Xe	1.64E-08	
Cumulative	1.64E-08	1.64E-08
^{132}Xe	3.29E-08	
Cumulative	3.29E-08	3.29E-08
^{134}Xe	4.93E-08	
Cumulative	4.93E-08	4.93E-08
^{136}Xe	8.22E-08	
Cumulative	8.22E-08	8.22E-08
Σ Xe	1.81E-07	0.00E+00
Cumulative	1.81E-07	1.81E-07

Table 4.23. Net and Cumulative Quantities of Gas Evolved for KC-2/3 P250 at Hot Cell Temperature (~32°C)

Gas	Gas Quantities, moles, at Sampling Times			
	453.67 hr	**3785.67 hr**	**4665.33 hr**	**6144.67 hr**
CO_2	1.20E-04	1.90E-04	1.56E-04	1.90E-04
Cumulative	1.20E-04	3.10E-04	4.66E-04	6.56E-04
H_2	4.09E-06	1.16E-05	5.89E-06	8.83E-06
Cumulative	4.09E-06	1.57E-05	2.16E-05	3.04E-05
N_2	-5.14E-05	-1.64E-05	-1.43E-06	-5.87E-06
Cumulative	-5.14E-05	-6.77E-05	-6.92E-05	-7.50E-05
O_2	-4.59E-05	-4.57E-06	-1.65E-06	-2.19E-06
Cumulative	-4.59E-05	-5.05E-05	-5.21E-05	-5.43E-05
CH_4		2.65E-07		
Cumulative	0.00E+00	2.65E-07	2.65E-07	2.65E-07
C_2H_x				
Cumulative	0.00E+00	0.00E+00	0.00E+00	0.00E+00
$\geq C_3H_x$				
Cumulative	0.00E+00	0.00E+00	0.00E+00	0.00E+00
Σ C_yH_x C		2.65E-07		
Cumulative	0.00E+00	2.65E-07	2.65E-07	2.65E-07
^{83}Kr				
Cumulative	0.00E+00	0.00E+00	0.00E+00	0.00E+00
^{84}Kr				
Cumulative	0.00E+00	0.00E+00	0.00E+00	0.00E+00
^{85}Kr				
Cumulative	0.00E+00	0.00E+00	0.00E+00	0.00E+00
^{86}Kr				
Cumulative	0.00E+00	0.00E+00	0.00E+00	0.00E+00
Σ Kr	0.00E+00	0.00E+00	0.00E+00	0.00E+00
Cumulative	0.00E+00	0.00E+00	0.00E+00	0.00E+00
^{130}Xe				2.60E-09
Cumulative	0.00E+00	0.00E+00	0.00E+00	2.60E-09
^{131}Xe				2.60E-09
Cumulative	0.00E+00	0.00E+00	0.00E+00	2.60E-09
^{132}Xe				5.20E-09
Cumulative	0.00E+00	0.00E+00	0.00E+00	5.20E-09
^{134}Xe				7.79E-09
Cumulative	0.00E+00	0.00E+00	0.00E+00	7.79E-09
^{136}Xe				
Cumulative	0.00E+00	0.00E+00	0.00E+00	0.00E+00
Σ Xe	0.00E+00	0.00E+00	0.00E+00	1.82E-08
Cumulative	0.00E+00	0.00E+00	0.00E+00	1.82E-08

Table 4.24. Maximum Gas Generation Rates for Large-Scale Tests at ~32°C

Gas	Rate of Gas Generation for Large-Scale Tests at ~32°C, ml/kg settled sludge-day			
	KC-4	KC-4 Dup	KC-5	KC-2/3 P250
H_2	0.016	0.016	0.0089	0.079
CO_2	0.015	0.024	0.029	2.3
Total gas	0.031	0.040	0.038	2.4

small-scale test data (Figure 4.2) is about 10 times higher. On this basis, it seems that the hydrogen-mediated corrosion reaction has not yet reached its maximum rate.

Consumption of O_2 and N_2 occurred in all the large-scale tests [exception: KC-4 Dup showed no N_2 consumption]. The measured O_2 and N_2 depletion can be used to calculate the moles of uranium metal oxidized by Reactions 2 and 3 in the K Basin sludge. The quantity of uranium metal oxidized by water according to Reaction 1 can be determined by the measured hydrogen production. Table 4.25 shows estimates of the quantities of uranium metal reacted with water, oxygen, and nitrogen, and the total uranium reacted.

The rates of uranium reacted (g U/kg settled sludge-day) were estimated from the calculated total mass of uranium reacted, the mass of sample used in each test, and the test duration. The calculated rate values are provided at the bottom of Table 4.25. The reactions with air (N_2 and O_2) are responsible for about 63% to 92% of the corrosion. The uranium reaction rate in aerated conditions is lower than in

Table 4.25. Metallic Uranium Reacted Calculated from Gas Generation and Depletion Reactions (in total moles during experiment), and Rate of Uranium Reacted (g U/kg settled sludge-day)

U Oxidation Based on H_2, O_2, and N_2 Gas Analysis				
Reaction	Moles U Reacted Based on Various Reactions			
	KC-4	KC-4 Dup	KC-5	KC-2/3 P250
Reaction 1 $U + 2\ H_2O \rightarrow UO_2 + 2\ H_2$	2.96E-5	2.02E-5	1.39E-5	1.52E-5
Reaction 2 $U + O_2 \rightarrow UO_2$	1.85E-5	1.53E-4	2.26E-5	5.43E-5
Reaction 3 $U + 0.875\ N_2 \rightarrow UN_{1.75}$	3.35E-5	0[(a)]	3.24E-5	8.58E-5
Total Moles U (Σ Equations 1-3)	8.16E-5	1.73E-4	6.89E-5	1.55E-4
Settled Sludge Mass in Test, g	421.51	378.25	439.45	65.98
total mass U reacted, g	0.019	0.041	0.016	0.037
U Metal, Wt% Settled Sludge	4.5E-3	1.1E-2	3.6E-3	5.6E-2
Rate of Uranium Reacted (all reactions), g U/kg settled sludge-day				
Rate	2.1E-4	4.9E-4	1.7E-4	2.2E-3

(a) Negative oxidation value reported as zero.

non-aerated conditions. Until the oxygen and nitrogen are depleted and a higher overpressure of hydrogen established, the reaction rate is expected to remain relatively low (Montenyohl 1960).

The carbon concentration in the uranium metal, inferred from the quantities of hydrocarbon gas product, were about 1510, 1170, 1560, and 1790 ppm parts uranium in the KC-4, KC-4 Dup, KC-5, and KC-2/3 P250 large-scale materials, respectively. The low amounts of uranium corroded and possible contributions from other sources to produce hydrocarbon gas compromise the ability to determine carbon concentrations in the uranium metal from these data.

The Kr and Xe gas concentrations expected in the gas product can be calculated based on the estimated amount of uranium reacted and the estimated burn-up of the uranium samples. However, only gases from the first sampling of the KC-4 and KC-4 Dup tests had reliable isotopic analyses for both Kr and Xe; Xe released in the corrosion of metal from test KC-5 also was above the detection limit. The fission product gases were below detection in the KC-2/3 P250 test. A burn-up value of 2900 MWD/TeU, typical of power-mode N Reactor operation, was assumed for this estimate, and the Kr and Xe produced from this burn-up were determined based on ORIGEN code calculations for N Reactor Mark IV fuel. A more accurate estimate for the burn-up may be possible based on the KE Basin fuel storage map to reflect the actual burn-up of the fuel stored in these locations. A 2900 MWD/TeU burn-up produces 0.016 mole% Kr/mole U and 0.134 mole% Xe/mole U. Table 4.26 shows the sum of all isotopes for Kr and Xe liberated, in moles, based on the total uranium reactions occurring at the time of the first sampling (~1484 hours) and the burn-up value of 2900 MWD/TeU.

The moles of fission gas measured from direct gas mass spectral analysis can be compared with the values for these gases based on reaction of the uranium metal. Table 4.27 shows the comparison of these values as a ratio of the gas measured (e.g., $Kr_{measured}$) divided by the fission product gas calculated based on uranium reaction (e.g., $Kr_{calculated}$). For the KC-4 and KC-5 large-scale tests, the (measured/calculated) ratios are unity within a factor of 2 and range from ~0.4 to ~2 for both Kr and Xe. The variation from unity probably arises from inaccuracies in fission product gas analyses near the analytical detection limit.

Table 4.26. Sum of Fission Gases Based on Uranium Reacted at the Time of the First Sampling and Uranium Burn-up at 2900 MWD/TeU

Sum of Fission Gases Based on U Oxidation, moles			
Gas	**KC-4**	**KC-4 Dup**	**KC-5**
Kr	1.31E-8	2.77E-8	(a)
Xe	1.09E-7	2.32E-7	9.24E-8

(a) Below detection limit.

Table 4.27. Ratio of Fission Gas Measured to Fission Gas Calculated

Ratio of Fission Gas Measured (by Mass Spectrometry) to Fission Gas Calculated (Based on U Burn-up and Reaction at the First Sampling)			
Gas Ratio	**KC-4**	**KC-4 Dup**	**KC-5**
$Kr_{measured}/Kr_{calculated}$	0.64	0.39	(a)
$Xe_{measured}/Xe_{calculated}$	1.04	0.53	1.96

(a) Below detection limit.

4.5 Gas Generation Results from 1996 KE Basin Canister Sludge Samples

This section discusses the gas generation observed from KE canister sludge samples collected in 1996. The conditions and results of gas analyses from these studies (published previously in Appendix B of Makenas et al. 1997) are presented here for comparison with the present findings.

From June 11 through June 20, 1996, nine K Basin canister sludge samples were moved from the 327 Building pool to the 325 Building. Seven of the samples were collected from fueled canisters, with the remaining two samples collected from empty canisters. During recovery of the sludge samples from the shipping containers, evidence of significant pressurization (from gas generation) was observed in four of the containers. Further observations indicated that a fifth canister sludge sample was also generating gas. Therefore, of the seven samples from fueled canisters, five samples generated gas. The two samples from empty canisters did not appear to generate gas.

When the canister sludge samples were transferred from the shipping containers to 2-L graduated glass cylinders, the formation of gas bubbles was observed in the same samples that had shown evidence of pressurization. After being transferred, the samples were sparged with air to mobilize the settled sludge and obtain a homogeneous slurry for settling rate studies. In the graduated cylinder containing canister sludge sample 96-05, a plug of sludge was pushed up by generated gas. The graduated cylinders were then stoppered with gas sampling tubing leading outside the hot cell. The evolved gases were collected from samples 96-05 and 96-06. Next, the sludge samples were resuspended using helium sparging, and another gas sample was collected from sample 96-06 (gas generation was not sufficient to collect a good sample from the 96-05 sludge). Finally, gas samples were collected from sludge shipping containers 96-13 and 96-15. The mole percent compositions of the five gas samples taken in the 1996 tests are shown in Table 4.28. The compositions of the gas samples from 96-05 and 96-06 were: H_2, 98% to 99%; CO_2, 0.1% to 1.1%; and CH_4, 0.3% to 1.4%. In comparison, the gas composition for the KC-2/3 P250 40°C test in the linear region was as follows: H_2, 99%; CO_2, 0.4% to 1.1%; and CH_4, 0.1% to 1.2%.

In addition to the gas composition, estimates were made of the gas generation rates over several days for samples 96-05 and 96-06 (Table 4.29). Two techniques were used: in the first technique, generation rates were estimated by measuring the size of the gas pockets in the sludge column over time; for the second technique, the gas generation rate was determined by estimating the volume of gas collected over time in a Tedlar bag. The error associated with the Tedlar bag approach was estimated to be plus or minus 50%. The gas generation rates calculated from measuring the size of the gas pockets are expected to be more accurate.

The gas generation rates at ambient hot cell temperature (35ºC) from the canister sludge samples collected in 1996 ranged from 0 to 150 ml/kg settled sludge-day. The average gas generation rates for samples 96-05 and 96-06 were 27 and 59 ml/kg settled sludge-day, respectively. The rates for samples 96-05 and 96-06 are much higher than observed for the large-scale test with KC-2/3 P250-L at ambient hot cell temperature (2.4 ml/kg settled sludge-day). Furthermore, while more than 80% of the gas generated from KC-2/3 P250-L was CO_2, greater than 98% of the gas from the 96-05 and 96-06 sludge samples was H_2. The high H_2 content in the gas generated from 96-05 and 96-06 indicates that these samples were beyond an induction period and actively corroding by Reaction 1 with water. Upon completion of the induction period, it is possible that the rate of gas generation from KC-2/3 P250-L will approach the average rates measured for samples 96-05 and 96-06 at ambient hot cell temperature, but even after 1 year of testing, the induction time for KC-2/3 P250-L has not yet been completed.

Table 4.28. Compositions of Gases Sampled and Generated (shaded) from KE Basin Canisters in 1996 at Hot Cell Temperature

96-05 Air Sparge

Sample	He	Ar	H_2	CO_2	CH_4	C_2 hydrocarbons	other hydrocarbons	N_2	O_2
1		0.5	56.6	0.26	0.15	0.012		33.9	8.5
			99.20	0.46	0.26	0.02			

Kr 83	Kr 84	Kr 85	Kr 86	Xe 130	Xe 131	Xe 132	Xe 134	Xe 136
	2.0E-03		3.0E-03		4.0E-03	6.0E-03	9.0E-03	1.3E-02
	3.5E-03		5.3E-03		7.1E-03	1.0E-03	1.6E-02	2.3E-02

96-06 Air Sparge

Sample	He	Ar	H_2	CO_2	CH_4	C_2 hydrocarbons	other hydrocarbons	N_2	O_2
1		0.58	53.4	0.17	0.17	0.013		36.7	9
			99.30	0.32	0.32	0.02			

Kr 83	Kr 84	Kr 85	Kr 86	Xe 130	Xe 131	Xe 132	Xe 134	Xe 136
	2.0E-03	3.0E-03			3.0E-03	5.0E-03	7.0E-03	1.0E-02
	3.7E-03	5.6E-03			5.6E-03	9.3E-03	1.3E-02	1.9E-02

96-06 Helium Sparge

Sample	He	Ar	H_2	CO_2	CH_4	C_2 hydrocarbons	other hydrocarbons	N_2	O_2
1	0.83	0.82	12.6	0.14	0.04		0.01	68.1	17.4
			98.40	1.09	0.31		0.08		

Kr 83	Kr 84	Kr 85	Kr 86	Xe 130	Xe 131	Xe 132	Xe 134	Xe 136
	1.4E-03		1.7E-03		1.7E-03	2.0E-03	3.0E-03	4.0E-03
	1.1E-02		1.3E-02		1.3E-02	1.6E-02	2.3E-02	3.1E-02

96-13 Shipping Canister

Sample	He	Ar	H_2	CO_2	CH_4	C_2 hydrocarbons	other hydrocarbons	N_2	O_2
1	0.014	0.26	72.1	0.044	0.43	0.024	0.03	21.2	5.8
			99.20	0.06	0.59	0.03	0.04		

Kr 83	Kr 84	Kr 85	Kr 86	Xe 130	Xe 131	Xe 132	Xe 134	Xe 136
	2.0E-03		3.0E-03		4.0E-03	5.0E-03	8.0E-03	1.2E-02
	2.8E-03		4.1E-03		5.5E-03	6.9E-03	1.1E-02	1.7E-02

96-15 Shipping Canister

Sample	He	Ar	H_2	CO_2	CH_4	C_2 hydrocarbons	other hydrocarbons	N_2	O_2
1		0.296	75.6	0.234	1.11	0.062	0.03	19.3	3.37
			98.10	0.30	1.44	0.08	0.04		

Kr 83	Kr 84	Kr 85	Kr 86	Xe 130	Xe 131	Xe 132	Xe 134	Xe 136
					2.3E-03	3.8E-03	6.4E-03	9.1E-03
					3.0E-03	4.9E-03	8.3E-03	1.2E-02

Note: Blank entries are below detection limits.
Shaded Values denote the composition of the gas generated (i.e., contribution of neon cover gas has been subtracted out).

Table 4.29. Estimated Total Gas Generation Rates from KE Canister Sludge Samples in 1996 at Hot Cell Temperature

Sludge Mass and Gas Generation Rates	Date and (Method of Estimate)	KE Canister Sludge Sample 96-05	KE Canister Sludge Sample 96-06
Mass of Settled Solids	N/A	667 g	733 g
Rates on a Per Sample Basis – STP			
Gas Generation Rate	7/31/96 (gas pocket)	1.7 ml/sample-hr (for 16 hr)	Not measured
Gas Generation Rate (After 5-min air sparge)	8/19/96 (Tedlar bag)	0.4 to 0.6 ml/sample-hr (for 107 hr)	0.6 to 1.2 ml/sample-hr (for 107 hr)
Gas Generation Rate (After 5-min helium sparge)	8/22/96 (Tedlar bag)	0.4 to 0.7 ml/sample-hr (for 40 hr)	0.9 to 1.7 ml/sample-hr (for 40 hr)
Gas Generation Rate (ml/sample-hr)	9/3/96 (gas pocket)	Not measured	4.6 ml/sample-hr (for 95 hr)
Average Gas Generation Rate	N/A	0.7 ml/sample-hr	1.8 ml/sample-hr
Rates on a Per kg Settled Sludge Basis			
Average Gas Generation Rate	N/A	**27 ml/kg settled sludge-day**	**59 ml/kg settled sludge-day**
MaximumGas Generation Rate	**(gas pocket)**	**61 ml/kg settled sludge-day**	**150 ml/kg settled sludge-day**

N/A – not applicable.

The larger relative volume of the vapor space to sludge in the KC-2/3 P250-L test compared to the smaller-scale tests (e.g., KC-2/3 P250 40), about 10:1, may be responsible for the delayed onset of the linear kinetics region. The additional vapor space may be diluting the hydrogen concentration necessary to form the reactive uranium hydride layer.

The apparent lack of an induction period for samples 96-05 and 96-06 may partially be attributed to differences in how the samples were handled. The KC-2/3 P250 material was briefly exposed to air during the wet sieving process before the gas generation testing. This exposure to air may have contributed to the duration of the induction period.

The gas generation rates of KC-2/3 P250 small-scale tests during the linear phase were 4600, 1600, 440, and 82 ml/kg settled sludge-day at 95°C, 80°C, 60°C, and 40°C, respectively. The projected rate at 35°C based on the Arrhenius equation (Figure 4.2), 53 ml/kg settled sludge-day, is comparable to the average rates observed for the 96-05 and 96-06 samples at 35°C. However, the KC-2/3 P250 sample only represents the fraction (~25 wt%) of the sample containing the particles greater than 250 μm, while the 96-05 and 96-06 samples represented the entire samples. On a whole sample basis, the average gas generation rates from 96-05 and 96-06 are two to four times greater than what would be expected from the whole KC-2/3 sample (i.e., accounting for the 75% of the sample made up of the essentially

unreactive particles less than 250 μm). On a whole sample basis at the maximum observed gas generation rate for 96-06 (150 ml/kg settled sludge-day, for ~95 hours), the gas generation rate for 96-06 was about 11 times greater than what would be expected from an equivalent mass of KC-2/3 (whole) sludge at 35°C. Therefore, for a period of time, 96-06 was much more reactive than the KC-2/3 sludge. This higher apparent reactivity of these individual samples may have been the result of a higher uranium metal content and/or finer metallic particles (i.e., greater surface area). These results show the potential of individual samples to deviate from the gas generation rate derived from a composite sample (i.e., KC-2/3 was created from sample material collected from six locations). [Long-term gas generation studies were not performed with canister sludge in 1996. Recent gas generation testing in 2000 included a longer-term test with a sample of the 96-06 material. After storage at room temperature for 4 years, the 96-06 sludge showed no propensity for any gas generation. Details on the results of this test will be included in the Series II Gas Generation Testing report.]

In summary, while the compositions and average rates (considering the temperature differences) are comparable for the 96-05 and 96-05 samples and the KC-2/3 P250 test at 40ºC, on a whole sample basis, the 96-05 and 96-06 samples were significantly more reactive over initial periods of time and exhibited little or no induction period. While several of the individual samples exhibited a higher apparent reactivity than KC-2/3 canister sludge, several of the other canister samples collected in 1996 generated little or no gas. The KC-2/3 canister material was a fairly large composite (several kilograms) created from sludge collected from 10 sampling locations, and its gas generation behavior was monitored for more than 3000 hours. The gas generation behavior of KC-2/3 is expected to best represent nominal canister sludge collected from canisters containing moderately and severely damaged fuel.

4.6 Evaluation of Reaction Surface Area and Size of the Uranium Metal Particles in KE Canister Sludge Sample KC-2/3 P250

Evaluations of the reaction surface area per unit mass of settled sludge were performed using the results from the gas generation testing with sample KC-2/3 P250. The uranium metal surface area to volume ratio is an important parameter for predicting heat and gas generation rates in the K Basin sludge from the reaction of uranium metal with water. The Spent Nuclear Fuel Project Technical Databook (Reilly 1998) provides reaction rates for the KE and KW Basin fuel with water. For design basis and safety basis calculations, the rate is multiplied by a factor (i.e., the reactivity enhancement factor). A portion of this reactivity enhancement factor is to account for uncertainties associated with the reaction surface area. Consequently, analysis of the surface area to sludge mass ratio can potentially decrease some of the conservatism in the reaction rate (Reilly 1998) and the reactivity enhancement factor.

In addition to the reaction surface area evaluation, the measured uranium metal corrosion rate (from gas generation data) was compared to the rates predicted by the rate equation given by Reilly (1998) as a function of the initial metallic uranium particle size. This comparison gives an indication of the initial uranium particle size distribution within the KC-2/3 P250 sludge sample.

From the gas generation rate data collected during the second gas sampling event from KC-2/3 P250-80, the uranium metal reaction rate was calculated to be 0.26 mg uranium metal/gram settled sludge-hour. The second sampling event was used since it best represented the linear portion of the gas generation rate curve. The first sampling event included an induction period. After the second sampling event, the gas generation rates began to decrease, indicating that some uranium metal particles were either oxidized to

extinction or no longer participated in gas generation reactions (e.g., uranium metal particles may have become coated). The kinetic behavior of the KC-2/3 P250 materials is examined in Section 4.2.1.

Based on Reilly (1998) and Pajunen (1999), the reaction rate of uranium with water to form UO_2 by Reaction 1 is:

$$\log \text{rate}\left(\frac{\text{mg wt gain}}{\text{cm}^2 \cdot \text{hr}}\right) = 7.634 - \frac{3016}{\text{T}} \qquad \text{(Rate 1)}$$

Solving for uranium oxidation (corrosion rate) at 80°C:

$$\text{rate}\left(\frac{\text{mg U oxidized}}{\text{cm}^2 \cdot \text{hr}}\right) = \frac{238}{32} \times 10^{7.634} \times 10^{\frac{-3016}{(273+80)}} = \frac{0.915 \text{ mg U}}{\text{cm}^2 \cdot \text{hr}}$$

Using the reaction rate from Reilly (1998) and the measured reaction rate determined from the tests with KC-2/3 P250 at 80°C, the effective uranium metal surface area (i.e., the uranium metal surface area available to react with water) can be calculated:

$$\text{Calculated U metal surface area} = \frac{\left[\frac{\text{measured reaction rate}}{\text{mass settled sludge, g}}\right]}{[\text{Reilly (1998) corrosion rate, surface area basis}]}$$

$$= \frac{\left[\frac{0.26 \text{ mg U}}{\text{g settled sludge} \cdot \text{hr}}\right]}{\left[\frac{0.915 \text{ mg U}}{\text{cm}^2 \cdot \text{hr}}\right]}$$

$$= \frac{0.28 \text{ cm}^2}{\text{g settled sludge}} \text{ (for KC-2/3 P250).}$$

With the surface area to sludge mass ratio, and the uranium content and particle size distribution of the sludge, the distribution of uranium metal reactive surface area with respect to the sludge particles can be evaluated. In the analysis provided below, the calculated reaction surface area is compared with the theoretical surface area determined by assuming all of the uranium particles are perfectly spherical. An understanding of how the actual surface area compares to the surface area of spheres is very important, since the uranium particles are modeled as perfect spheres within the thermal stability safety analyses for transporting and storing the sludge (Plys et al. 1999).

In Section 4.2.2 of this report, gas generation results indicate that KC-2/3 P250-80 originally contained approximately 6.4% (by weight) uranium metal on a settled-sludge basis. Furthermore, results from dissolution enthalpy measurements (Bredt et al. 1999) indicate that KC-2/3 P250 may contain 4% to 9% uranium metal (settled-sludge basis). If KC-2/3 P250-80 contains 6.4% uranium metal, and all uranium metal in the sample exists as discrete spherical particles, and the uranium metal particles follow the overall sample particle size distribution (PSD), then the theoretical surface area of the uranium particles

can be calculated per unit mass of settled sludge. In Table 4.30, the theoretical surface area of the uranium particles in 1 gram of KC-2/3 P250 is calculated.

As shown in Table 4.30, each gram of settled sludge theoretically will have approximately 0.40 cm^2 of uranium metal surface area. As shown above, the reaction surface area calculated from the gas generation testing and the rate equation for the uranium reaction with oxygen-free water (Reilly 1998) is 0.28 cm^2/gram settled sludge for KC-2/3 P250. The calculated surface area thus is 70% of the theoretical value determined from assuming spherical particles. However, if all assumptions were correct, and the rate equation used (Reilly 1998) accurately represented the reaction rate obtained, the measured surface area would be expected to be one to three times larger than calculated for spheres. This is because actual uranium fuel fragments have irregular surfaces and exhibit a surface roughness that should yield a greater surface area than a perfect sphere of identical mass.

Table 4.30. Theoretical Uranium Metal Surface Area for KC-2/3 P250 – 1 g Settled Sludge (assuming 6.4% U metal content, and spherical particles)

Particle Size Distribution of KC-2/3 P250 (Bredt et al. 1999)			Number of U Metal Particles per g Settled Sludge	Surface Area of Spherical U Metal Particles per g Settled Sludge, cm^2
Tyler Screen Size No.	Mass Fraction of Sample Retained on Tyler Screen	Avg. Diameter of Particles Retained on Screen, µm		
5	0.032	5200	0.0014	0.0012
12	0.12	2700	0.039	0.0089
32	0.21	960	1.5	0.044
60	0.64	375	78	0.34
Total	1.0	---	79	0.40

The results of this surface area evaluation can be interpreted in several ways. First, the rate equation for the uranium reaction with oxygen-free water (Reilly 1998), which is based on a correlation of literature data, agrees fairly well with the measured rate if the actual uranium particles closely resemble spheres. Eliminating the rate enhancement factor should be considered when using the rate equation given by Reilly (1998) to describe the behavior of the uranium particles in sludge.

A second interpretation of the results of the surface area evaluation is that incorrect assumptions may have been used (e.g., uranium PSD follows the overall sample PSD). Assumptions used for this analysis that could affect the interpretation of the surface area results are listed in Table 4.31. For example, the surface area could be affected by a change in the assumption that the actual uranium metal content in the vessel containing KC-2/3 P250-80 is 3% instead of the assumed value of 6.4%. With the 3% metal concentration, the theoretical surface area of spherical uranium particles would be only 0.18 cm^2/gram settled sludge, yielding in turn a measured surface area about 1.5 times larger than calculated for spheres.

Another type of analysis was used to compare the measured corrosion rate against the rate given by Reilly (1998). For this analysis, the uranium corrosion rates observed for the KC-2/3 P250 samples at the 40°C, 60°C, 80°C, and 95°C test temperatures (the latter for the test begun at 40°C) were compared with the corrosion rates expected for uranium metal spheres of varying sizes in water. As shown above (Rate 1), the expected rates as a function of temperature may be expressed as weight gain, according to Reaction 1,

Table 4.31. Assumptions for Surface Area Evaluation/Calculations

Number	Assumption
1	For determining the theoretical uranium metal surface area, it was assumed that the distribution of uranium metal particles followed that of the overall sample. [Data in Bredt et al. (1999) show that dry particle density increases as particle size decreases for KC-2/3 P250. This finding would indicate that higher concentrations of uranium are probably associated with smaller particles. However, the dry particle density data cannot be used to distinguish uranium metal from uranium oxide particles.]
2	All uranium metal in sample KC-2/3 P250-80 contributed to the gas generation rate, which was used to calculate the uranium metal reaction rate (i.e., metallic uranium reactions with water were not limited by mass transfer resistances).
3	The gas generated that was represented by the second gas sampling from KC-2/3 P250-80 occurred under oxygen-free conditions. [This assumption is partially justified by the fact that no oxygen was found in the gas sample; however, the presence of argon indicates some air was present for a portion of this gas generation period.]
4	The rate equation given by Reilly (1998), derived from a correlation of data found in the literature, is applicable to uranium metal particles in K Basin Sludge.
5	KC-2/3 P250-80 contains 6.4% by weight uranium metal (settled-sludge basis). [Assumption based on Section 4.2.1 and Bredt et al. (1999).]
6	The surface area of uranium metal particles should be one to three times greater than that of a sphere of equal mass (due to surface irregularities). This assumption has not been validated.

caused by the uptake of oxygen on uranium to form UO_2 (Reilly 1998). The rate equation may be restated in terms of linear penetration rate into the uranium by dividing the rate given in terms of surface area by the density of uranium (19.05 g/cm^3) and multiplying by the gravimetric factor relating uranium metal mass to oxygen mass (238/32):

$$\log \text{rate } (\mu\text{m penetration/hour}) = 8.226 - 3016/T(K)$$

The linear penetration corrosion rates are 0.0389, 0.147, 0.481, and 1.071 μm/hour at 40°C, 60°C, 80°C, and 95°C, respectively. At these rates, the times to corrode a 1000-μm-diameter sphere (500-μm corrosion penetration to reach the center) are about 13,000, 3400, 1000, and 470 hours, respectively.

The calculated percentages of uranium metal corroded for nominal 250-, 500-, 750-, 1000-, and 1500-μm spheres at 40°C, 60°C, 80°C, and 95°C as functions of time are given in Figures 4.6 through 4.9, respectively. Note that the predicted reaction rates of the various uranium metal spheres are nearly linear over the first 20-30% of reaction. This is because the gas generation rate, which is proportional to the sphere surface area (and radius squared), changes more slowly than the total fraction of gas evolved, which is proportional to sphere volume (and radius cubed). This near linearity of the initial rate was characteristic of the gas generation rates observed in the present testing.

The corrosion rates modeled by spheres in Figures 4.6 through 4.9 are compared with the uranium corrosion rates, based on H_2 generation observed in the KC-2/3 P250 small-scale tests run at the same respective temperatures. The contributions to corrosion by nitrogen and oxygen represent less than 2.5% of the total uranium corrosion in all cases and are neglected in the present analysis. The KC-2/3 P250 reaction time data plotted in the figures also have been corrected by subtracting the observed

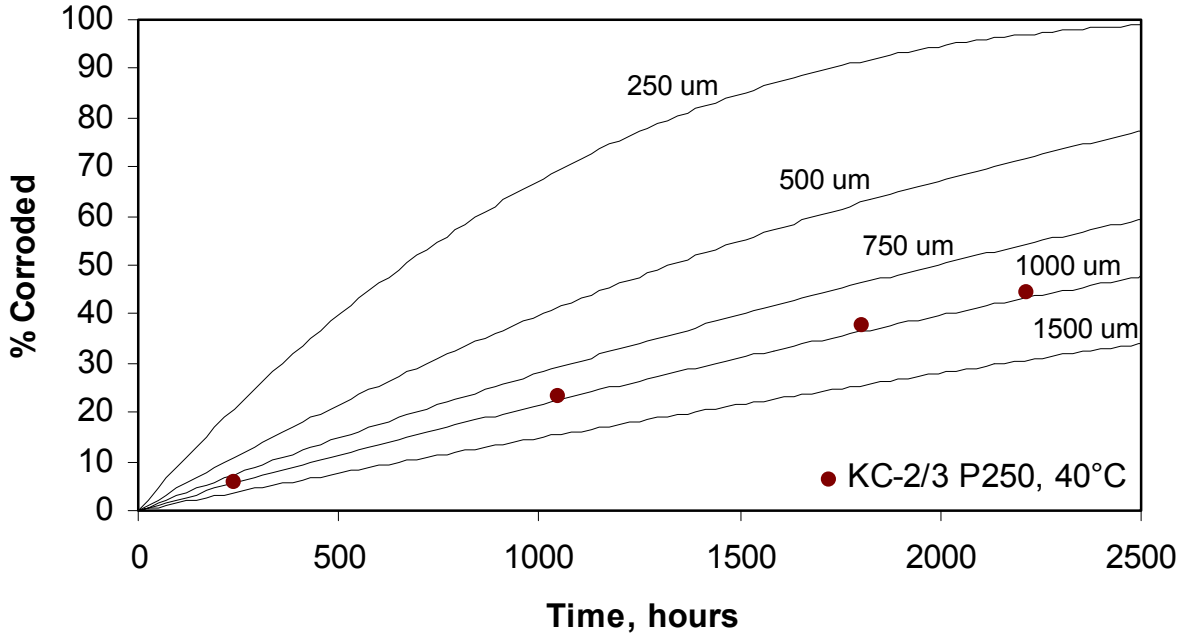

Figure 4.6. Uranium Metal Corrosion in Water Observed in the KC-2/3 P250 Test at 40°C Compared with Uranium Metal Sphere Corrosion Rates Under Similar Conditions

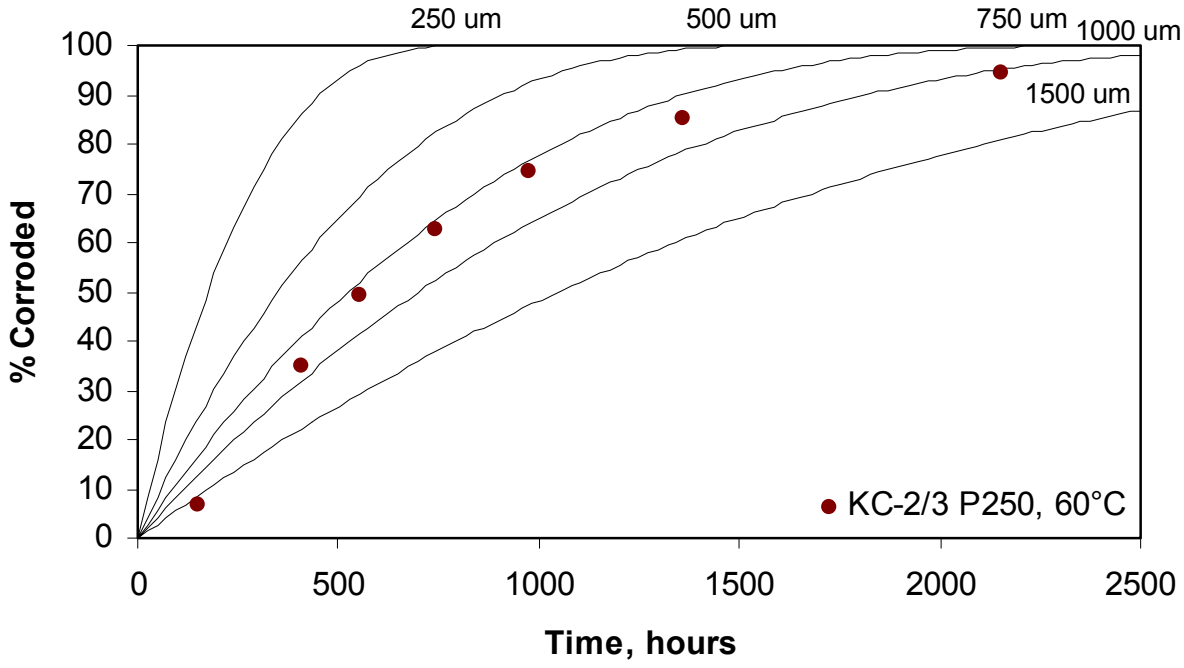

Figure 4.7. Uranium Metal Corrosion in Water Observed in the KC-2/3 P250 Test at 60°C Compared with Uranium Metal Sphere Corrosion Rates Under Similar Conditions

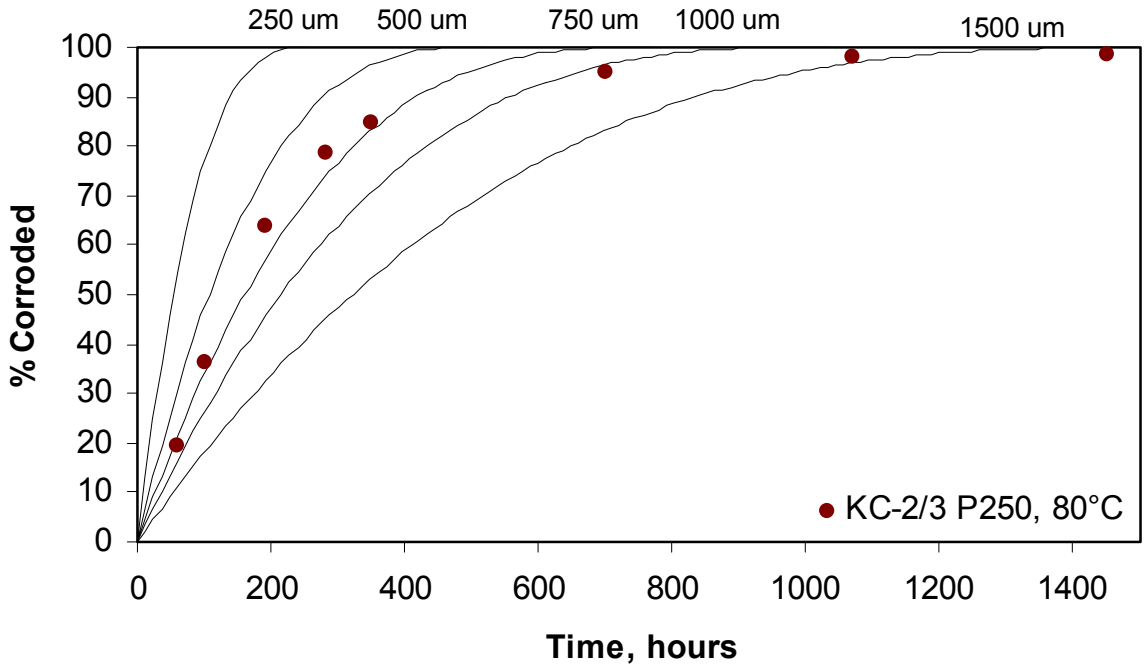

Figure 4.8. Uranium Metal Corrosion in Water Observed in the KC-2/3 P250 Test at 80°C Compared with Uranium Metal Sphere Corrosion Rates Under Similar Conditions

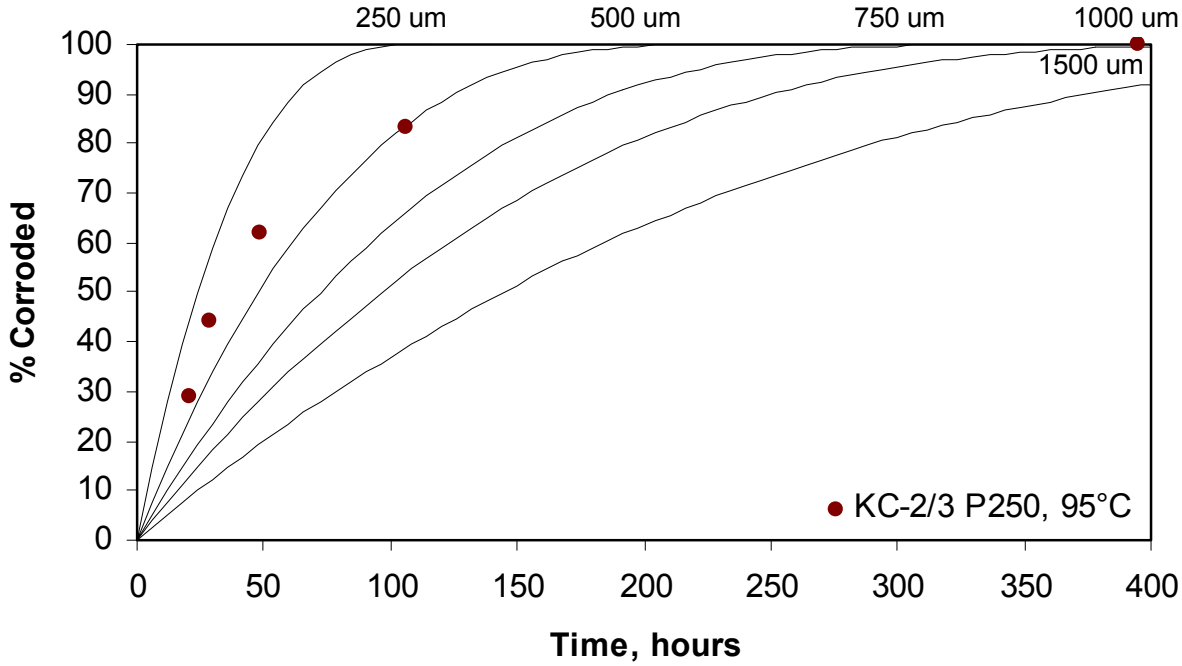

Figure 4.9. Uranium Metal Corrosion in Water Observed in the KC-2/3 P250 Test at 95°C Compared with Uranium Metal Sphere Corrosion Rates Under Similar Conditions

26.9-, 205-, and 1340-hour induction times at 40°C, 60°C, and 80°C. Zero induction time was used for the 95°C results because the reaction already was underway in the 40°C test when the temperature was increased to 95°C.

As shown in Figures 4.6 through 4.8, the observed KC-2/3 P250 corrosion rates at 40°C to 80°C are consistent with the rates expected from a distribution of uranium metal particles in the size range between 500 μm and 1500 μm. The 95°C data (Figure 4.9) are consistent with particles in the range ~250 to 500 μm. The lower size distribution at 95°C may be attributed to the predicted 170-μm (in diameter) corrosion incurred by 2200 hours of reaction (after the induction time) at 40°C.

The kinetics of the corrosion of a spherical particle or a cube (or collection of equal-sized spherical or cubic particles) also may be expressed analytically for reactions, such as that of uranium, whose rates are proportional to the instantaneous surface area of the solid being corroded. The relevant rate law for spheres (derivation given in Appendix D) has the following inverse cubic dependence:

$$(1-f)^{\frac{1}{3}} = 1 - \frac{kt}{r_0 \rho} = 1 - \frac{k't}{r_0}$$

in which f is the fraction reacted at time t, r_0 is the initial radius in μm, ρ is the material density in μg/μm^3, and k is the areal reaction rate expressed in μg/μm^2-hour. Dividing the areal corrosion rate, k, by the material density, ρ, gives k', the linear penetration corrosion rate in μm/hour. A plot of $(1- f)^{1/3}$ versus time (in hours) has a slope of k'/r_0 (or $k/r_0\rho$) and intercept on the vertical axis of 1. The radii of hypothetically spherical uranium metal particles thus may be calculated by dividing the known uranium metal linear penetration corrosion rate at the experimental temperature by the slope of the inverse cubic kinetics plot.

The corrosion rate of uranium metal by water is reflected in the H_2 gas generation rate. The observed H_2 gas generation data for the KC-2/3 P250 small-scale tests, abstracted from Tables 4.7 through 4.9, are presented in Table 4.32. These data are plotted according to the inverse cubic corrosion rate equation in Figure 4.10. As seen in Figure 4.10, the reactions at 60°C, 80°C, and 95°C followed the surface-area-dependent rate law to the consumption of about 75% of the uranium. The test at 40°C was following the rate law through about 40% completion when the temperature of the test apparatus was boosted to 95°C. The associated best-fit equations for the initial linear regions of the plots in Figure 4.10 have slopes of -0.0000803/hour, -0.000366/hour, -0.00142/hour, and -0.00461/hour at 40°C, 60°C, 80°C, and 95°C, respectively.

As shown previously in this section, the linear penetration rates of uranium metal corrosion by water at 40°C, 60°C, 80°C, and 95°C are 0.0389, 0.147, 0.481, and 1.071 μm/hour. Dividing the linear penetration corrosion rates by the respective slopes from Figure 4.10 provides an estimate of the radii of the initial hypothetical spherical uranium metal particles. The particle diameters (2 x radii) thus calculated are 970, 810, and 680 μm for the test data at 40°C, 60°C, and 80°C, respectively. The diameter derived from the 95°C test data is about 470 μm. As before, the diameter from the 95°C test is lower because the corrosion that occurred when this system was at 40°C removed about 170 μm from the initial diameter. The initial particle diameter in the 40/95°C test thus was about 470 + 170 = 640 μm. As shown in Appendix D, cubic particles would have the same dimensions on a side as the diameters of the spheres.

The actual size of the initial uranium metal particles is not monodisperse because the plots deviate from linearity above 75% reaction. The deviation, in the direction of lower rate, indicates the presence of some

Table 4.32. Hydrogen Gas Generation Rate Data for Small-Scale Tests of KC-2/3 P250

40°C			
Run Time, hr	**Reaction Time (-1340 hr induction), hr**	**H_2, moles**	**Fraction, f, of total H_2**
425	-915	2.12E-7	0.000014
770	-570	1.89E-6	0.00012
1195	-145	1.78E-4	0.012
1577	237	8.50E-4	0.056
2387	1047	3.49E-3	0.230
3146	1806	5.73E-3	0.377
3556	2216	6.75E-3	0.444
60°C			
Run Time, hr	**Reaction Time (-205 hr induction), hr**	**H_2, moles**	**Fraction, f, of total H_2**
353	148	8.19E-4	0.067
612	407	4.26E-3	0.346
762	557	6.06E-3	0.493
946	741	7.68E-3	0.624
1181	976	9.13E-3	0.742
1563	1358	1.05E-2	0.854
2361	2156	1.16E-2	0.943
80°C			
Run Time, hr	**Reaction Time (-26.9 hr induction), hr**	**H_2, moles**	**Fraction, f, of total H_2**
89	62	1.43E-3	0.196
130	103	2.64E-3	0.362
219	192	4.65E-3	0.638
309	282	5.71E-3	0.783
376	349	6.19E-3	0.849
728	701	6.93E-3	0.951
1123	1096	7.13E-3	0.978
1500	1473	7.19E-3	0.986
2265	2238	7.24E-3	0.993
95°C			
Run Time, hr	**Reaction Time (0 hr induction), hr**	**H_2, moles**	**Fraction, f, of total H_2**
3556.3	0.0	6.75E-3	0.000
3574.7	18.3	9.18E-3	0.288
3585.3	29.0	1.05E-2	0.444
3605.3	49.0	1.20E-2	0.621
3662.3	106.0	1.38E-2	0.834
3951.0	394.7	1.52E-2	1.000

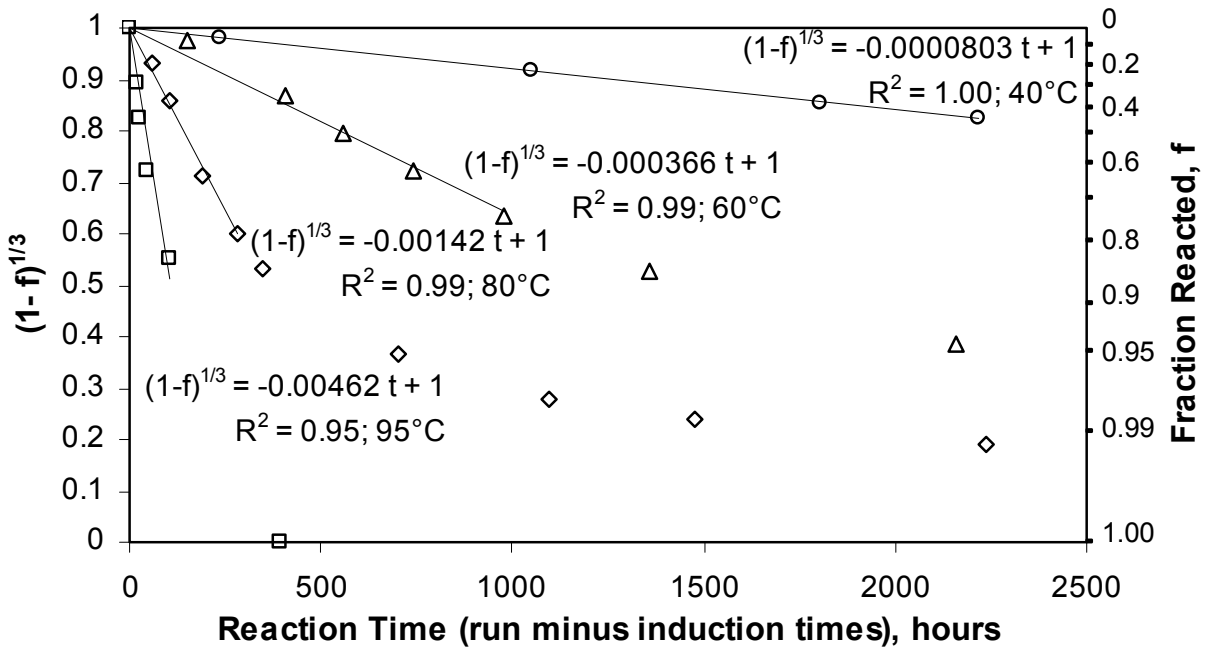

Figure 4.10. Inverse Cubic Function Uranium Metal Corrosion Kinetics Plot in the KC-2/3 P250 Tests

larger particles. Similarly, the uranium metal particles likely are not perfect spheres or cubes. However, uranium metal corrosion in the KC-2/3 P250 sludge sample seems to be well modeled as spheres or cubes of about 800-μm axial dimension. [Note, sludge containing 7.4 wt% uranium metal – all existing as 800-μm spheres – will initially provide 0.29 cm^2/gram of reaction surface area (i.e., approximately equal to the calculated uranium metal surface area provided earlier in this discussion).]

By use of the Arrhenius equation, the logarithm of the observed rate $k/r_0\rho$ may be plotted against inverse absolute temperature to determine the activation energy (E_a) of the uranium corrosion reaction. Data from the tests at 40°C, 60°C, and 80°C were used; the 95°C data could not be used because the prior reaction at 40°C had altered the radii of the particles. The fit was excellent ($R^2 = 1.000$), and the E_a derived from the slope found to be 15.8 kcal/mole (66.0 kJ/mole). This value is consistent with the 16.1 kcal/mole E_a value found for the same reaction based on the technical literature (Pajunen 1999) and the 15.1 kcal/mole value found for the KC-2/3 P250 tests at all four temperatures based on maximum H_2 gas generation rates (Figure 4.2).

The estimate of the initial particle size for the uranium metal in KC-2/3 P250 (i.e., 500 to 1500 μm) is in general agreement with earlier particle size observations of disintegrated spent nuclear fuel samples during thermogravimetric analysis (TGA) testing (Appendix E). Microcracks were observed in the uranium fuel that was sectioned from corroded/damaged regions of the fuel that had been stored in the K Basins. During the TGA testing, spent fuel samples were subjected to dry air and moist helium atmospheres to temperatures up to 160°C. In this environment, three of the fuel samples disintegrated and were subsequently examined to determine the PSD. The average particle sizes (number average) for the disintegrated samples were: 852 μm (standard deviation of 729 μm); 2241 μm (standard deviation of 1201 μm); and 1160 μm (standard deviation of 896).

For the reaction surface area evaluation, it was assumed that the metallic uranium particles followed the same PSD as the entire KC-2/3 P250 sample (e.g., 64% of material mass was between 250 μm and 500 μm). The analysis above shows that this assumption may be very conservative with respect to the reactivity of the sludge, since the metallic uranium particles appear to be larger than those of the bulk samples.

In conclusion, this reaction surface area and particle evaluation indicates that the reaction rate given for uranium metal with oxygen-free water in the Spent Nuclear Fuel Project Technical Databook (Reilly 1998) may be slightly conservative for uranium metal particles in sludge, and, within the stated assumptions (e.g., PSD of uranium = PSD of sludge), a reaction enhancement factor probably is not needed.

4.7 Evaluation of CO_2 Production Kinetics Data for the Small-Scale Tests KC-2/3 M250, KC-4 M250, KC-4 P250, KC-5 M250, and KC-5 P250

As shown in Section 4.3, the gas produced for the small-scale tests KC-2/3 M250, KC-4 M250, KC-4 P250, KC-5 M250, and KC-5 P250 was predominantly CO_2. The CO_2 likely arises from the reaction of solid phase calcite and schoepite (Reaction 5). Because the reaction involves the disappearance of these solid phases, the kinetics may be surface-area-dependent and subject to an inverse cubic rate law similar to that described in Section 4.6 for uranium metal corrosion. Accordingly, total gas generation data for these five tests at 95°C were plotted in the same manner as shown in Figure 4.10. The 95°C data were used because the reaction rates were higher and the gas product richer in CO_2 than was observed at 80°C. Data from the first several hours following the temperature elevation to 95°C were not used because of exsolution of gas dissolved during the time at the lower hot cell temperature.

The inverse cubic relationship plots for the 95°C data from tests KC-2/3 M250, KC-4 M250, KC-4 P250, KC-5 M250, and KC-5 P250 are shown in Figures 4.11 through 4.15, respectively. Also given on the plots are the equations for the best-fit line through the data and the resulting correlation coefficient, R^2.

Several observations are made concerning these results. First, the variability ("noise") of the data in all cases increases with reaction time. This is expected because the absolute rate of gas production decreases at advanced times and becomes more subject to random pressure and temperature fluctuations. Similarly, the variability of the data from test to test also increases with decreasing amount of total gas produced. To the extent of measurement accuracy, the reactions follow the inverse cubic rate law to 90% or greater reaction completion [i.e., $(1-f)^{1/3} < 0.4$]. Finally, all tests show comparable slopes (i.e., k'/r_0 or $k/r_0\rho$) ranging from $(0.74 \text{ to } 1.22)\times10^{-3}$/hour at 95°C.

Because the rate-determining mineral (calcite or schoepite in the case of Reaction 5), the associated densities of the minerals, and the mass-specific rates k or k' are unknown, the nominal particle size of the rate-determining material cannot be determined. However, the consistency of the slopes suggests that the same material, of essentially the same particle size, controls the CO_2-generating reaction rate in all five tests. Because the original test materials arose from diverse areas of the KE Basin (floor, near the canisters, and within the canisters), the rate-determining reactant is broadly distributed, though with varying concentrations, in the KE Basin.

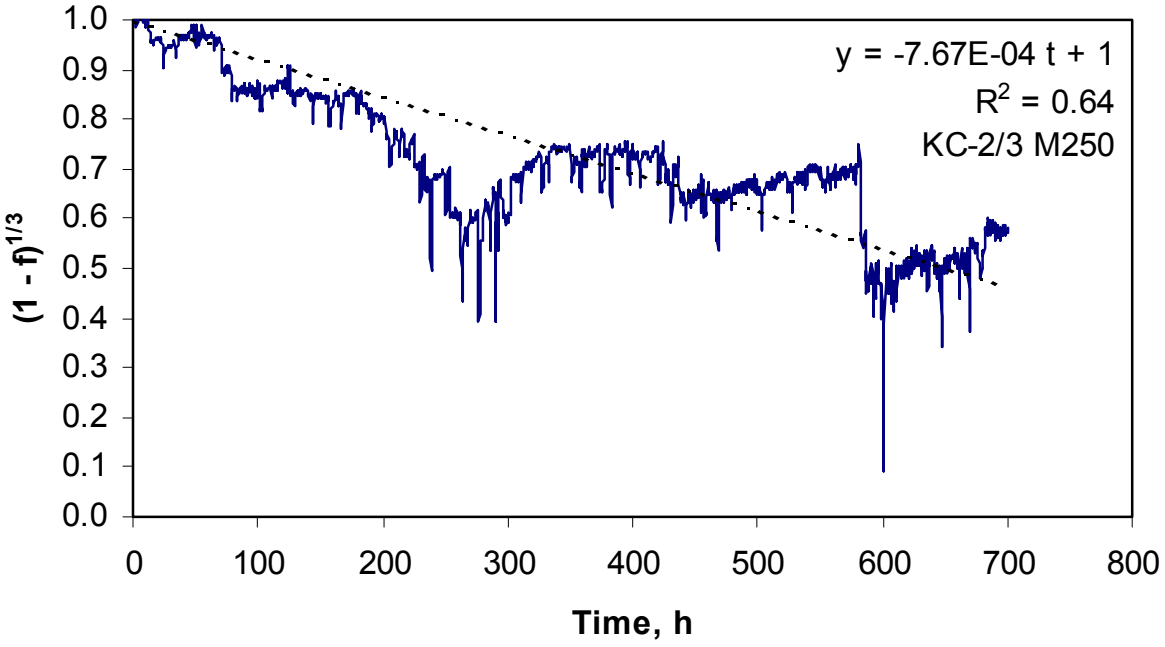

Figure 4.11. Inverse Cubic Function CO_2 Generation Kinetics Plot in the KC-2/3 M250 Test at 95°C

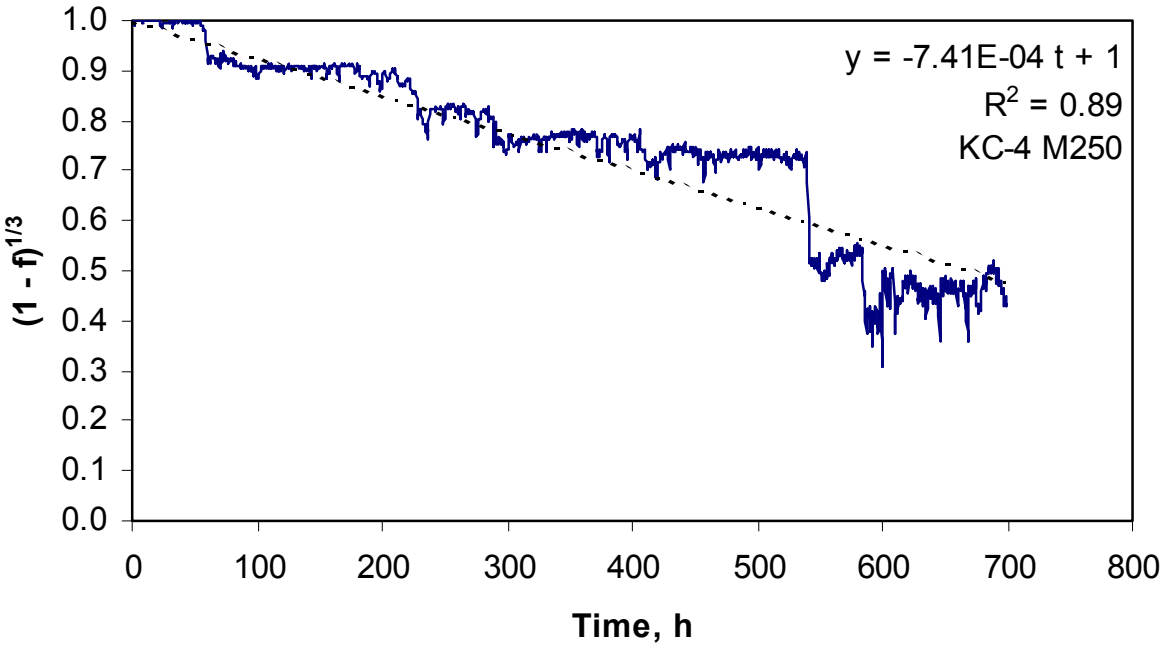

Figure 4.12. Inverse Cubic Function CO_2 Generation Kinetics Plot in the KC-4 M250 Test at 95°C

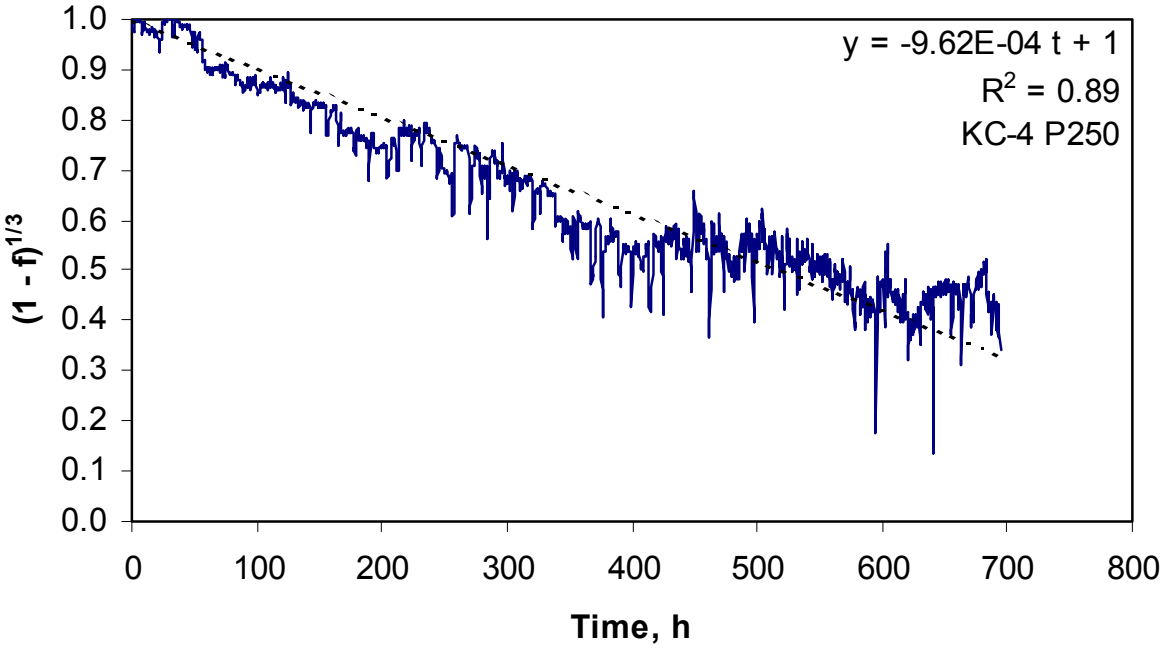

Figure 4.13. Inverse Cubic Function CO_2 Generation Kinetics Plot in the KC-4 P250 Test at 95°C

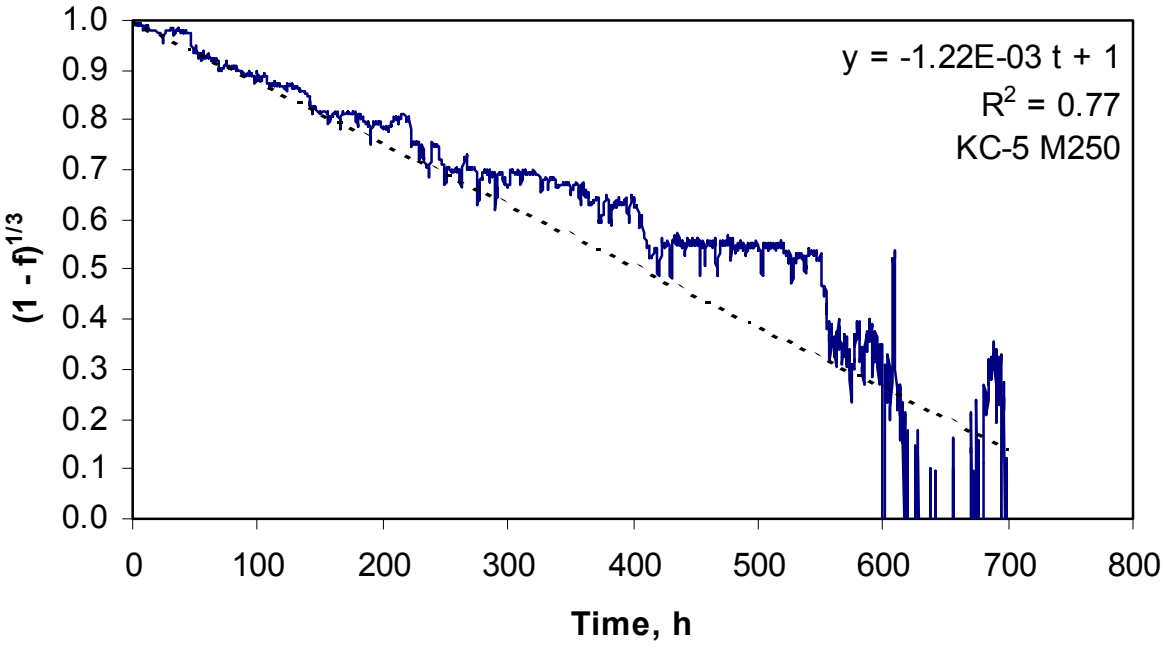

Figure 4.14. Inverse Cubic Function CO_2 Generation Kinetics Plot in the KC-5 M250 Test at 95°C

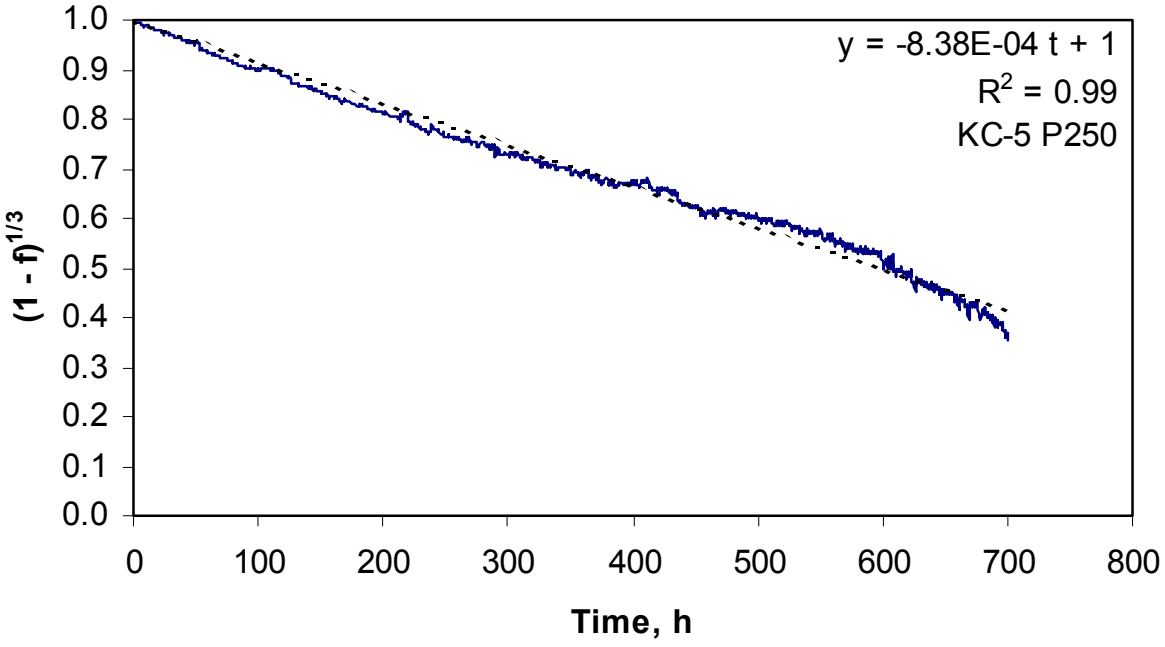

Figure 4.15. Inverse Cubic Function CO_2 Generation Kinetics Plot in the KC-5 P250 Test at 95°C

5.0 References

Bradley, M. J., and L. M. Ferris. 1962. "Hydrolysis of Uranium Carbides between 25 and 100º. I. Uranium Monocarbide." *Inorganic Chemistry* 1(3):683-687.

Bradley, M. J., and L. M. Ferris. 1964. "Hydrolysis of Uranium Carbides between 25 and 100º. II. Uranium Dicarbide, Uranium Metal-Monocarbide Mixtures, and Uranium Monocarbide-Dicarbide Mixtures." *Inorganic Chemistry* 3(2):189-195.

Bredt, P. R., C. H. Delegard, A. J. Schmidt, and K. L. Silvers. 1999. *Testing and Analysis of Consolidated Sludge Sample from 105K East Basin Floor and Canisters.* PNNL-13341, Pacific Northwest National Laboratory, Richland, Washington.

Bryan, S. A., and L. R. Pederson. 1995. *Thermal and Combined Thermal and Radiolytic Reactions Involving Nitrous Oxide, Hydrogen, and Nitrogen in the Gas Phase: Comparison of Gas Generation Rates in Supernate and Solid Fractions of Tank 241-SY-101 Simulated Wastes.* PNL-10490, Pacific Northwest National Laboratory, Richland, Washington.

Bryan, S. A., L. R. Pederson, C. M. King, S. V. Forbes, and R. L. Sell. 1996. *Gas Generation from Tank 241-SY-103 Waste.* PNL-10798, Pacific Northwest National Laboratory, Richland, Washington.

Chen, F., R. C. Ewing, and S. B. Clark. 1999. "The Gibbs Free Energies and Enthalpies of Formation of U^{6+} Phases: An Empirical Method of Prediction." *American Mineralogist* 84:650-664.

Cordfunke, E.H.P. 1969. *The Chemistry of Uranium*, p. 188. Elsevier Publishing Company, Amsterdam, Netherlands.

Finch, R. J. 1997. "Thermodynamic Stabilities of U(VI) Minerals: Estimated and Observed Relationships." In *Scientific Basis for Nuclear Waste Management XX*, pp. 1185-1192, W. J. Gray and I. R. Triay, editors. Materials Research Society, Pittsburgh.

Finch, R. J., and R. C. Ewing. 1991. "Phase Relation of the Uranyl Oxide Hydrates and Their Relevance to the Disposal of Spent Fuel." in *Scientific Basis for Nuclear Waste Management XIV*, pp. 241-246, T. Abrajano, Jr. and L. H. Johnson, editors. Materials Research Society, Pittsburgh.

Finch, R., and T. Murakami. 1999. "Systematics and Paragenesis of Uranium Minerals." In *Uranium: Mineralogy, Geochemistry and the Environment*, pp. 91-180, P. C. Burns and R. Finch, editors. Mineralogical Society of America, Washington, DC.

Johnson, A. B., R. G. Ballinger, and K. A. Simpson. 1994. "Kinetic and Thermodynamic Bases to Resolve Issues Regarding Conditioning of Uranium Metal Fuels." PNL-SA-24458, Pacific Northwest Laboratory, Richland, Washington.

King, C. M., L. R. Pederson, and S. A. Bryan. 1997. *Thermal and Radiolytic Gas Generation from Tank 241-S-102 Waste.* PNNL-11600, Pacific Northwest National Laboratory, Richland, Washington.

Makenas, B. J., T. L. Welsh, R. B. Baker, D. R. Hansen, and G. R. Golcar. 1996. *Analysis of Sludge from Hanford K East Basin Floor and Weasel Pit.* WHC-SP-1182, Westinghouse Hanford Company, Richland, Washington.

Makenas, B. J., T. L. Welsh, R. B. Baker, E. W. Hoppe, A. J. Schmidt, J. Abrefah, J. M. Tingey, P. R. Bredt, and G. R. Golcar. 1997. *Analysis of Sludge from Hanford K East Basin Canisters.* HNF-SP-1201, DE&S Hanford, Inc., Richland, Washington.

Makenas, B. J., T. L. Welsh, R. B. Baker, G. R. Golcar, P. R. Bredt, A. J. Schmidt, and J. M. Tingey. 1998. *Analysis of Sludge from Hanford K West Basin Canisters.* HNF-1728, Rev. 0, Fluor Daniel Hanford, Richland, Washington.

Makenas, B. J., A. J. Schmidt, K. L. Silvers, P. R. Bredt, C. H. Delegard, E. W. Hoppe, J. M. Tingey, A. H. Zacher, T. L. Welsh, R. B. Baker. 1999. *Supplementary Information on K-Basin Sludges.* HNF-2367, Rev. 0, Fluor Daniel Hanford, Richland, Washington.

Marschman, S. C., T. D. Pyecha, and J. Abrefah. 1997. *Metallographic Examination of Damaged N Reactor Spent Nuclear Fuel Element SFEC5,4378*. PNNL-11438, Pacific Northwest National Laboratory, Richland, Washington.

Montenyohl, V. I. 1960. "Corrosion of Uranium." Chapter 7, *Reactor Handbook*, 2nd edition, Vol. I, Materials, C. R. Tipton, Jr., editor. Interscience Publishers, Inc., New York.

Pajunen, A. L. 1999. *Uranium Oxidation Rate Summary for the Spent Nuclear Fuel Project.* HNF-4165, Rev. 0, DE&S Hanford, Inc., Richland Washington.

Pearce, K. L., and S. C. Klimper. 2000. *105-K Basin Material Design Basis Feed Description for Spent Nuclear Fuel Project Facilities, Volume 2, Sludge.* HNF-SD-SNF-TI-009, Rev. 3, Fluor Hanford, Inc., Richland, Washington.

Plys, M. G., B. Malinovic, and D. R. Duncan. 1999. *IWTS Metal-Water Reaction Rate Evaluation.* (Fauske and Associates Report 99-26). SNF-4266, Rev. 0, DE&S Hanford, Inc., Richland, Washington.

Pitner, A. L. 1999a. *K East Basin Sludge/Sampling 1999 Campaigns.* HNF-4746, Rev. 0, Numatec Hanford Corporation, Richland, Washington.

Pitner, A. L. 1999b. *Revised Estimates of K East Basin Canister Type Distribution and Sludge Content.* HNF-5362, Rev. 0, Numatec Hanford Corporation, Richland, Washington.

Reilly, M. A. 1998. *Spent Nuclear Fuel Project Technical Databook.* HNF-SD-SNF-TI-015, Rev. 6, DE&S Hanford, Inc., Richland Washington.

Sandino, M., C. Amaia, and B. Grambow. 1994. "Solubility Equilibria in the U(VI)-Ca-K-Cl-H_2O System: Transformation of Schoepite into Becquerelite and Compreignacite." *Radiochimica Acta* 66/67:37-43.

Schmidt, A. J., C. H. Delegard, K. L. Silvers, P. R. Bredt, C. D. Carlson, E. W. Hoppe, J. C. Hayes, D. E. Rinehart, S. R. Gano, and B. M. Thornton. 1999. *Validation Testing of the Nitric Acid Dissolution Step Within the K Basin Sludge Pretreatment Process.* PNNL-12120, Pacific Northwest National Laboratory, Richland, Washington.

Sowder, A. G., S. B. Clark, and R. A. Fjeld. 1996. "The Effect of Silica and Phosphate on the Transformation of Schoepite to Becquerelite and Other Uranyl Phases." *Radiochimica Acta* 74:45-49.

Sowder, A. G., S. B. Clark, and R. A. Fjeld. 1999. "The Transformation of Uranyl Oxide Hydrates: The Effect of Dehydration on Synthetic Metaschoepite and Its Alteration to Becquerelite." *Environmental Science and Technology* 33:3552-3557.

Vochten, R., and L. Van Haverbeke. 1990. "Transformation of Schoepite into the Uranyl Oxide Hydrates: Becquerelite, Billietite and Wölsendorfite." *Mineralogy and Petrology* 43:65-72.

Wagman, D. D., W. H. Evans, V. B. Parker, R. H. Schumm, I. Halow, S. M. Bailey, K. L. Churney, and R. L. Nuttall. 1982. "The NBS Tables of Chemical Thermodynamic Properties - Selected Values for Inorganic and C_1 and C_2 Organic Substances in SI Units." *Journal of Physical and Chemical Reference Data* 11 (Supplement 2).

Weakley, E. A. 1979. *Fuels Engineering Technical Handbook.* UNI-M-61, UNC Nuclear Industries, Richland, Washington.

Wilkinson, W. D. 1962. *Uranium Metallurgy,* p. 1411. Interscience Publishers, New York.

Wronkiewicz, D. J., J. K. Bates, S. F. Wolf, and E. C. Buck. 1996. "Ten-Year Results from Unsaturated Drip Tests with UO_2 at 90°C: Implications for the Corrosion of Spent Nuclear Fuel." *Journal of Nuclear Materials* 238:78-95.

Appendix A

Verification of the Gas Generation System Reliability and Performance

Appendix A

Verification of the Gas Generation System Reliability and Performance

To ensure that the moles of gas could be measured correctly when the reaction vessel temperature was changed, a known quantity of gas was measured at various reaction vessel temperatures. The reaction vessel temperature was changed from a starting temperature of 60ºC to 90ºC and finally to 120ºC, then decreased through 90ºC to 60ºC as the final temperature. This temperature range encompasses the experimental range that will be encountered during gas generation tests. The pressure increased as the temperature increased, following the Ideal Gas Law. The moles of gas within the closed reaction system remained constant throughout the experiment.

The temperature of a reaction vessel attached to the gas manifold line in the same configuration used for gas generation experiments is shown in Figure A.1. The temperature of the reaction vessel was initially regulated at 60ºC for approximately 20 hours. The reaction vessel temperature then was quickly increased to 90ºC and allowed to stay at this temperature for approximately 5 hours. The temperature again was increased to 120ºC and allowed to stay at that temperature for several days. The temperature then was lowered to 90ºC for a short time (about 1 hour), followed by a return to the original temperature of 60ºC. The pressure of the gas in the system increased as the temperature increased and decreased as the temperature decreased, as expected for a fixed volume system; the pressure data are shown in Figure A.2. Comparing Figures A.1 and A.2, we see that the pressure tracks the temperature very well.

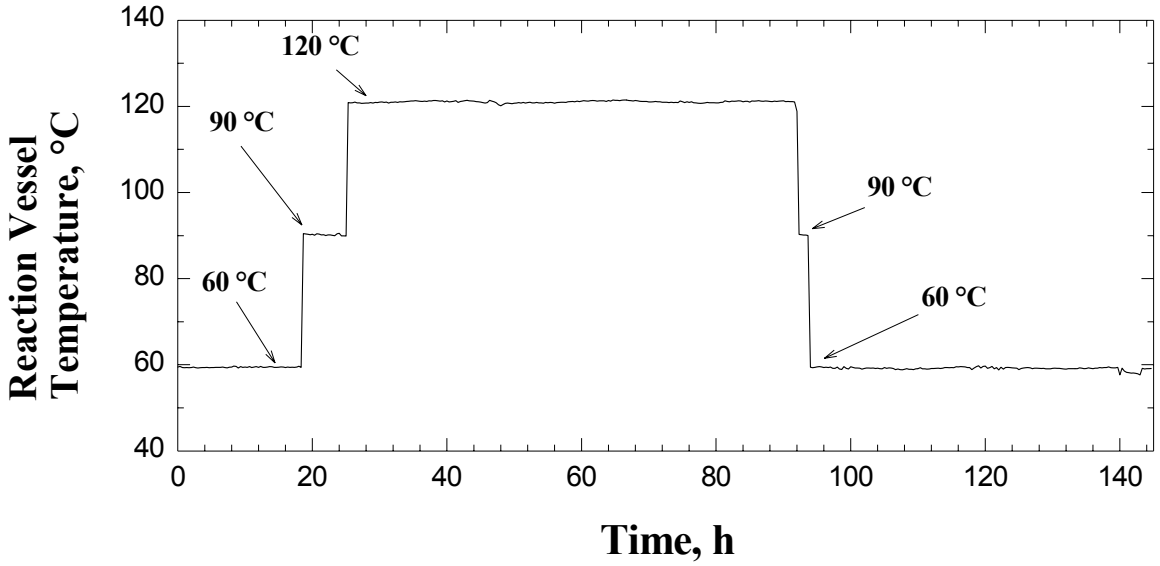

Figure A.1. Reaction Vessel Temperature During Initial Testing (Temperature of the reaction vessel was changed from 60ºC to 90ºC to 120ºC and back to 60ºC during this experiment.)

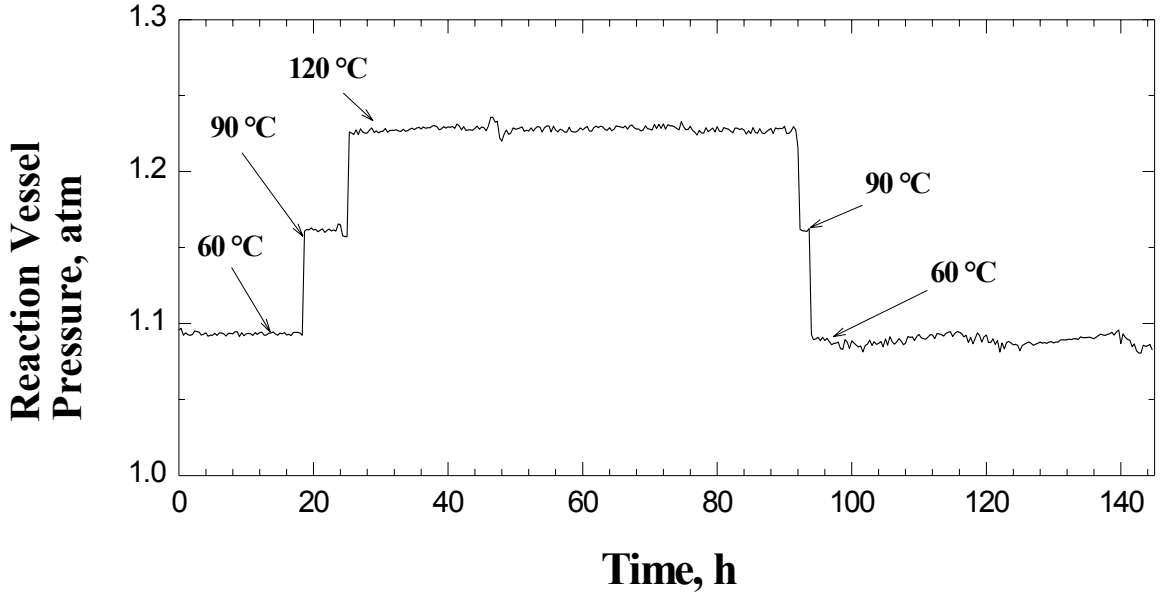

Figure A.2. Reaction Vessel Pressure During Initial Testing (Temperature of the reaction vessel was changed from 60ºC to 90ºC to 120ºC and back to 60ºC during this experiment.)

The moles of gas were calculated using pressure-volume-temperature relationships in which the volume and temperature were measured for each portion of the reaction system and the total pressure of the system was known. For example, in system 1, the total moles present, 0.00155, ranged from a maximum of 0.00157 to a minimum of 0.00152 over the entire temperature range. The relative standard deviation (RSD) of total moles during this experiment was only 0.56%. For the system integrity check shown in Figures A.1 and A.2, the total moles of gas within the reaction system as a function of time was calculated and is shown in Figure A.3. The calculated moles of gas were constant over the entire experimental duration, in which the temperature was changed from 60°C to 120°C and then back to 60°C.

This experiment was repeated for all of the reaction systems used in actual sludge testing. Each reaction vessel was attached to a separate gas manifold line and increased from 60ºC to 120ºC and back to 60ºC, as described for reaction vessel 1. The pressures, temperatures, and moles of gas were monitored for each reaction system. Table A.1 contains the results for reaction systems 1 through 10. In each case, the error in moles calculated was less than 2% RSD, ranging from 0.19% to 1.99%. In all cases, the ability of each system to measure its quantity of gas was reproducible and excellent.

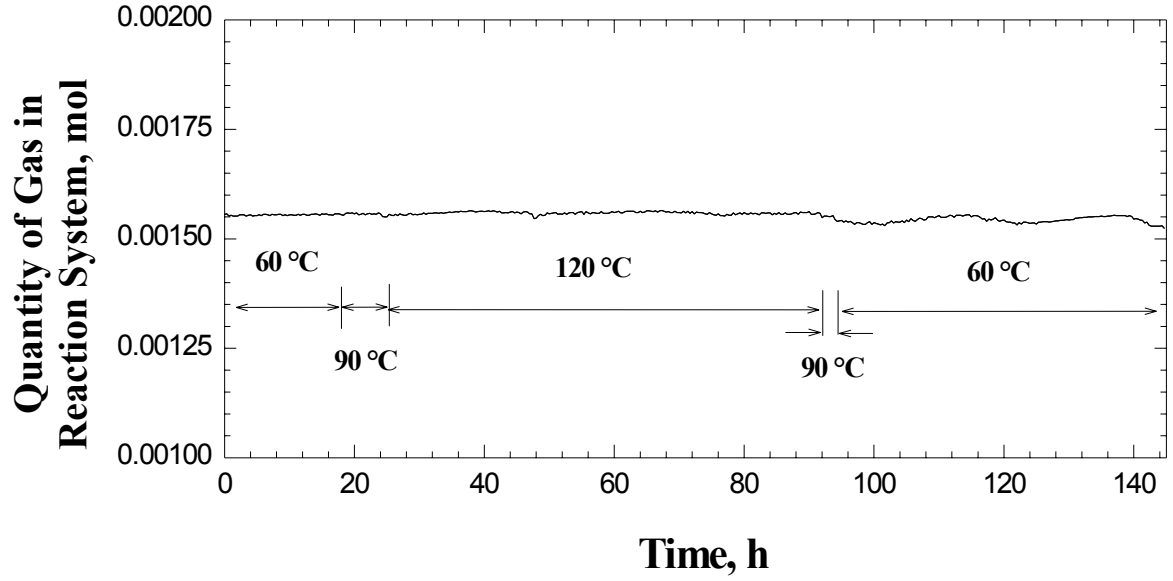

Figure A.3. Total Moles of Gas in Reaction System 1 During Initial Testing (Temperature of the reaction vessel was changed from 60ºC to 90ºC to 120ºC and back to 60ºC during this experiment.)

Table A.1. Measured Moles of Gas Contained in Gas Manifold System During Heating and Cooling System Check

System	1	2	3	4	5	6	7	8	9	10
Moles (average)	1.55E-3	1.69E-3	1.67E-3	1.95E-3	5.21E-3	2.35E-3	1.67E-3	1.68E-3	1.56E-3	1.69E-3
Maximum Moles	1.57E-3	1.70E-3	1.69E-3	1.97E-3	6.42E-3	2.40E-3	1.69E-3	1.70E-3	1.64E-3	1.71E-3
Mimimum Moles	1.52E-3	1.68E-3	1.65E-3	1.94E-3	5.13E-3	2.30E-3	1.65E-3	1.67E-3	1.54E-3	1.67E-3
Standard Deviation	8.72E-6	3.08E-6	9.34E-6	1.02E-5	1.04E-4	3.39E-5	1.32E-5	9.26E-6	2.22E-5	8.43E-6
RSD	0.56%	0.18%	0.56%	0.52%	1.99%	1.44%	0.79%	0.55%	1.43%	0.50%

Appendix B

Gas Analysis and Gas Generation Rate Data

Table B.1. Gas Analyses for Test KC-2/3 P250 at 40°C

Run Sys -5	Temp. °C	Ne	Ar	H_2	CO_2	CH_4	C_2 HC	$C_{>2}$ HC	N_2	O_2	Kr 83	Kr 84	Kr 85	Kr 86	Xe 130	Xe 131	Xe 132	Xe 134	Xe 136	Time, h
1	40	94.3	0.057	0.02	0.72	0.085	0.002		3.92	0.84	5.0E-04	1.0E-03	5.0E-05	1.6E-03	9.0E-06	3.3E-03	5.4E-03	8.9E-03	1.2E-02	425
21H133				2.6	82	9.6	0.226				5.7E-02	1.1E-01	5.7E-03	1.8E-01	1.0E-03	3.7E-01	6.1E-01	1.0E+00	1.4E+00	
2	40	56.1	0.41	0.182	0.3	0.170	0.003		33.80	9.00	7.0E-04	1.4E-03	7.0E-05	2.4E-03	2.0E-05	4.0E-03	6.4E-03	1.1E-02	1.5E-02	344
21H134				25	42	24	0.419				9.8E-02	2.0E-01	9.8E-03	3.4E-01	2.8E-03	5.6E-01	8.9E-01	1.5E+00	2.1E+00	
3	40	82.8	0.002	16.2	0.49	0.239	0.017	0.009	0.10	0.02	1.2E-03	2.3E-03	8.0E-05	4.3E-03	2.0E-05	7.3E-03	1.2E-02	1.9E-02	2.7E-02	425
21H136				95.03	2.9	1.40	0.100	0.053			7.0E-03	1.3E-02	4.7E-04	2.5E-02	1.2E-04	4.3E-02	6.9E-02	1.1E-01	1.6E-01	
4	40	56.9	0.001	42.5	0.417	0.099	0.011	0.006	0.06	0.01	6.0E-04	1.2E-03	6.0E-05	2.3E-03	9.0E-06	3.8E-03	6.1E-03	1.0E-02	1.4E-02	382
21H139				99	0.97	0.230	0.026	0.014	-0.06	-0.03	1.4E-03	2.8E-03	1.4E-04	5.3E-03	2.1E-05	8.8E-03	1.4E-02	2.4E-02	3.2E-02	
5	40	26.0	0.001	73.5	0.303	0.088	0.010	0.003	0.09	0.01	6.0E-04	1.2E-03		2.0E-03		3.5E-03	5.7E-03	9.5E-03	1.3E-02	810
21H144				99	0.41	0.119	0.014	0.004	0.01	-0.02	8.1E-04	1.6E-03		2.7E-03		4.7E-03	7.7E-03	1.3E-02	1.8E-02	
6	40	28.9	0.001	70	0.8	0.063	0.009	0.003	0.14	0.01	5.0E-04	9.0E-04		1.7E-03		2.9E-03	4.7E-03	7.8E-03	1.1E-02	759
21H148				99	1.13	0.089	0.013	0.004	0.08	-0.02	7.0E-04	1.3E-03		2.4E-03		4.1E-03	6.6E-03	1.1E-02	1.5E-02	
7	40	46.5	0.001	52	1.25	0.048	0.006	0.002	0.19	0.02	4.0E-04	7.0E-04		1.2E-03	5.0E-06	2.1E-03	3.5E-03	5.8E-03	8.0E-03	411
21H150				97	2.34	0.090	0.011	0.004	0.20	-0.01	7.5E-04	1.3E-03		2.2E-03	9.4E-06	3.9E-03	6.6E-03	1.1E-02	1.5E-02	
8	95	24.6	0.003	53.4	21.3	0.520	0.061	0.015	0.15	0.01	4.0E-04	8.0E-04		1.2E-03	1.0E-04	2.1E-03	3.5E-03	6.1E-03	8.3E-03	18
21H151				71	28.2	0.689	0.081	0.020	-0.02	-0.05	5.3E-04	1.1E-03		1.6E-03	1.3E-04	2.8E-03	4.6E-03	8.1E-03	1.1E-02	
9	95	34.2	0.002	43.40	21.7	0.460	0.052	0.013	0.12	0.01	4.0E-04	8.0E-04		1.1E-03	6.0E-06	1.9E-03	3.0E-03	5.0E-03	7.0E-03	11
21H152				66	33	0.700	0.079	0.020			6.1E-04	1.2E-03		1.7E-03	9.1E-06	2.9E-03	4.6E-03	7.6E-03	1.1E-02	
10	95	33.6	0.002	50.3	15.5	0.384	0.046	0.013	0.15	0.01	4.0E-04	7.0E-04		1.1E-03	7.0E-06	2.2E-03	3.5E-03	5.9E-03	8.2E-03	20
22K3				76	23	0.579	0.069	0.020			6.0E-04	1.1E-03		1.7E-03	1.1E-05	3.3E-03	5.3E-03	8.9E-03	1.2E-02	
11	95	32.6	0.002	54.8	12.2	0.190	0.031	0.011	0.12	0.02	5.0E-04	9.0E-04		1.6E-03		2.8E-03	4.4E-03	7.3E-03	1.0E-02	57
22K4				81	18.1	0.282	0.046	0.016			7.4E-04	1.3E-03		2.4E-03		4.2E-03	6.5E-03	1.1E-02	1.5E-02	
12	95	37.8	0.003	51.2	10.6	0.173	0.038	0.017	0.15	0.02	6.0E-04	1.1E-03		1.7E-03	1.0E-05	3.2E-03	5.4E-03	8.7E-03	1.3E-02	289
22K7				82	17.1	0.278	0.061	0.027	-0.03	-0.04	9.7E-04	1.8E-03		2.7E-03	1.6E-05	5.2E-03	8.7E-03	1.4E-02	2.0E-02	

Blank entries are below detection limits.
Shaded values denote the composition of the gas generated (i.e., contribution of neon cover gas has been deducted).

Table B.2. Gas Analyses for Test KC-2/3 P250 at 60°C

Run Sys -8	Temp. °C	Ne	Ar	H_2	CO_2	CH_4	C_2 HC	$C_{>2}$ HC	N_2	O_2	Kr 83	Kr 84	Kr 85	Kr 86	Xe 130	Xe 131	Xe 132	Xe 134	Xe 136	Time, h
1	60	69.2	0.076	25.9	1.4	0.180	0.022	0.016	2.64	0.52	6.0E-04	1.1E-03	6.0E-05	2.0E-03	8.0E-06	3.3E-03	5.2E-03	8.7E-03	1.2E-02	353
21H132				94	5.1	0.653	0.080	0.058			2.2E-03	4.0E-03	2.2E-04	7.3E-03	2.9E-05	1.2E-02	1.9E-02	3.2E-02	4.4E-02	
2	60	22.6	0.001	74.2	2.93	0.166	0.022	0.020	0.05	0.002	5.0E-04	1.0E-03	5.0E-05	1.9E-03	8.0E-06	3.1E-03	5.1E-03	8.3E-03	1.2E-02	259
21H134				96	3.8	0.214	0.028	0.026			6.5E-04	1.3E-03	6.5E-05	2.5E-03	1.0E-05	4.0E-03	6.6E-03	1.1E-02	1.6E-02	
3	60	36.9	0.003	59.2	3.51	0.189	0.024	0.020	0.17	0.01	4.0E-04	8.0E-04	8.0E-05	1.4E-03		2.2E-03	3.7E-03	6.0E-03	8.3E-03	151
21H134				94	5.6	0.300	0.038	0.032			6.4E-04	1.3E-03	1.3E-04	2.2E-03		3.5E-03	5.9E-03	9.5E-03	1.3E-02	
4	60	38.7	0.001	56.8	4.06	0.252	0.028	0.023	0.06	0.01	4.0E-04	8.0E-04		1.3E-03	6.0E-06	2.3E-03	3.7E-03	6.1E-03	8.5E-03	184
21H135				93	6.6	0.412	0.046	0.038	-0.04	-0.03	6.5E-04	1.3E-03		2.1E-03	9.8E-06	3.8E-03	6.0E-03	1.0E-02	1.4E-02	
5	60	39.9	0.002	55.5	4.14	0.275	0.032	0.024	0.10	0.01	4.0E-04	8.0E-04	1.0E-04	1.3E-03	6.0E-06	2.3E-03	3.6E-03	6.0E-03	8.4E-03	235
21H136				92	6.9	0.458	0.053	0.040	0.03	-0.03	6.7E-04	1.3E-03	1.7E-04	2.2E-03	1.0E-05	3.8E-03	6.0E-03	1.0E-02	1.4E-02	
6	60	41.5	0.001	54.4	3.55	0.296	0.033	0.020	0.11	0.01	4.0E-04	8.0E-04	4.0E-05	1.4E-03	7.0E-06	2.3E-03	3.8E-03	6.2E-03	8.8E-03	382
21H139				93	6.1	0.507	0.057	0.034	0.04	-0.02	6.9E-04	1.4E-03	6.9E-05	2.4E-03	1.2E-05	3.9E-03	6.5E-03	1.1E-02	1.5E-02	
7	60	48.7	0.002	46.4	4.37	0.209	0.027	0.010	0.23	0.01	4.0E-04	8.0E-04		1.4E-03	8.0E-06	2.5E-03	4.2E-03	6.8E-03	9.6E-03	798
21H144				91	8.6	0.409	0.053	0.020	0.29	-0.02	7.8E-04	1.6E-03		2.7E-03	1.6E-05	4.9E-03	8.2E-03	1.3E-02	1.9E-02	
8	60	48.8	0.003	27.4	23.3	0.175	0.046	0.024	0.25	0.02	3.0E-04	7.0E-04		9.0E-04	8.0E-06	2.0E-03	3.3E-03	5.5E-03	8.2E-03	1173
22K7	95			54	45.7	0.343	0.090	0.047	0.15	-0.05	5.9E-04	1.4E-03		1.8E-03	1.6E-05	3.9E-03	6.5E-03	1.1E-02	1.6E-02	671

Blank entries are below detection limits.
Shaded values denote the composition of the gas generated (i.e., contribution of neon cover gas has been deducted).

Table B.3. Gas Analyses for Test KC-2/3 P250 at 80°C

Run Sys -12	Temp. °C	Ne	Ar	H_2	CO_2	CH_4	C_2 HC	$C_{>2}$ HC	N_2	O_2	Kr 83	Kr 84	Kr 85	Kr 86	Xe 130	Xe 131	Xe 132	Xe 134	Xe 136	Time, h
1	80	36.5	0.0060	48.40	14.30	0.361	0.051	0.048	0.29	0.003	1.1E-03	1.8E-03	6.0E-05	3.0E-03	1.1E-05	4.8E-03	7.9E-03	1.3E-02	1.8E-02	89
21H130				77	22.7	0.573	0.081	0.076	-0.20	-0.17	1.7E-03	2.9E-03	9.5E-05	4.8E-03	1.7E-05	7.6E-03	1.3E-02	2.1E-02	2.9E-02	
2	80	39.7	0.0020	46.88	13.17	0.133	0.019	0.020	0.09	0.01	5.0E-04	9.0E-04	1.0E-04	1.5E-03	7.0E-06	2.4E-03	3.9E-03	6.3E-03	8.5E-03	41
21H131				78	21.9	0.221	0.032	0.034	0.01	-0.03	8.3E-04	1.5E-03	1.7E-04	2.5E-03	1.2E-05	4.0E-03	6.5E-03	1.0E-02	1.4E-02	
3	80	32.2	0.0019	57	10.5	0.242	0.030	0.030	0.05	0.01	6.0E-04	9.0E-04	1.0E-04	1.4E-03	7.0E-06	2.6E-03	4.3E-03	6.9E-03	9.6E-03	90
21H132				84	15.5	0.357	0.044	0.044	-0.04	-0.02	8.9E-04	1.3E-03	1.5E-04	2.1E-03	1.0E-05	3.8E-03	6.3E-03	1.0E-02	1.4E-02	
4	80	46.9	0.0016	42.10	10.6	0.215	0.028	0.026	0.05	0.01	4.0E-04	8.0E-04	2.0E-04	1.3E-03	6.0E-06	2.2E-03	3.6E-03	5.8E-03	8.2E-03	89
21H132				79	20.0	0.406	0.053	0.049	0.01	-0.01	7.5E-04	1.5E-03	3.8E-04	2.5E-03	1.1E-05	4.2E-03	6.8E-03	1.1E-02	1.5E-02	
5	80	65.5	0.0013	26.03	8.24	0.149	0.019	0.019	0.05	0.01	2.4E-04	4.8E-04		7.8E-04		1.4E-03	2.2E-03	3.7E-03	5.3E-03	67
21H133				75	23.9	0.432	0.056	0.054	0.07		7.0E-04	1.4E-03		2.3E-03		4.0E-03	6.5E-03	1.1E-02	1.5E-02	
6	80	56.7	0.0030	35.1	7.6	0.400	0.048	0.039	0.11	0.02	4.0E-04	8.0E-04	1.0E-04	1.4E-03	8.0E-06	2.3E-03	4.0E-03	6.4E-03	9.2E-03	352
21H134				81	17.6	0.927	0.111	0.090	-0.13	-0.07	9.3E-04	1.9E-03	2.3E-04	3.2E-03	1.9E-05	5.3E-03	9.3E-03	1.5E-02	2.1E-02	
7	80	79.7	0.0040	12.8	7	0.238	0.032	0.027	0.19	0.02	2.0E-04	4.0E-04	8.0E-05	6.0E-04	3.0E-06	9.0E-04	1.5E-03	2.5E-03	3.6E-03	395
21H136				64	35	1.189	0.160	0.135	-0.28	-0.25	1.0E-03	2.0E-03	4.0E-04	3.0E-03	1.5E-05	4.5E-03	7.5E-03	1.2E-02	1.8E-02	
8	80	90.4	0.0020	4.17	5.2	0.076	0.013	0.011	0.11	0.02	6.0E-05	1.0E-04	6.0E-06	1.0E-04	1.0E-06	3.0E-04	5.0E-04	8.0E-04	1.2E-03	377
21H139				44	55	0.799	0.137	0.116	0.25	0.00	6.3E-04	1.1E-03	6.3E-05	1.1E-03	1.1E-05	3.2E-03	5.3E-03	8.4E-03	1.3E-02	
9	80	90.3	0.0060	3.24	6.1	0.043	0.016	0.009	0.29	0.02	1.0E-04	1.0E-04	5.0E-06	1.0E-04	4.0E-06	2.0E-04	3.0E-04	4.0E-04	6.0E-04	765
21H144				35	66	0.465	0.173	0.097	-1.41	-1.00	1.1E-03	1.1E-03	5.4E-05	1.1E-03	4.3E-05	2.2E-03	3.2E-03	4.3E-03	6.5E-03	
10	80	86.8	0.0060	3.22	9.6	0.031	0.023	0.012	0.32	0.03	1.0E-04	1.0E-04	5.0E-06	1.0E-04	2.0E-06	1.0E-04	2.0E-04	4.0E-04	5.0E-04	335
22K7	95			25.2	75	0.243	0.180	0.094	-0.75	-0.65	7.8E-04	7.8E-04	3.9E-05	7.8E-04	1.6E-05	7.8E-04	1.6E-03	3.1E-03	3.9E-03	733

Blank entries are below detection limits.
Shaded values denote the composition of the gas generated (i.e., contribution of neon cover gas has been deducted).

Table B.4. Gas Generation Rates from KC-2/3 P250 at 40°C

Run	Temp. °C	Gas Generation Rate, moles/kg-day															
		H_2	CO_2	CH_4	C_2 HC	$C_{>2}$ HC	N_2	O_2	Kr 83	Kr 84	Kr 85	Kr 86	Xe 130	Xe 131	Xe 132	Xe 134	Xe 136	Time, h
1	40	5.04E-07	1.58E-05	1.9E-6	4.4E-8		-1.7E-5	-9.1E-6	1.1E-8	2.2E-8	1.1E-9	3.5E-8	2.0E-10	7.2E-8	1.2E-7	2.0E-7	2.7E-7	425
2	40	4.94E-06	8.15E-06	4.6E-6	8.1E-8		-1.1E-5	-4.7E-6	1.9E-8	3.8E-8	1.9E-9	6.5E-8	5.4E-10	1.1E-7	1.7E-7	3.0E-7	4.1E-7	344
3	40	4.19E-04	1.27E-05	6.2E-6	4.4E-7	2.3E-7	4.8E-7	-1.7E-7	3.1E-8	5.9E-8	2.1E-9	1.1E-7	5.2E-10	1.9E-7	3.1E-7	5.0E-7	6.9E-7	425
4	40	1.78E-03	1.75E-05	4.2E-6	4.6E-7	2.5E-7	-1.1E-6	-4.8E-7	2.5E-8	5.0E-8	2.5E-9	9.6E-8	3.8E-10	1.6E-7	2.6E-7	4.3E-7	5.8E-7	382
5	40	3.31E-03	1.36E-05	4.0E-6	4.5E-7	1.3E-7	3.3E-7	-7.4E-7	2.7E-8	5.4E-8		9.0E-8		1.6E-7	2.6E-7	4.3E-7	5.9E-7	810
6	40	2.99E-03	3.41E-05	2.7E-6	3.8E-7	1.3E-7	2.4E-6	-6.2E-7	2.1E-8	3.8E-8		7.3E-8		1.2E-7	2.0E-7	3.3E-7	4.6E-7	759
7	40	2.53E-03	6.07E-05	2.3E-6	2.9E-7	9.7E-8	5.2E-6	-3.6E-7	1.9E-8	3.4E-8		5.8E-8	2.4E-10	1.0E-7	1.7E-7	2.8E-7	3.9E-7	411
8	95	1.34E-01	5.34E-02	1.3E-3	1.5E-4	3.8E-5	-3.8E-5	-9.2E-5	1.0E-6	2.0E-6		3.0E-6	2.5E-7	5.3E-6	8.8E-6	1.5E-5	2.1E-5	18
9	95	1.26E-01	6.30E-02	1.3E-3	1.5E-4	3.8E-5	9.4E-5	-3.6E-5	1.2E-6	2.3E-6		3.2E-6	1.7E-8	5.5E-6	8.7E-6	1.5E-5	2.0E-5	11
10	95	7.83E-02	2.41E-02	6.0E-4	7.2E-5	2.0E-5	1.1E-4	-2.4E-5	6.2E-7	1.1E-6		1.7E-6	1.1E-8	3.4E-6	5.4E-6	9.2E-6	1.3E-5	20
11	95	3.14E-02	7.00E-03	1.1E-4	1.8E-5	6.3E-6	2.1E-5	-3.7E-6	2.9E-7	5.2E-7		9.2E-7		1.6E-6	2.5E-6	4.2E-6	5.9E-6	57
12	95	4.94E-03	1.02E-03	1.7E-5	3.7E-6	1.6E-6	-1.8E-6	-2.2E-6	5.8E-8	1.1E-7		1.6E-7	9.7E-10	3.1E-7	5.2E-7	8.4E-7	1.2E-6	289
Blank entries are below detection limits.																		

Table B.5. Gas Generation Rates from KC-2/3 P250 at 60°C

Run	Temp. °C	Gas Generation Rate, moles/kg-day																
		H_2	CO_2	CH_4	C_2 HC	$C_{>2}$ HC	N_2	O_2	Kr 83	Kr 84	Kr 85	Kr 86	Xe 130	Xe 131	Xe 132	Xe 134	Xe 136	Time, h
1	60	2.98E-03	1.61E-04	2.1E-5	2.5E-6	1.8E-6	-4.2E-4	-1.3E-4	6.9E-8	1.3E-7	6.9E-9	2.3E-7	9.2E-10	3.8E-7	6.0E-7	1.0E-6	1.4E-6	353
2	60	1.71E-02	6.76E-04	3.8E-5	5.1E-6	4.6E-6	-7.8E-6	-4.7E-6	1.2E-7	2.3E-7	1.2E-8	4.4E-7	1.8E-9	7.2E-7	1.2E-6	1.9E-6	2.8E-6	259
3	60	1.54E-02	9.12E-04	4.9E-5	6.2E-6	5.2E-6	1.5E-6	3.3E-5	1.0E-7	2.1E-7	2.1E-8	3.6E-7		5.7E-7	9.6E-7	1.6E-6	2.2E-6	151
4	60	1.13E-02	8.10E-04	5.0E-5	5.6E-6	4.6E-6	-4.3E-6	-3.1E-6	8.0E-8	1.6E-7		2.6E-7	1.2E-9	4.6E-7	7.4E-7	1.2E-6	1.7E-6	184
5	60	7.92E-03	5.91E-04	3.9E-5	4.6E-6	3.4E-6	2.2E-6	-2.2E-6	5.7E-8	1.1E-7	1.4E-8	1.9E-7	8.6E-10	3.3E-7	5.1E-7	8.6E-7	1.2E-6	235
6	60	4.61E-03	3.01E-04	2.5E-5	2.8E-6	1.7E-6	2.2E-6	-1.1E-6	3.4E-8	6.8E-8	3.4E-9	1.2E-7	5.9E-10	1.9E-7	3.2E-7	5.3E-7	7.5E-7	382
7	60	1.71E-03	1.61E-04	7.7E-6	9.9E-7	3.7E-7	5.4E-6	-4.2E-7	1.5E-8	2.9E-8		5.2E-8	2.9E-10	9.2E-8	1.5E-7	2.5E-7	3.5E-7	798
8	60 95	5.02E-04	4.27E-04	3.2E-6	8.4E-7	4.4E-7	1.4E-6	-4.4E-7	5.5E-9	1.3E-8		1.6E-8	1.5E-10	3.7E-8	6.0E-8	1.0E-7	1.5E-7	1173 671
Blank entries are below detection limits.																		

Table B.6. Gas Generation Rates from KC-2/3 P250 at 80°C

Run	Temp. °C	Gas Generation Rate, moles/kg-day																
		H_2	CO_2	CH_4	C_2 HC	$C_{>2}$ HC	N_2	O_2	Kr 83	Kr 84	Kr 85	Kr 86	Xe 130	Xe 131	Xe 132	Xe 134	Xe 136	Time, h
1	80	2.81E-02	8.31E-03	2.1E-4	3.0E-5	2.8E-5	-7.3E-5	-6.3E-5	6.4E-7	1.0E-6	3.5E-8	1.7E-6	6.4E-9	2.8E-6	4.6E-6	7.7E-6	1.1E-5	89
2	80	5.19E-02	1.46E-02	1.5E-4	2.2E-5	2.3E-5	6.6E-6	-1.8E-5	5.5E-7	1.0E-6	1.1E-7	1.7E-6	7.8E-9	2.7E-6	4.3E-6	7.0E-6	9.4E-6	41
3	80	3.91E-02	7.20E-03	1.7E-4	2.1E-5	2.1E-5	-1.9E-5	-1.0E-5	4.1E-7	6.2E-7	6.9E-8	9.6E-7	4.8E-9	1.8E-6	3.0E-6	4.7E-6	6.6E-6	90
4	80	2.08E-02	5.24E-03	1.1E-4	1.4E-5	1.3E-5	2.1E-6	-3.3E-6	2.0E-7	4.0E-7	9.9E-8	6.4E-7	3.0E-9	1.1E-6	1.8E-6	2.9E-6	4.1E-6	89
5	80	1.25E-02	3.96E-03	7.2E-5	9.3E-6	8.9E-6	1.2E-5	1.7E-6	1.2E-7	2.3E-7		3.8E-7		6.6E-7	1.1E-6	1.8E-6	2.5E-6	67
6	80	3.68E-03	7.97E-04	4.2E-5	5.0E-6	4.1E-6	-5.9E-6	-3.0E-6	4.2E-8	8.4E-8	1.0E-8	1.5E-7	8.4E-10	2.4E-7	4.2E-7	6.7E-7	9.6E-7	352
7	80	9.03E-04	4.94E-04	1.7E-5	2.3E-6	1.9E-6	-4.0E-6	-3.5E-6	1.4E-8	2.8E-8	5.6E-9	4.2E-8	2.1E-10	6.4E-8	1.1E-7	1.8E-7	2.5E-7	395
8	80	2.72E-04	3.39E-04	5.0E-6	8.5E-7	7.2E-7	1.5E-6	-2.8E-8	3.9E-9	6.5E-9	3.9E-10	6.5E-9	6.5E-11	2.0E-8	3.3E-8	5.2E-8	7.8E-8	377
9	80	1.06E-04	2.00E-04	1.4E-6	5.2E-7	3.0E-7	-4.3E-6	-3.0E-6	3.3E-9	3.3E-9	1.6E-10	3.3E-9	1.3E-10	6.6E-9	9.8E-9	1.3E-8	2.0E-8	765
10	80 95	8.80E-05	2.62E-04	8.5E-7	6.3E-7	3.3E-7	-2.6E-6	-2.3E-6	2.7E-9	2.7E-9	1.4E-10	2.7E-9	5.5E-11	2.7E-9	5.5E-9	1.1E-8	1.4E-8	335 733
Blank entries are below detection limits.																		

Table B.7. Gas Analyses for Test KC-4 P250 at 80°C

Run Sys -11	Temp. °C	Ne	Ar	H_2	CO_2	CH_4	C_2 HC	$C_{>2}$ HC	N_2	O_2	Kr 83	Kr 84	Kr 85	Kr 86	Xe 130	Xe 131	Xe 132	Xe 134	Xe 136	Time, h
1	80	93.1	0.022	0.04	5.700	0.002	0.002	0.004	0.99	0.17										425
21H133				0.68	99	0.035	0.035	0.069												
2	80	94.3	0.005	0.05	5.300			0.001	0.19	0.10						3.0E-05	2.0E-05	2.0E-05	3.0E-05	295
21H134				0.95	99			0.019								5.6E-04	3.7E-04	3.7E-04	5.6E-04	
3	80	93.9	0.01	0.10	5.400	0.001	0.001	0.002	0.36	0.20										814
21H139				1.88	97.7	0.018	0.018	0.036												
4	80	94.3	0.008	0.13	5.200	0.001		0.001	0.35	0.04										802
21H144				2.48	96	0.019		0.019	-4.40	-2.26										
5	80	88.7	0.021	0.35	9.600	0.002			0.89	0.375										403
22K11	95			3.55	96.4	0.020			-7.86	-0.74										769

Blank entries are below detection limits.
Shaded values denote the composition of the gas generated (i.e., contribution of neon cover gas has been deducted).

Table B.8. Gas Analyses for Test KC-5 P250 at 80°C

Run Sys -6	Temp. °C	Ne	Ar	H_2	CO_2	CH_4	C_2 HC	$C_{>2}$ HC	N_2	O_2	Kr 83	Kr 84	Kr 85	Kr 86	Xe 130	Xe 131	Xe 132	Xe 134	Xe 136	Time, h
1	80	77.2	0.018	1.73	20.1	0.021	0.009	0.018	0.85	0.01	7.0E-04	4.0E-04		1.0E-04	3.0E-06	2.0E-04	3.0E-04	5.0E-04	7.0E-04	425
21H133				7.9	92	0.096	0.041	0.082			3.2E-03	1.8E-03		4.6E-04	1.4E-05	9.1E-04	1.4E-03	2.3E-03	3.2E-03	
2	80	75.5	0.002	0.58	23.8	0.007	0.004	0.008	0.12	0.03					2.0E-06	1.0E-04	2.0E-04	3.0E-04	4.0E-04	296
21H134				2.4	97	0.029	0.016	0.033							8.2E-06	4.1E-04	8.2E-04	1.2E-03	1.6E-03	
3	80	72.1	0.002	0.19	27.6	0.004	0.004	0.009	0.09	0.03							1.0E-04	2.0E-04	2.0E-04	814
21H139				0.7	99	0.014	0.014	0.032									3.6E-04	7.2E-04	7.2E-04	
4	80	72.3	0.002	0.12	27.4	0.003	0.004	0.003	0.11	0.02							3.0E-05	3.0E-05	5.0E-05	802
21H144				0.4	99	0.011	0.014	0.011	0.11	-0.03							1.1E-04	1.1E-04	1.8E-04	
5	80	62	0.005	0.22	37.5	0.003	0.004	0.002	0.218	0.071										403
22K11	95			0.6	99.40	0.01	0.01	0.005	-0.309	-0.0496										769

Blank entries are below detection limits.
Shaded values denote the composition of the gas generated (i.e., contribution of neon cover gas has been deducted).

Table B.9. Gas Analyses for Test KC-2/3 M250 at 80°C

Run Sys -7	Temp. °C	Ne	Ar	H_2	CO_2	CH_4	C_2 HC	$C_{>2}$ HC	N_2	O_2	Kr 83	Kr 84	Kr 85	Kr 86	Xe 130	Xe 131	Xe 132	Xe 134	Xe 136	Time, h
1	80	80.2	0.023	0.04	18.3	0.004	0.002	0.002	1.23	0.22	2.0E-05	5.0E-05		9.0E-05		3.0E-04	4.0E-04	8.0E-04	1.1E-03	425
21H133				0.196	100	0.022	0.011	0.011			1.1E-04	2.7E-04		4.9E-04		1.6E-03	2.2E-03	4.4E-03	6.0E-03	
2	80	87.1	0.014	0.05	11.5	0.002			1.02	0.29	1.0E-05	3.0E-05	3.0E-06	4.0E-05		1.0E-05	2.0E-04	3.0E-04	5.0E-04	296
21H134				0.43	99	0.017					8.6E-05	2.6E-04	2.6E-05	3.5E-04		8.6E-05	1.7E-03	2.6E-03	4.3E-03	
3	80	91.1	0.018	0.05	7.2	0.004			1.28	0.35	5.0E-05	9.0E-05	5.0E-06	2.0E-04		2.0E-04	3.0E-04	6.0E-04	8.0E-04	814
21H139				0.69	99	0.055					6.9E-04	1.2E-03	6.9E-05	2.7E-03		2.7E-03	4.1E-03	8.2E-03	1.1E-02	
4	80	92.7	0.006	0.05	6.9	0.004		0.001	0.25	0.07	2.0E-05	4.0E-05		7.0E-05		2.0E-04	3.0E-04	5.0E-04	6.0E-04	802
21H144				0.71	98	0.057		0.014	-2.41	-0.59	2.9E-04	5.7E-04		1.0E-03		2.9E-03	4.3E-03	7.1E-03	8.6E-03	
5	80	90.7	0.018	0.08	8.200	0.008	0.002		0.82	0.18	6.0E-05	9.0E-05		2.0E-04		4.0E-04	7.0E-04	1.1E-03	1.5E-03	403
22K11	95			1	98.9	0.1	0.02		-7.25	-2.43	7.2E-04	1.1E-03		2.4E-03		4.8E-03	8.4E-03	1.3E-02	1.8E-02	769

Blank entries are below detection limits.
Shaded values denote the composition of the gas generated (i.e., contribution of neon cover gas has been deducted).

Table B.10. Gas Analyses for Test KC-4 M250 at 80°C

Run Sys -10	Temp. °C	Ne	Ar	H_2	CO_2	CH_4	C_2 HC	$C_{>2}$ HC	N_2	O_2	Kr 83	Kr 84	Kr 85	Kr 86	Xe 130	Xe 131	Xe 132	Xe 134	Xe 136	Time, h
1	80	95	0.023	0.09	3.850	0.004	0.003	0.004	0.97	0.03										425
21H133				2.24	97	0.10	0.08													
2	80	96.4	0.004	0.098	3.24	0.00	0.002	0.002	0.23	0.05						3.0E-05	4.0E-05	6.0E-05	8.0E-05	296
21H134				2.91	96	0.06	0.06	0.06								8.9E-04	1.2E-03	1.8E-03	2.4E-03	
3	80	96.0	0.004	0.172	3.58	0.00	0.003	0.004	0.18	0.01										812
21H139				4.55	95	0.08	0.08	0.11												
4	80	95.6	0.005	0.19	3.95	0.00	0.003	0.003	0.21	0.03						2.0E-05	3.0E-05	3.0E-05	4.0E-05	802
21H144				4.51	94	0.10	0.07	0.07	-2.98	-1.51						4.8E-04	7.1E-04	7.1E-04	9.5E-04	
5	80	87.5	0.01	0.394	11.5	0.00	0.003	0.002	0.45	0.128										403
22K11	95			3	96.6	0.0	0.03	0.02	-2.52	-0.62										769

Blank entries are below detection limits.
Shaded values denote the composition of the gas generated (i.e., contribution of neon cover gas has been deducted).

Table B.11. Gas Analyses for Test KC-5 M250 at 80°C

Run Sys -9	Temp. °C	Ne	Ar	H_2	CO_2	CH_4	C_2 HC	$C_{>2}$ HC	N_2	O_2	Kr 83	Kr 84	Kr 85	Kr 86	Xe 130	Xe 131	Xe 132	Xe 134	Xe 136	Time, h
1	80	86.2	0.015	0.04	8.300	0.003	0.003	0.005	0.72	4.69										425
21H133				0.44	99	0.036	0.036	0.060												
2	80	91.9	0.003	0.049	7.9	0.002	0.003	0.004	0.14	0.04		3.0E-05		3.0E-05		3.0E-05	4.0E-05	6.0E-05	8.0E-05	296
21H134				0.61	99	0.025	0.038	0.050				3.8E-04		3.8E-04		3.8E-04	5.0E-04	7.5E-04	1.0E-03	
3	80	90.8	0.002	0.107	9	0.003	0.003	0.005	0.11	0.02										814
21H139				1.17	98	0.033	0.033	0.055												
4	80	75.9	0.151	0.114	7.6	0.002	0.002	0.002	12.90	3.35										802
21H144				1.47	98	0.026	0.026	0.026	4.62	-0.18										
5	80	85.0	0.005	0.326	14.3	0.00	0.004	0.002	0.25	0.081										403
22K11	95			2	97.7	0.0	0.03	0.01	-0.59	-0.060										769

Blank entries are below detection limits.
Shaded values denote the composition of the gas generated (i.e., contribution of neon cover gas has been deducted).

Table B.12. Gas Generation Rates from KC-4 P250 at 80°C

Run	Temp. °C	Gas Generation Rate, moles/kg-day																
		H_2	CO_2	CH_4	C_2 HC	$C_{>2}$ HC	N_2	O_2	Kr 83	Kr 84	Kr 85	Kr 86	Xe 130	Xe 131	Xe 132	Xe 134	Xe 136	Time, h
1	80	3.63E-06	5.31E-04	1.9E-7	1.9E-7	3.7E-7	-7.1E-5	-2.8E-5										425
2	80	6.87E-06	7.14E-04			1.3E-7	-2.0E-5	1.9E-6						4.0E-9	2.7E-9	2.7E-9	4.0E-9	295
3	80	5.01E-06	2.60E-04	4.8E-8	4.8E-8	9.6E-8	-1.9E-5	-3.3E-7										814
4	80	6.60E-06	2.56E-04	4.9E-8		4.9E-8	-1.2E-5	-6.0E-6										802
5	80, 95	1.44E-05	3.91E-04	8.1E-8			-3.2E-5	-3.0E-6										1146
Blank entries are below detection limits.																		

Table B.13. Gas Generation Rates from KC-5 P250 at 80°C

Run	Temp. °C	Gas Generation Rate, moles/kg-day																
		H_2	CO_2	CH_4	C_2 HC	$C_{>2}$ HC	N_2	O_2	Kr 83	Kr 84	Kr 85	Kr 86	Xe 130	Xe 131	Xe 132	Xe 134	Xe 136	Time, h
1	80	8.17E-05	9.50E-04	9.9E-7	4.3E-7	8.5E-7	-2.7E-5	-1.8E-5	3.3E-8	1.9E-8		4.7E-9	1.4E-10	9.4E-9	1.4E-8	2.4E-8	3.3E-8	425
2	80	3.92E-05	1.61E-03	4.7E-7	2.7E-7	5.4E-7	2.1E-6	4.4E-7					1.4E-10	6.8E-9	1.4E-8	2.0E-8	2.7E-8	296
3	80	4.99E-06	7.25E-04	1.1E-7	1.1E-7	2.4E-7	1.7E-7	2.3E-7							2.6E-9	5.3E-9	5.3E-9	813
4	80	3.11E-06	7.10E-04	7.8E-8	1.0E-7	7.8E-8	7.6E-7	-1.9E-7							7.8E-10	7.8E-10	1.3E-9	802
5	80, 95	5.12E-06	8.80E-04	7.0E-8	9.4E-8	4.7E-8	-2.7E-6	-4.4E-7										1151
Blank entries are below detection limits.																		

Table B.14. Gas Generation Rates from KC-2/3 M250 at 80°C

Run	Temp. °C	Gas Generation Rate, moles/kg-day																
		H_2	CO_2	CH_4	C_2 HC	$C_{>2}$ HC	N_2	O_2	Kr 83	Kr 84	Kr 85	Kr 86	Xe 130	Xe 131	Xe 132	Xe 134	Xe 136	Time, h
1	80	1.71E-06	8.70E-04	1.9E-7	9.5E-8	9.5E-8	-2.9E-5	-1.3E-5	9.5E-10	2.4E-9		4.3E-9		1.4E-8	1.9E-8	3.8E-8	5.2E-8	425
2	80	3.17E-06	7.30E-04	1.3E-7			-4.2E-6	-3.6E-8	6.3E-10	1.9E-9	1.9E-10	2.5E-9		6.3E-10	1.3E-8	1.9E-8	3.2E-8	296
3	80	1.12E-06	1.61E-04	9.0E-8			-3.2E-6	-6.3E-7	1.1E-9	2.0E-9	1.1E-10	4.5E-9		4.5E-9	6.7E-9	1.3E-8	1.8E-8	814
4	80	1.11E-06	1.53E-04	8.9E-8		2.2E-8	-3.7E-6	-9.1E-7	4.4E-10	8.9E-10		1.6E-9		4.4E-9	6.6E-9	1.1E-8	1.3E-8	802
5	80, 95	1.37E-06	1.42E-04	1.4E-7	3.5E-8		-1.0E-5	-3.5E-6	1.0E-9	1.6E-9		3.5E-9		6.9E-9	1.2E-8	1.9E-8	2.6E-8	1152
Blank entries are below detection limits.																		

Table B.15. Gas Generation Rates from KC-4 M250 at 80°C

Run	Temp. °C	Gas Generation Rate, moles/kg-day																
		H_2	CO_2	CH_4	C_2 HC	$C_{>2}$ HC	N_2	O_2	Kr 83	Kr 84	Kr 85	Kr 86	Xe 130	Xe 131	Xe 132	Xe 134	Xe 136	Time, h
1	80	3.87E-06	1.67E-04	1.7E-7	1.3E-7	1.7E-7	-3.8E-5	-2.0E-5										425
2	80	6.06E-06	2.00E-04	1.2E-7	1.2E-7	1.2E-7	-1.2E-6	-1.3E-6						1.9E-9	2.5E-9	3.7E-9	4.9E-9	296
3	80	3.82E-06	7.94E-05	6.7E-8	6.7E-8	8.9E-8	-1.6E-6	-1.3E-6										812
4	80	4.38E-06	9.10E-05	9.2E-8	6.9E-8	6.9E-8	-2.9E-6	-1.5E-6						4.6E-10	6.9E-10	6.9E-10	9.2E-10	802
5	80, 95	7.61E-06	2.22E-04	7.7E-8	5.8E-8	3.9E-8	-5.8E-6	-1.4E-6										1152
Blank entries are below detection limits.																		

Table B.16. Gas Generation Rates from KC-5 M250 at 80°C

Run	Temp. °C	Gas Generation Rate, moles/kg-day																
		H_2	CO_2	CH_4	C_2 HC	$C_{>2}$ HC	N_2	O_2	Kr 83	Kr 84	Kr 85	Kr 86	Xe 130	Xe 131	Xe 132	Xe 134	Xe 136	Time, h
1	80	2.32E-06	5.19E-04	1.9E-7	1.9E-7	3.1E-7	-2.8E-5	2.7E-4										425
2	80	4.09E-06	6.59E-04	1.7E-7	2.5E-7	3.3E-7	-2.6E-6	-4.9E-7		2.5E-9		2.5E-9		2.5E-9	3.3E-9	5.0E-9	6.7E-9	296
3	80	3.33E-06	2.80E-04	9.3E-8	9.3E-8	1.6E-7	9.2E-7	4.9E-8										814
4	80	3.68E-06	2.45E-04	6.4E-8	6.4E-8	6.4E-8	1.2E-5	-4.6E-7										802
5	80, 95	8.81E-06	3.87E-04	8.1E-8	1.1E-7	5.4E-8	-2.3E-6	-2.4E-7										1152
Blank entries are below detection limits.																		

Table B.17. Gas Analyses for Test KC-4 at Ambient Hot Cell Temperature (~32°C)

Run Sys -1	Temp. °C	Ne	Ar	H_2	CO_2	CH_4	C_2 HC	$C_{>2}$ HC	N_2	O_2	Kr 83	Kr 84	Kr 85	Kr 86	Xe 130	Xe 131	Xe 132	Xe 134	Xe 136	Time, h
1	~32	99.56	0.006	0.091	0.098	0.002			0.24	0.003		2.0E-05		3.0E-05		8.0E-05	1.0E-04	2.0E-04	3.0E-04	1483
21H126				45	48	0.987			-88.79	-53.84		9.9E-03		1.5E-02		3.9E-02	4.9E-02	9.9E-02	1.5E-01	
2	~32	99.4	0.003	0.256	0.103				0.17	0.04						3.0E-04	3.0E-04	5.0E-04	6.0E-04	3788
21H149				61	24.5				0.90	-0.44						7.1E-02	7.1E-02	1.2E-01	1.4E-01	

Blank entries are below detection limits.
Shaded values denote the composition of the gas generated (i.e., contribution of neon cover gas has been deducted).

Table B.18. Gas Analyses for Test KC-4 Dup at Ambient Hot Cell Temperature (~32°C)

Run Sys -2	Temp. °C	Ne	Ar	H_2	CO_2	CH_4	C_2 HC	$C_{>2}$ HC	N_2	O_2	Kr 83	Kr 84	Kr 85	Kr 86	Xe 130	Xe 131	Xe 132	Xe 134	Xe 136	Time, h
1	~32	95.9	0.042	0.001	0.131	0.001			3.51	0.41	1.0E-05	2.0E-05		3.0E-05		8.0E-05	1.0E-04	2.0E-04	3.0E-04	1484
21H126				1	91	0.691			56.88	-349.98	6.9E-03	1.4E-02		2.1E-02		5.5E-02	6.9E-02	1.4E-01	2.1E-01	
2	~32	96.4	0.033	0.2113	0.11	0.002			2.90	0.39										3788
21H149				55	28.7	0.522			58.63	-84.45										

Blank entries are below detection limits.
Shaded values denote the composition of the gas generated (i.e., contribution of neon cover gas has been deducted).

Table B.19. Gas Analyses for Test KC-5 at Ambient Hot Cell Temperature (~32°C)

Run Sys -3	Temp. °C	Ne	Ar	H_2	CO_2	CH_4	C_2 HC	$C_{>2}$ HC	N_2	O_2	Kr 83	Kr 84	Kr 85	Kr 86	Xe 130	Xe 131	Xe 132	Xe 134	Xe 136	Time, h
1	~32	99.5	0.007	0.012	0.196				0.28	0.001						1.0E-04	2.0E-04	3.0E-04	5.0E-04	1484
21H126				5	89				-100.23	-60.69						4.5E-02	9.1E-02	1.4E-01	2.3E-01	
2	~32	99.5	0.002	0.144	0.197	0.001			0.13	0.02										3788
21H149				36	49.0	0.249			11.04	-0.85										

Blank entries are below detection limits.
Shaded values denote the composition of the gas generated (i.e., contribution of neon cover gas has been deducted).

Table B.20. Gas Analyses for Test KC-2/3 at Ambient Hot Cell Temperature (~32°C)

Run Sys -4	Temp. °C	Ne	Ar	H_2	CO_2	CH_4	C_2 HC	$C_{>2}$ HC	N_2	O_2	Kr 83	Kr 84	Kr 85	Kr 86	Xe 130	Xe 131	Xe 132	Xe 134	Xe 136	Time, h
1	~32	98.8	0.011	0.014	0.41				0.66	0.07										454
21H133				3.2	92				-39.64	-35.42										
2	~32	99	0.004	0.044	0.72	0.001			0.19	0.05										3332
21H149				5.3	87	0.121			-7.49	-2.10										
3	~32	99.3	0.001	0.023	0.61				0.08	0.02										880
22K7				3.3	88				-0.81	-0.93										
4	~32	99.2	0.001	0.034	0.73				0.061	0.014					1.0E-05	1.0E-05	2.0E-05	3.0E-05		1479
22K11				4	96				-2.96	-1.10					1.3E-03	1.3E-03	2.6E-03	3.9E-03		

Blank entries are below detection limits.
Shaded values denote the composition of the gas generated (i.e., contribution of neon cover gas has been deducted).

Table B.21. Gas Generation Rates from KC-4 at Ambient Hot Cell Temperature (~32°C)

Run	Temp. °C	Gas Generation Rate, moles/kg-day																
		H_2	CO_2	CH_4	C_2 HC	$C_{>2}$ HC	N_2	O_2	Kr 83	Kr 84	Kr 85	Kr 86	Xe 130	Xe 131	Xe 132	Xe 134	Xe 136	Time, h
1	~32	5.82E-07	6.27E-07	1.3E-8			-1.2E-6	-7.0E-7		1.3E-10		1.9E-10		5.1E-10	6.4E-10	1.3E-9	1.9E-9	1483
2	~32	6.62E-07	2.66E-07				9.8E-9	-4.8E-9						7.8E-10	7.8E-10	1.3E-9	1.6E-9	3788
Blank entries are below detection limits.																		

Table B.22. Gas Generation Rates from KC-4 Dup at Ambient Hot Cell Temperature (~32°C)

Run	Temp. °C	Gas Generation Rate, moles/kg-day																
		H_2	CO_2	CH_4	C_2 HC	$C_{>2}$ HC	N_2	O_2	Kr 83	Kr 84	Kr 85	Kr 86	Xe 130	Xe 131	Xe 132	Xe 134	Xe 136	Time, h
1	~32	7.71E-09	1.01E-06	7.7E-9			6.3E-7	-3.9E-6	7.7E-11	1.5E-10		2.3E-10		6.2E-10	7.7E-10	1.5E-9	2.3E-9	1484
2	~32	6.74E-07	3.51E-07	6.4E-9			7.2E-7	-1.0E-6										3788
Blank entries are below detection limits.																		

Table B.23. Gas Generation Rates from KC-5 at Ambient Hot Cell Temperature (~32°C)

Run	Temp. °C	Gas Generation Rate, moles/kg-day																
		H_2	CO_2	CH_4	C_2 HC	$C_{>2}$ HC	N_2	O_2	Kr 83	Kr 84	Kr 85	Kr 86	Xe 130	Xe 131	Xe 132	Xe 134	Xe 136	Time, h
1	~32	7.26E-08	1.19E-06				-1.3E-6	-8.1E-7						6.1E-10	1.2E-9	1.8E-9	3.0E-9	1484
2	~32	3.73E-07	5.10E-07	2.6E-9			1.1E-7	-8.9E-9										3788
Blank entries are below detection limits.																		

Table B.24. Gas Generation Rates from KC-2/3 at Ambient Hot Cell Temperature (~32°C)

Run	Temp. °C	Gas Generation Rate, moles/kg-day																
		H_2	CO_2	CH_4	C_2 HC	$C_{>2}$ HC	N_2	O_2	Kr 83	Kr 84	Kr 85	Kr 86	Xe 130	Xe 131	Xe 132	Xe 134	Xe 136	Time, h
1	~32	3.28E-06	9.60E-05				-4.1E-5	-3.7E-5										454
2	~32	1.27E-06	2.08E-05	2.9E-8			-1.8E-6	-5.0E-7										3332
3	~32	2.43E-06	6.46E-05				-5.9E-7	-6.8E-7										880
4	~32	2.2E-06	4.7E-05				-1.4E-6	-5.4E-7					6.4E-10	6.4E-10	1.3E-09	1.9E-09		1479
Blank entries are below detection limits.																		

Appendix C

Evaluation of Radiolysis as a Source of Hydrogen Production from K Basin Sludge

Appendix C

Evaluation of Radiolysis as a Source of Hydrogen Production from K Basin Sludge

[Note: This discussion was previously provided to Duke Engineering & Services Hanford by PNNL in a Letter Report and Supporting Data Package (Appendix E1) of KE Basin Canister Sludge Sampling and Analysis, Rev. 0, March 7, 1997, prepared by K. L. Silvers.]

For the KE canister sludge samples collected in April 1996 (Makenas et al. 1997), estimates were made for the production of hydrogen by radiolysis. From the following evaluation, it does not appear that radiolysis is a major source of hydrogen.

Since the nuclide analysis provided seemed either incomplete or inconsistent with what was expected to be found, data from the ORIGEN2 run (SD-CP-TI-077 rev 0) were used instead. Data used were for the 12% Pu-240 case (80 wt% Mark IV, 20 Mark IA).

The principal heat-producing fission products after 25 years are Sr-Y-90, Cs-Ba-137, Eu-154, and Kr-85. Of these, only the first two pairs are significant. The estimated power based on uranium fuel is 70 W/t after 25 years of storage. It is unknown how much of these nuclides may be retained in the sludge samples. If we assume about 50%, then about 35 watts per ton are available.

The range of the beta particles (Sr-Y) is calculated to be about 180 mg/cm^2, or roughly 0.015 cm (150 μm) in UO_2. The (photons will escape the sludge particles, but only a fraction will be absorbed by the relatively small amount of water present. If we assume 50%, the fission product energy used for radiolysis is about 17 W/t (W = J/s, 1.0E6 g/t), or 1.1E17 eV/kg-s.

The total α energy increases very slightly with time due to the growth of Am-241. The principal contributions should be from Pu-238,239,240, and Am-241 with small contributions from Pu-241 and Cm-244. At 25 years, the actinide power should be about 14 W/t.

The average α energy is about 5 MeV, but this is greatly reduced for the particles exiting the surface of a UO_2 particle. The ranges for 5, 4, 3, and 2 MeV in air are 4.0, 2.8, 1.8, and 1.0 mg/cm^2, respectively. Using relations given by Friedlander and colleagues (1981), the corresponding values for water are 3.21, 2.22, 1.41, and 0.7, for UO_2 10.2, 7.2, 4.6, 2.7, and for U metal 13.0, 9.1, 5.9, and 3.4 mg/cm^2. Division by the densities gives the linear range. In UO_2, the ranges for 5, 4, and 3 MeV are calculated to be 9.4, 6.6, and 4.2 μm, respectively. For a 5 MeV α particle, the remaining range after passing through 7 μm UO_2 is 2.6 mg/cm^2, which is equivalent to about 2 MeV. For 5-μm thickness, the energy remaining is 3 MeV.

A detailed calculation of the fraction escaping and the effective energy is unlikely to produce any additional valuable information. It is noted, though, that if we assume a 9.4-μm path in UO_2, about 31% of the α-particles could escape a spherical particle of a 60-μm radius, and about 18% from one of 100-μm radius. The actual particle size (i.e., surface area) is unknown. We will use a conservative assumption that 50% escape, retaining 60% of the energy of the particle. Thus, the 14 W/t is reduced to 4.2 W/t or 2.6E16 eV/kg-s. We will assume that all of this is used in radiolysis.

Another uncertainty is the "G" value for hydrogen production, if indeed it does apply to a heterogeneous system such as this. If we use conventional values of 0.45 for β-γ and 1.5 for α, we can estimate the hydrogen production:

Assume 1 kg of U metal and sufficient water to absorb all the effective radiation as estimated above.

(2.6E16 eV/kg-s)(1.5 molecules H_2)(25000ml/mol)/100eV(6.02E23) = 1.6E-5 ml/s, and

(1.1E17)(0.45)(25000)/100(6.02E23) = 2.0E-5 ml/s

or a total of about 0.13 ml/hr. If we use an arbitrary "G" value of 10 for all radiations, we find about 2.0 ml/hr.

The yields calculated are probably on the conservative (high) side. For example, the γ absorption is certainly less than 50% unless a large amount of water is present. The absorption by 1 mm of water is about 0.3% at 1 MeV.

Reference

Friedlander, G., J. W. Kennedy, and J. M. Miller. 1981. *Nuclear and Radiochemistry*, 2nd edition. Wiley-Interscience, New York.

Appendix D

Derivations of Surface-Area-Dependent Corrosion Rate Laws

Appendix D

Derivations of Surface-Area-Dependent Corrosion Rate Laws

As shown in a review of the technical literature (Pajunen 1999), the corrosion rate of the uranium metal in its reaction with water is proportional to the exposed surface area of the uranium solid phase. Dividing the linear areal rate, k, by the material density produces the linear penetration rate, k'. Many other irreversible dissolution or corrosion reactions (e.g., the dissolution of uranium metal and uranium dioxide in acid) also show the same linear dependence of rate on surface area. It follows that the observed surface area-limited mass rates of disappearance of solid phase particles depend on the relationships between the exposed surface area and the volumes (masses) of the starting solid.

Derivations of the rates of disappearance of various geometric solids (sphere, cube, and bar and plate rectangular solids) are considered in this Appendix. In all cases, the surface area-limited rates are assumed to be isotropic (i.e., the same in all directions on all material faces).

Sphere

The corrosion of a sphere is based on the kinetic model developed for reactions of spherical particles (Carter 1961).

The linear penetration rate of corrosion, k', is expressed by the following differential equation:

$$\frac{dy}{dt} = k'$$

in which the rate of penetration in depth y over time t is constant at rate k'. Integrating, the depth penetrated at time t is:

$$y_t = k't$$

The volume, V_s, of material remaining from a corroding sphere after a period of time t may be expressed by two alternative equations:

$$V_s = \frac{4}{3}\pi(r_0 - y_t)^3 = \frac{4}{3}\pi r_0^3(1 - f)$$

in which r_0 is the sphere's original radius, y_t is the depth removed by corrosion, and f is the fraction of the original material which has been corroded. Dividing and taking cube roots yields, in order, the following two equations:

$$(r_0 - y_t)^3 = r_0^3(1 - f)$$

$$(r_0 - y_t) = r_0(1 - f)^{\frac{1}{3}}$$

By substituting k't for y_t and rearranging:

$$(1-f)^{\frac{1}{3}} = 1 - \frac{k't}{r_0}$$

This is the equation used in Section 4.6 to describe the corrosion of a hypothetical uranium metal sphere or collection of equal-sized spheres.

Cube

As was done for the sphere considered in the previous section, the volume of a cube remaining after a period of linear penetration corrosion, V_c, may be expressed by two alternative equations:

$$V_c = (s_0 - 2y_t)^3 = s_0^3(1-f)$$

in which s_0 is the initial length of the side of the cube and the corrosion is occurring to the same penetrating depth y_t from opposite sides over time, t. Taking cube roots, substituting k't for y_t, and rearranging yields:

$$(1-f)^{\frac{1}{3}} = 1 - \frac{2k't}{s_0}$$

It is seen that this equation is identical to that of a sphere because the sphere has axial dimension, or diameter (analogous to s_0), of $2r_0$. Substituting $2r_0$ for s_0 in the equation for the cube produces the equation for the sphere.

Bar

The bar shape considered in this section is a right rectangular solid of initial dimension $s_0 \times s_0 \times l_0$ in which $l_0 >> s_0$. As in the previous sections, the volume of the bar, V_b, may be expressed by two alternative equations:

$$V_b = (s_0 - 2y_t)^2(l_0 - 2y_t) = s_0^2 l_0(1-f)$$

However, because $l_0 >> s_0$, the surface area and relative loss of volume at the two $s_0 \times s_0$ ends is negligible compared with the area and loss of volume along the four $s_0 \times l_0$ sides. The dimension l_0 thus remains relatively constant (i.e., $l_0 - 2y_t \cong l_0$) compared with the s_0 dimensions. Therefore, the first volume equation may be approximated by:

$$V_b \cong (s_0 - 2y_t)^2 l_0 \cong s_0^2 l_0(1-f)$$

Taking square roots this time, substituting k't for y_t, and rearranging yields:

$$(1-f)^{\frac{1}{2}} = 1 - \frac{2k't}{s_0}$$

This equation is of the same form as that for the cube, except the exponent on the (1 - f) term is 1/2 instead of 1/3.

Plate

The plate shape considered in this section is another right rectangular solid. The initial dimensions are $s_0 \times l_0 \times l_0$ with $l_0 >> s_0$. The volume of the plate, V_p, may be expressed by the two alternative equations:

$$V_b = (s_0 - 2y_t)(l_0 - 2y_t)^2 = s_0 l_0^2 (1-f)$$

Because $l_0 >> s_0$, the area and relative loss of volume at the four narrow $s_0 \times l_0$ edges is negligible compared with the area and loss of volume of along the two large $l_0 \times l_0$ faces. The l_0 dimensions remain relatively constant (i.e., $l_0 - 2y_t \cong l_0$) compared with the s_0 dimension. Therefore, the first volume equation may be approximated by:

$$V_b \cong (s_0 - 2y_t) l_0^2 \cong s_0 l_0^2 (1-f)$$

Substituting k't for y_t and rearranging yields:

$$(1-f) = 1 - \frac{2k't}{s_0}$$

This equation is of the same form as those for the cube and bar, except that the exponent on (1 - f) is unity instead of 1/3 and 1/2, respectively.

Reference

Carter, R. E. 1961. "Kinetic Model for Solid-State Reactions." *Journal of Chemical Physics* 34(6):2010-2015.

Pajunen, A. L. 1999. *Uranium Oxidation Rate Summary for the Spent Nuclear Fuel Project.* HNF-4165, Rev. 0, DE&S Hanford, Inc., Richland Washington.

Appendix E

Particle Sizes of Disintegrated SNF Samples from TGA Testing

J. Abrefah, PNNL

Prepared for Numatec Hanford Company

Particle Sizes of Disintegrated SNF Samples from TGA Testing

Background

Microcracks were observed in the uranium matrix that were sectioned from the corroded/damaged region of Spent Nuclear Fuel (SNF) stored in the water-filled K-Basins at the Hanford site. These microcraks likely resulted in the rubbleization of SNF samples during oxidation studies in dry air and moist helium (Abrefah 1999[1]) atmospheres. The presence of these microcracks are shown in the photomicrographs of SNF sample sectioned from the damaged/corroded region of SNF element SFEC5,4378 and published in a report by Marschman (1997[2]). While these cracks may propagate along grain boundaries, the cracks are large and have straight sections that would transcend many grains. Depending on the density of the crack network, particulates resulting from the disintegration process will vary in sizes.

A particle size analyses for the disintegrated SNF samples using either photomicrograph and/or filtration techniques were not performed. These methods would have accurately determined the varying sizes and distribution of the particulates generated. However, a simplified method was used to estimate the range of particle sizes from the photographs taken of the three disintegrated SNF samples. This letter provides the method and results of the measurement.

Particle Size Estimate

To correlate photographic images with the actual sample size, a dimension was measured off a photograph. The measurement was performed on photograph of either the pre-test sample or the biggest post-test sample piece. The photographic dimension was compared to the pre-test sample dimension (see attachment for SNF samples pre-test dimensional measurements data) for the purpose of estimating a scale factor. The scale factor was used to determine the actual particle sizes for all subsequent measurements. The scales shown in the post-test photographs in Figures 1 through 3 were estimated using the same factor.

The particle sizes were measured with a handheld magnifying lens, a compass, a caliper and a ruler. The compass was used to determine the outline of the particles on the photographs with the aid of the magnifying lens. Parallel lines were drawn in cases of larger pieces to enclose the particle and then the measurement determined using the compass and ruler. The measurements themselves have a very good accuracy with error band of less than 1 % but the maximum uncertainty in the method was the determination of the boundaries around the particles and the irregularity associated with the particles. It is very difficult to estimate the exact error band of the estimates because of the latter

[1] Abrefah, J. and R. L. Sell. 1999. *Oxidation of K-West Basin Spent Nuclear Fuel in Moist Helium Atmosphere*. PNNL-12167, Pacific Northwest National Laboratory, Richland, Washington.
[2] Marschman, S. C., T. D. Pyecha and J. Abrefah. 1997. *Metallographic Examination of Damaged N Reactor Spent Nuclear Fuel Element SFEC5,4378*. PNNL-11438, Pacific Northwest National Laboratory, Richland, Washington.

except to mention that the estimate sizes should be better than a factor of two of the accurate particle sizes. The data obtained from the measurements are summarized in the Table 1 below.

Table 1. Particle Sizes of Three Disintegrated SNF Samples

Measurement #	Particle Size (micron)		
	TGA Run 80 (5-S1A-J2B1)	TGA Run 81 (5-S1A-J2A2)	TGA Run 82 (5-S1A-J4B)
1	4300	5900	4000
2	810	3800	3800
3	726	3100	870
4	500	2000	640
5	1080	1520	860
6	710	2130	450
7	600	2130	520
8	700	1490	740
9	1020	1430	850
10	540	3380	720
11	1090	1160	910
12	370	2590	540
13	510	1250	850
14	470	3050	680
15	480	2130	1260
16	730	2470	1430
17	630	3630	1170
18	680	1830	570
19	740	2560	740
20	750	2260	1100
21	590	3320	790
22	690	1520	930
23	990	400	660
24	590	520	1730
25	960	460	2180
TGA = Thermogravimetric Analysis System 5-S1A-… are the SNF Sample identifications			

Summary

The average particle sizes for the three disintegrated SNF samples (Figures 1 to 3) are; (a) 852 microns with a standard deviation of 729 for 5-S1A-J2B1 (TGA Run 80), (b) 2241 microns with a standard deviation of 1201 for 5-S1A-J2A2 (TGA Run 81), and (c) 1160 microns with a standard deviation of 896 for 5-S1A-J4B (TGA Run 82). Note that the method used will bias the measurement to larger particles compared to the smaller particles and it is recommended that an accurate particle size determination be performed.

The photographs shown in Figures 1 through 3 were used in the measurements. Further expansion of these photographs resulted in particulate images with blurred boundaries that would have increased the error in the measurement. The best attempt method was used to measure these SNF particle sizes from the photographs, but the method may not provide an accurate measurement of particle size distribution. This limitation should be considered when using the data in the Table 1.

The average particle sizes of the three SNF samples are larger than the expected average grain size of N-Reactor fuel. However, a typical grain-size particle could also be part of the wide size distribution of the disintegrated rubble.

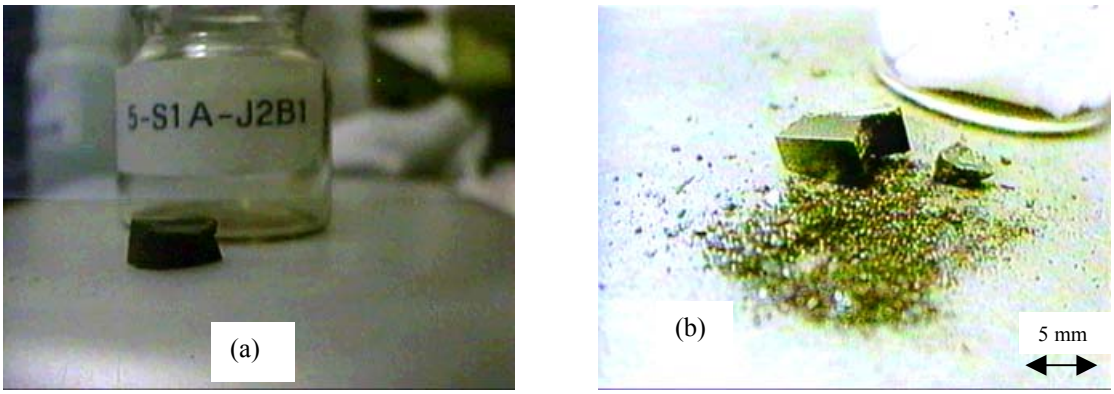

Figure 1. Photographs of (a) Pre- and (b) Post-Test SNF Sample (5-S1A-J2A2) That Disintegrated After Oxidation in Moist-Helium Atmosphere at 160°C, TGA Run 80

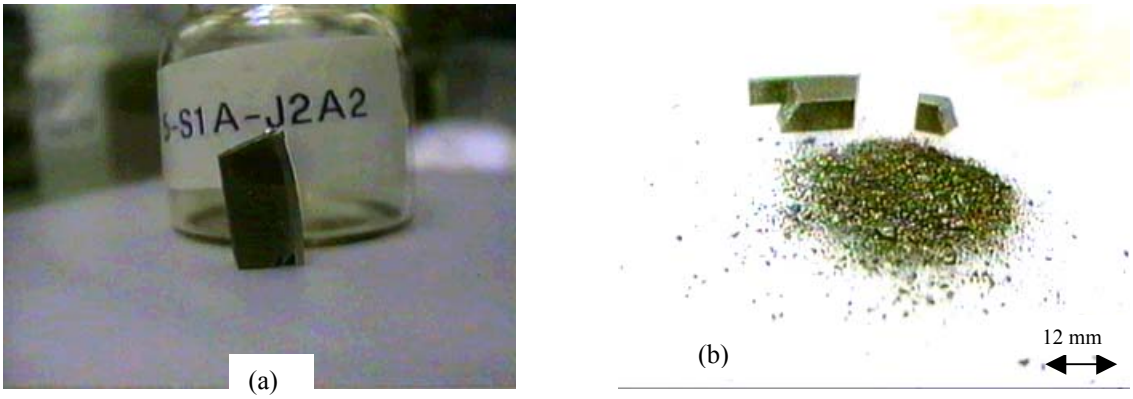

Figure 2. Photographs of (a) Pre- and (b) Post-Test SNF Sample (5-S1A-J2A2) That Disintegrated After Oxidation in Moist-Helium Atmosphere at 160°C, TGA Run 81

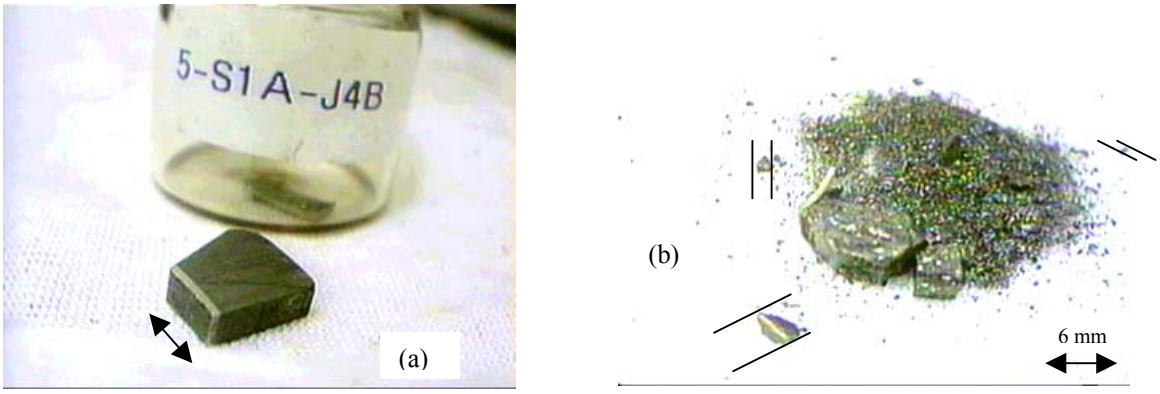

Figure 3. Photographs of (a) Pre- and (b) Post-Test SNF Sample (5-S1A-J4B) That Disintegrated After Oxidation in Moist-Helium Atmosphere at 160°C, TGA Run 82

Attachments

SNF Sample Dimensional Measurement

SPENT FUEL SAMPLE SKETCH
AND
DIMENSIONAL MEASUREMENTS
for
Thermogravimetric Analysis Testing

Hanford Spent Nuclear Fuel Characterization Project

TGA Test Number: TGA 80 (1)

Test Instruction Number: SNF-CT-131 (2)

Sample Identification Number: S-S1A-J261 (3)

Gauge Block Calibration No.	Calibration Due Date	Gauge Block as Measured	Gauge Block Indicated Thickness	
670-10-01-018 (4)	6-25-99. (5)	.250 (6)	.250 (7)	.250 (8)

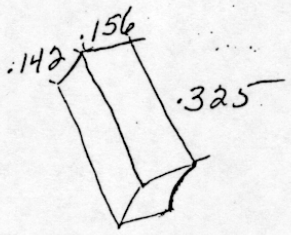

Video Made 10/15/98

SNF-TP-011, Rev. 0
Attachment 1
Page 1 of 1

SPENT FUEL SAMPLE SKETCH
AND
DIMENSIONAL MEASUREMENTS
for
Thermogravimetric Analysis Testing

Hanford Spent Nuclear Fuel Characterization Project

81
~~80~~

TGA Test Number: TGA ~~81~~ RTS 10/12/98 (1)

Test Instruction Number: SNF-CT-~~131~~ 132 RTS 10/12/98 (2)

Sample Identification Number: S-S1A-J2A2 (3)

Gauge Block Calibration No.	Calibration Due Date	Gauge Block as Measured	Gauge Block Indicated Thickness	
670-10-01-018 (4)	6/25/99 (5)	.250 (6)	.249 (7)	.250 (8)

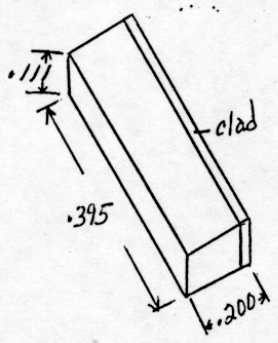

Video mode 10/12/98

SPENT FUEL SAMPLE SKETCH
AND
DIMENSIONAL MEASUREMENTS
for
Thermogravimetric Analysis Testing

Hanford Spent Nuclear Fuel Characterization Project

TGA Test Number: TGA82 (1)

Test Instruction Number: SNF-CT-133 (2)

Sample Identification Number: 5-51A-J48 (3)

Gauge Block Calibration No.	Calibration Due Date	Gauge Block as Measured	Gauge Block Indicated Thickness	
670-10-01-018 (4)	6/25/99 (5)	.250 (6)	.251 (7)	.250 (8)

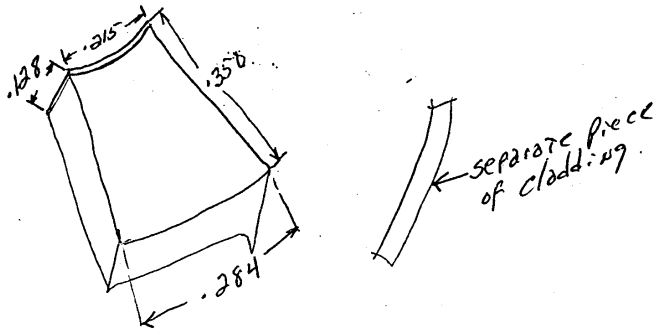

SNF-TP-011, Rev. 0
Attachment 1
Page 1 of 1